Satellite glial contact enhances differentiation and maturation of human iPSC-derived sensory neurons

Chelsey J. LeBlang[1,2], Maria F. Pazyra-Murphy[1], Elizabeth S. Silagi[1,2], Srestha Dasgupta[1,2], Marianna Tsolias[1], Toussaint Miller[1], Veselina Petrova[2,3], Shannon Zhen[3], Vukasin Jovanovic[4], David Castellano[4], Kathryn Gerrish[4], Pinar Ormanoglu[4], Carlos Tristan[4], Ilyas Singeç[4], Clifford J. Woolf[2,3], Ozge Tasdemir-Yilmaz[1,2,5], Rosalind A. Segal*[1,2,5].

[1]Department of Cancer Biology, Dana Farber Cancer Institute, Boston, MA 02215

[2]Department of Neurobiology, Harvard Medical School, Boston, MA 02215

[3]F.M. Kirby Neurobiology Center, Boston Children's Hospital, Boston, MA 02215

[4]Stem Cell Translation Laboratory, National Center for Advancing Translational Science, National Institute of Health, Bethesda, MD, 20892

[5]co-senior author

*corresponding author: rosalind_segal@dfci.harvard.edu

Abstract: Sensory neurons generated from induced pluripotent stem cells (iSNs) are used to model human peripheral neuropathies, however current differentiation protocols produce sensory neurons with an embryonic phenotype. Peripheral glial cells contact sensory neurons early in development and contribute to formation of the canonical pseudounipolar morphology, but these signals are not encompassed in current iSN differentiation protocols. Here, we show that terminal differentiation of iSNs in co-culture with rodent Dorsal Root Ganglion satellite glia (rSG) advances their differentiation and maturation. Co-cultured iSNs develop a pseudounipolar morphology through contact with rSGs. This transition depends on semaphorin-plexin guidance cues and on glial gap junction signaling. In addition to morphological changes, iSNs terminally differentiated in co-culture exhibit enhanced spontaneous action potential firing, more mature gene expression, and increased susceptibility to paclitaxel induced axonal degeneration. Thus, iSNs differentiated in coculture with rSGs provide a better model for investigating human peripheral neuropathies.

Keywords: Satellite Glia, Pseudounipolar, iSN, Sensory Neuron, DRG, Neuropathy, CIPN.

34 **Introduction:**

35 Dorsal Root Ganglion (DRG) neurons are responsible for communicating somatosensory input
36 from the outside world to the central nervous system[1]. They relay these signals through a single
37 specialized T-shaped axon, which projects to both the periphery and the spinal cord[1–3]. DRG
38 neurons include multiple phenotypic subtypes, which respond to specific stimuli and exhibit
39 distinct patterns of gene expression[1,4,5]. DRG neurons are subject to a large number of disorders
40 including hereditary neuropathies, diabetic neuropathy, and chemotherapy induced peripheral
41 neuropathy[6], therefore developing appropriate human model systems is a major goal for
42 researchers.

43 The use of differentiated human induced pluripotent stem cells (hiPSCs) has become a gold
44 standard for studying disease pathology in relevant cell types and is increasingly accessible[7,8].
45 Over the past decade, several protocols have been generated to differentiate standard and patient
46 derived hiPSCs into somatosensory neurons (iSNs, hiPSC-derived sensory neurons)[9–15].
47 Researchers have developed these protocols and utilized iSNs to study neuropathic pain
48 signaling[10,16–18], mechanisms underlying debilitating and painful neuropathies[19–24], and
49 development of treatments for these disorders[17,23,25,26].

50 During sensory neuron differentiation, iPSCs undergo changes mimicking embryonic
51 development, altering their transcriptional program to progressively resemble neuroectoderm,
52 neural crest progenitor cells, and ultimately sensory neurons, through treatment with
53 combinations of small molecules over time and/or genetic manipulation[9–15]. Cells produced using
54 these protocols express many hallmark proteins associated with sensory neuron identity, however
55 iSNs exhibit an embryonic phenotype, different from that of postnatal neurons[4]. In the developing
56 mammalian embryo, DRG neurons initially are bipolar in morphology and undergo a series of
57 morphological changes leading to a pseudounipolar morphology before birth[27–29]. Current
58 differentiation protocols generate iSNs that are predominantly bipolar in morphology, reflecting

59 the early embryonic state, or a multipolar morphology, similar to that observed following an acute
60 injury *in vivo*[30–32]. While developing sensory neurons alter their transcriptome over the course of
61 prenatal development and express transcription factors that contribute to neuronal subtyping[1,33],
62 iSNs remain functionally unspecialized. Therefore, modifications of sensory neuron differentiation
63 protocols to achieve a further differentiated phenotype would greatly advance efforts to study
64 postnatal homeostasis and disease at a molecular level, in a way that is more translatable to
65 human health or disease conditions.

66 We have sought to leverage developmental cues to advance the maturation of differentiated
67 sensory neurons. While specific mechanisms underlying pseudounipolarization and subtyping are
68 unknown, *in vitro* studies show that primary sensory neurons co-cultured with mixed DRG glia,
69 including Schwann cells (SCs) and satellite glia (SGs), become pseudounipolar[34–36]. Yet, iSNs
70 differentiated in a co-culture with induced or primary SCs, undergo no morphological changes,
71 aside from myelination[16,37,38]. *In vivo,* intimate contact is initiated between sensory neurons and
72 satellite glia during the early developmental period[39,40], therefore we hypothesized that satellite
73 glia contribute to DRG sensory neuron maturation, and that terminal differentiation of iSNs in
74 coculture with satellite glial cells would advance this. Here, we show that physical contact between
75 satellite glia and iSNs during differentiation significantly advances morphological and
76 physiological development compared to those differentiated alone, and both semaphorin-plexin
77 signaling and gap junction signaling contribute to this maturation process. We also tested the
78 utility of this model and demonstrate that cocultured iSNs are more susceptible to toxic
79 neuropathy compared to iSNs alone. This work not only provides an advanced iSN model for use
80 by researchers in future studies, but also provides insight into mechanisms underlying sensory
81 neuron development.

82 **Results:**

83 **Human iSNs differentiated in coculture with embryonic rodent DRG glia exhibit advanced**
84 **morphology:**

85 Currently, differentiation protocols used to generate iSNs from iPSCs produce sensory
86 neurons with predominantly immature morphologies[9–15]. While the molecular mechanisms
87 underlying embryonic transition to pseudounipolar morphology are unknown, our data (Fig. S1A-
88 B) and others[36,40] suggest that satellite glia may play a pivotal role in morphological maturation,
89 through contact with sensory neurons during this developmental period. To test this, we used our
90 previously published protocol[15] to terminally differentiate human iPSC-derived neural crest
91 precursors (iNCPs) alone, or together with peripheral glia prepared from rat E14.5 DRGs (Fig.
92 1A). After one week, cells were fixed and stained to visualize neuronal morphology (TUJ1,
93 cytoskeletal marker, green) and contact with rDRG satellite glia (p75, NGF receptor, magenta)
94 (Fig 1B).

95 Morphologies of human neurons were identified and quantified using the rules specified in the
96 methods section. Morphology categories compared consisted of “immature” (including unipolar
97 and bipolar cells) “multipolar”, “Pseudounipolar Transition (PUT)” (including PUT-Bulge, PUT-Bell,
98 and PU-Associated Branch), and “pseudounipolar (PU)” (including PU-Short and PU-Long) (Fig.
99 1B). Frequencies observed for each morphology category (Table 1) indicate that iSNs
100 differentiated in coculture include significantly more transitioning and pseudounipolar cells (PUT
101 *adj. residual* = 7.215, PU *adj. residual* = 6.350) and fewer cells with an immature morphology
102 (immature *adj. residual* = -5.555, multipolar *adj. residual* = -3.653) compared to iSNs differentiated
103 alone (PUT *adj. residual* = -7.215, PU *adj. residual* = -6.350 ,immature *adj. residual* = 5.555,
104 multipolar *adj. residual* = 3.653) (Fig. 1C). No differences were observed between iSNs derived
105 from different iPSC cell lines. These results suggest that terminal differentiation in co-culture with
106 DRG glia enhances the maturation of sensory neuron morphology.

107 To determine whether the ability of peripheral glia to promote a mature, pseudounipolar
108 morphology is restricted to only one of the protocols used to generate iSNs, we also tested our
109 co-culture protocol using RealDRG™ neurons from Anatomic. RealDRGs were terminally

differentiated in coculture or alone, using Senso-MM maturation media by Anatomic as a control. RealDRGs cocultured with rDRG Glia in NCATS Maturation Media (NMM)[15] undergo extensive morphologic changes, although the frequency of transition to pseudounipolar morphology was reduced compared to Deng et al. 2023[15] generated iSNs (Fig S1C-D). Treatment of RealDRGs cultures alone with NMM did not impact observed cell health or morphology but did result in the presence of neural precursor cells, which are not typically observed in RealDRG cultures maintained in Anatomic Senso-MM Media (Fig S1C-D).

	Morphology Frequencies								
	Immature		**Multipolar**	**Pseudounipolar Transition (PUT)**			**Pseudounipolar (PU)**		
Condition	**Unipolar**	**Bipolar**	**Multipolar**	**PUT-Bulge**	**PUT-Bell**	**PUT-AB**	**PU-Short**	**PU-Long**	**Totals**
Coculture	30	22	151	43	31	9	34	9	329
iSN Alone	0	101	174	11	1	0	0	0	287
Totals	153		325	95			43		616

Table 1. Raw frequency of morphology subtypes observed in co-cultured iSNs vs. iSNs terminally differentiated alone. X^2 frequency statistic calculated for major morphology groups: Immature, Multipolar PUT, and PU. (X^2= 111, df=3, p<0.001).

Human iSNs differentiated in coculture with embryonic rodent DRG glia exhibit advanced physiology:

We next assessed the impact of the coculture strategy on development of spontaneous electrophysiologic signaling in iSNs. DRG sensory neurons can transmit sensory input to the CNS via single action potential spikes, as well as synchronous action potential bursts[41,42]. While spontaneous activity is relatively low[41–45] increased spiking and bursting is observed in models of neuropathic pain both *in vivo*[41,42,45–48] and *in vitro*[42,43,45,49]. Therefore, it is crucial that iSNs develop physiologic signaling capability to study the pathogenesis of neuropathies and develop potential treatments.

Characterization of action potential firing using Multi-Electrode Array (MEA) recordings shows that iSNs generated with the Deng et al. 2023[15] protocol exhibit nearly undetectable baseline

131 spontaneous activity after the typical two-week maturation period. Since peripheral satellite glial
132 cells play an important role in the regulation of somatosensory neuron firing[50–53], we tested the
133 hypothesis that iSNs differentiated in coculture would exhibit more mature electrophysiologic
134 properties by measuring spontaneous neural activity of iSNs differentiated in coculture, or alone,
135 using Axion MEA plates containing 16 electrodes/well. Activity was measured on the Maestro Pro
136 recording system for 5 minutes weekly over the span of 5-7 weeks, and neuronal spiking and
137 bursting was analyzed using AxIS software. Overall, cocultured iSNs became robustly active
138 earlier than iSNs differentiated alone, as indicated by a higher number of active electrodes
139 beginning around week 3 of maturation (Fig. S1E-H). Data was analyzed when an average of 7
140 or more electrodes were active per well in both iSN culture conditions (Fig. 1E), this occurred
141 between weeks 5-7 across 4 experimental replicates (Fig. S1E-G). Glia alone were inactive and
142 do not contribute to signals recorded in the coculture (Fig. 1E, Fig. S1E-H).

143 Mature iSNs differentiated in coculture were more active than iSNs differentiated alone (Fig.
144 1E), with a significantly higher number of spikes elicited over the recording period (Mann-Whitney
145 Test, $p= 0.0162$) (Fig. 1F), as well as a significantly higher Mean Firing Rate (MFR) (Mann-
146 Whitney Test, $p= 0.013$) (Fig. 1G). The average MFR observed in cocultured iSNs, 1.657 Hz, is
147 comparable to MFRs previously reported in primary DRG neurons[54,55] and iSNs cultured long-
148 term[56]. No significant difference was observed in the total number of bursts recorded, however
149 the range was quite different, with a maximum burst number of 971 detected in coculture and only
150 341 in iSNs alone (Fig. 1H). Interestingly, cocultured iSNs elicited significantly longer burst trains
151 (Mann-Whitney Test, $p= <0.0001$) (Fig. 1I), with a significantly shorter period between bursts
152 (Mann-Whitney Test, $p= 0.0376$) (Fig. 1J), thus spending more time in a burst state. These results
153 suggest that cocultured iSNs are more physiologically mature than iSNs cultured alone.

154 **iNCPs terminally differentiated in co-culture are advanced in neuronal differentiation:**

155 To identify the transcriptional programs that promote iSN maturation in coculture, we carried
156 out RNA sequencing of iSNs terminally differentiated in coculture or alone. mRNA reads from
157 cocultures were aligned to both the human and rat genome to distinguish mRNAs derived from
158 hiSNs and rDRG glia respectively. PCA analysis confirmed that iSNs terminally differentiated in
159 co-culture cluster separately from iSNs differentiated alone, illustrating transcriptional differences
160 between these two groups (Fig. S2). Differential gene expression analysis yielded 476
161 significantly ($p<0.05$) upregulated genes in cocultured iSNs (Fig. 2A, Table S1). Genes implicated
162 in posterior thoracic neural crest development[57,58] (*HoxB9*, p adj.=$6.922e^{-15}$) and proliferation[59]
163 (*ID3,* p adj.=$1.306e^{-09}$) were among the top genes upregulated. Importantly, the most highly
164 upregulated gene, *NFIX* (p adj.=$1.025e^{-16}$), is associated with onset of neuronal differentiation and
165 quiescence of neural stem cells [60–62] signaling a shift towards a more mature neuronal phenotype.
166 Interestingly, *NFIX*, has also been shown to regulate neuroblast branching in adult
167 neurogenesis[63]. Additional changes in expression of genes underlying neuronal morphogenesis
168 include significant upregulation of *GPRIN3* (p adj.=$6.437e^{-12}$) and *RAI14* (p adj.= $4.910e^{-09}$),
169 proteins essential to axonal outgrowth[64,65] and dendritic development[66,67] respectively, through
170 regulation of actin cytoskeletal structure. These changes illustrate potential transcriptional
171 differences that underly the morphological maturation in cocultured iSNs.

172 Gene Ontology (GO) analysis provided further information on the upregulated gene
173 programs, with 185 significantly upregulated gene terms in cocultured iSNs compared to iSNs
174 alone (Fig. 2B, Table S2). The most significantly upregulated biological processes include
175 increased Bone Morphogenesis Pathway (BMP) signaling and anterior/posterior pattern
176 specification, which confirm commitment to the neural crest cell lineage[33,68] (Table S2). Several
177 biological processes related to neuronal differentiation and morphogenesis were also significantly
178 upregulated, including neural precursor proliferation, neuronal differentiation, and neuronal fate
179 commitment, (Fig 2B). Interestingly, we also observed a significant upregulation of genes

180 associated with axonogenesis (Fig 2B). These genes specifically influence axonal specification,
181 outgrowth, guidance, branching, and synaptogenesis (Table 2, Table S2), and may potentially
182 drive the pseudounipolarization process.

183 Functional maturation was also evident with the upregulated expression of biological
184 processes and cellular components related to synaptic structure and development, including
185 synaptic membrane proteins, receptors, and ion channels localized to synapses in DRG
186 neurons[4,69] (Fig 2B). Specifically, we observed increased expression of genes encoding sodium
187 ion channels (*SCN7a*/*SCN10a*) (Table S2). *SCN10a* is highly expressed in DRG nociceptors,
188 encoding the sodium channel Nav1.8[4,70], critical for nociception[71–73]. We also observed
189 upregulation of muscarinic receptors (*CHRM2/CHRM3*) essential to cholinergic signaling in DRG
190 neurons[74–76], and increased expression of potassium ion channels (*KCNA1/KCNQ5)* that limit
191 action potential firing and maintain resting membrane potential in adult DRG sensory neurons[77–
192 79] (Table S2). Lastly, we observed significant upregulation in AMPAR gene *GRIA2* and GABA
193 receptors (*GABRA1/GABRA5*) which are expressed in several adult DRG neuronal subtypes[4,69]
194 (Table S2). Overall, these transcriptional changes may underly the observed physiologic
195 maturation of co-cultured iSN.

196 Conversely, 748 significantly ($p<0.05$) downregulated genes were identified in cocultured iSNs
197 compared to iSNs alone (Fig. 2A, Table S1). There was decreased expression of genes
198 implicated in early-stage neural crest development (*Lin28a*, p adj.=1.249^{-21}; *RTKN,* p adj.=9.661^{-}
199 ^{15})[80,81] as well as a gene integral to differentiation of neural crest progenitors into mesenchymal
200 lineage cells (*ADAM12*, p adj.=1.069^{-42})[82] (Fig. 2A). We also observed a highly significant
201 decrease in *RGMB* expression (p adj.=9.985^{-28}), a BMP signaling partner which has been shown
202 to promote ventral neuronal differentiation from neural crest cells[83] (Fig. 2A). Additionally, we
203 observed a significant decrease in expression of genes associated with peripheral gliogenesis,
204 including myelinating Schwann cell markers (*Pou3F1*[84]*,* p adj.=4.872^{-12}, *SVIP*[85] p adj.=5.928^{-15},

205 *GPR17*[86] p adj.= 7.605^{-1}, *MAL*[87] p adj.=1.120^{-8}, *PMP22*[88,89] p adj.=1.325^{-5}, satellite glial markers
206 (*TRDN*[89] p adj.=4.190^{-20}, *BCAN*[88,89] p adj.=7.605^{-11}, *CHL1*[90] p adj.=1.863^{-7}), and glial proteins
207 integral to axonal development (*S100A6*[91] p adj.=1.481^{-14}, *SEMA3B*[92] p adj.=8.410^{-10}, *SEMA3G*[92]
208 p adj.=9.360^{-8}) (Fig. 2A) suggesting enhanced commitment to a neuronal fate when iSNs are
209 differentiated in co-culture.

210 Gene Ontology analysis yielded 134 significantly downregulated gene programs in iSNs
211 differentiated in coculture compared to iSNs differentiated alone (Fig. 2C, Table S2). Gene
212 programs associated with MHC I/II complex assembly and antigen presentation were among the
213 most significantly downregulated biological processes in cocultured iSNs (Table S2), consistent
214 with recent data that iNCPs express these proteins at low levels, if at all[93,94]. We also observed
215 significant downregulation in gene programs associated with gliogenesis, glial differentiation,
216 myelination, and axon ensheathment (Fig. 2C), consistent with results suggesting iSNs
217 differentiated in coculture are committed to a neuronal, rather than a glial, fate. Interestingly, GO
218 terms also included transcription factors implicated in the early specification of DRG neuronal
219 subtypes including *NTRK3* and *SHOX2* (expressed in proprioceptors), *RET* (expressed in
220 nonpeptidergic nociceptors and mechanoreceptors) *POU4f3* (expressed in a subpopulation of
221 peptidergic nociceptors) and *GFRA3* (expressed in a subpopulation of peptidergic
222 nociceptors)[1,4,95,96] (Table S2). These results indicate that iSNs in co-culture are committed to a
223 sensory neuron fate and restrict their transcription factor repertoire, which may advance
224 development of functional DRG subtypes.

225 GO analysis also provides potential explanation for a change in neuronal physiology with
226 decreased expression of genes involved in the development, composition, and function of
227 synaptic membrane structures (Fig. 2C), including glutamate receptors, such as kainate receptors
228 (*GRIK1/GRIK3*), AMPAR *GRIA4,* and Delta receptor *GRID2*[97], as well as purinergic receptors
229 (*P2RY1, P2RX6*) (Table S2). Interestingly, potassium ion channel expression (*KNCT2, KNCJ3,*

230 *KCNJ12, KCNS1*) was also decreased, which could contribute to the increased excitability we
231 observe in cocultured iSNs compared to iSNs differentiated alone[79] (Table S2). Taken together
232 transcriptomic analyses indicate that coculture of iNCPs with peripheral glia enhances
233 differentiation into more mature sensory neurons.

Role in Axonogenesis	Gene Names
Specification	*CDKL5*[98]/*PICALM* [99]
Outgrowth	*CDKL5*[98,100]/*AUTS2*[101] /*LAMA2*[102] /*PRICKLE1*[103]/ *EIF4G2* [104]/ *TRPC5*[105] /*ADARB1*[106]/*ENAH*[107]/ *RAB10*[108]; *USP9X*[109]/ *SOCS3*[110]
Branching	*NTN1*[111] / *BCL11A*[112]
Guidance	*EXT1*[111] /*PAK3*[113] /*EFNB2*[114]/ *NTN1*[111,115]/ *UNC5C*[115], *GLI3*[116], *FOXD1*[117]
Synaptogenesis	*NTN1*[111]/*SLITRK1/3*[118] /*ADARB1*[119] / *BCL11A*[120] / *DLG5*[121]

234 **Table 2. Genes upregulated in cocultured iSNs that are implicated in aspects of axonogenesis.**

235 **Rodent DRG satellite glia (rSGs) are responsible for advanced maturation of iSNs:**

236 Our studies demonstrate that iSNs differentiated in coculture with embryonic rat DRG cells
237 mature at an expedited rate compared to iSNs differentiated alone, however due to the protocol
238 used to prepare the rDRG cells, the glial subtype(s) driving this maturation was not initially clear.
239 The rodent DRG cell population includes satellite glia (SGs), myelinating and non-myelinating
240 Schwann cells (SCs), glial progenitor cells (GPCs), fibroblasts, endothelial cells, and immune
241 cells. When initially plated (Fig. 1A, Day 0-7), rDRG cells display a multitude of morphologies,
242 with small islands of semilunar cells and large flat cells, and this variety in cellular profiles is
243 maintained as long as the cells remain in Glia Base Media (Fig. S3A-B). However, the morphology
244 and cell number of rDRG glia changes upon addition of Deng et al. 2023[15] NCATS Maturation
245 Media (NMM), which is required for terminal differentiation of iSNs (Fig S3A-B). We used RNA
246 sequencing to determine the impact of both NMM treatment and iSN contact on rodent glial
247 identity and function (Fig. S3C), mRNA reads from co-cultured RNAs were aligned to both the
248 human and rat genome to differentiate mRNAs derived from hiSNs and rDRG glia respectively.

249 PCA analysis and hierarchal clustering (Fig. S3D-E) showed that rDRG glia treated with NMM
250 cluster together with cocultured rDRG glia treated with NMM. All glia treated with NMM cluster
251 separately from rDRG Glia Alone maintained in base media, suggesting that media composition
252 drives the transcriptional changes observed, while iSN contact leads to minimal changes in the
253 glial transcriptome.

254 DGE analysis yielded 1160 significantly ($p<0.05$) upregulated genes in NMM treated rDRG
255 glia compared to rDRG glia in Glia media (Fig 3A, Table S3). Overall, top upregulated genes in
256 NMM treated glia are associated with mature satellite glia (SGs). The most upregulated genes,
257 *DDIT4* (p adj.=1.196^{-39}) and *INSIG1* (p adj.=1.196^{-39}), have previously been identified as DRG SG
258 specific markers in mouse sc-RNAseq studies[88,90]. *DDIT4* has been implicated in suppression of
259 myelination[122] and *INSIG1*[90] plays a role in cholesterol biosynthesis. Lipid synthesis and
260 metabolism are established functions of DRG SGs[123,124] and all top upregulated genes with NMM
261 treatment are involved in these processes including *PRR5*[125] (p adj.=2.185^{-23}), *PCSK9*[126] (p
262 adj.=2.067^{-21}), *HMGCS1*[89] (p adj.=5.928^{-21}), *TMEM97*[127] (p adj.=9.604^{-19}). and *SCD*[89,90] (p
263 adj.=2.762^{-18}). *HMGCS1* and *SCD*[89], and their related upregulated genes, *HMGCR* (p adj.=1.537^{-}
264 ^{12}) and *SCD2*[90] (p adj.=4.821^{-15}), have also previously been identified as DRG SG gene makers
265 in sc-RNA seq studies. GO analysis (Fig. 3B, Table S4) confirmed that lipid biosynthesis and
266 metabolism pathways were significantly upregulated in NMM cultures.

267 We also observed significant upregulation in biologic processes, cellular components, and
268 molecular functions related to extracellular matrix (ECM) production. These include increased
269 expression of SG genes related to collagen production, such as *COL16A1*, *COL1A1, COL3A1,*
270 and *COL5A1*[90], and other ECM related genes previously associated with SG identity, *FBLN5*[89,90]
271 and *ANXA5*[90] (Table S4). Significant upregulation in biological processes related to DNA
272 replication (Table S4) indicate that enrichment for SGs may be due to enhanced cellular

273 proliferation. Together these results support that treatment with NMM results in an increased
274 proportion of mature SGs in our cultures.

275 DGE analysis also yielded 933 significantly ($p<0.05$) downregulated genes in NMM treated
276 rDRG glia compared cultures maintained in base Glia Media (Fig. 3A, Table S3). Overall, these
277 results indicate a decrease in immune functions in NMM treated cultures. Top downregulated
278 genes were key markers of DRG macrophages including *STAB1*[128,129] (p adj.=2.984^{-30}), *LYZ2*[89]
279 (p adj.=4.974^{-22}), *CSF1R*[130] (p adj.=9.916^{-20}), *MSR1*[131] (p adj.=1.090^{-19}), and *AIF1*[89] (p adj.=4.859^{-}
280 ^{16}). GO analysis (Fig. 3C, Table S4) confirmed that the most downregulated biological processes
281 in NMM treated rDRG glia are related to various aspects of leukocyte function including leukocyte
282 differentiation, proliferation, homeostasis, activation, migration, cytokine production, and
283 chemotaxis. Significant decrease in expression of gene programs related to both mononuclear
284 cells (phagocytosis, macrophage activation, macrophage differentiation) and lymphocytes (T-cell
285 proliferation, T-cell activation, B-cell differentiation, B-cell activation, adaptive immune response)
286 are observed (Table S4). GO analysis also reveals decreased expression of genes related to
287 several aspects of actin cytoskeletal organization, which may contribute to morphologic changes
288 observed with NMM treatment. Together these data indicate the composition of NMM results in
289 an enrichment of SGs. When we compared transcriptomic differences between co-cultured rDRG
290 glia treated with NMM and rDRG glia maintained in Glia Media, we found that differentially
291 expressed genes were nearly identical to those identified in NMM treated cultures without iSN
292 contact (Fig. 3D-F, Table S5-6), indicating that NMM treatment drives an enrichment of SGs in
293 rDRG glial cultures.

294 To elucidate the impact of iSN contact on the transcriptome of SGs, we next compared gene
295 expression between co-cultured NMM treated glia and NMM treated glia alone. DGE analysis
296 yielded very few significant ($p<0.05$) differences, with only 20 significantly upregulated and 52
297 significantly downregulated genes in co-cultured NMM treated glia (Fig. 3G, Table S7). The

298 results indicate that iSN contact impacts the SG cell-cycle and morphology with upregulation of
299 genes related to DNA replication and repair (*CDC14A*[132], p adj.=0.0007), transcription (*ZSCAN18,*
300 p adj.= 0.0352; *TLE4* p adj.= 0.0393), translation (*QARS*[133], p adj.=8.165^{-10}), cytoskeletal
301 organization (*DNMBP*[134] p adj.= 0.047, *SRCIN1*[135] p adj.= 0.047), *SLITRK2*[136] p adj.=0.0007) and
302 ion channels (*TRPM3* p adj.= 0.047, *GRIK2* p adj.= 0.008, *KCNK5* p adj.= 0.007). Several
303 upregulated genes were previously linked to specialized SGs (*SLITRK2*[86], *TRPM3*[137], *ITGB4*[90],
304 *GBP2*[90,137]), which may indicate changes in SG specific functional phenotype when in contact with
305 iSNs. Conversely, downregulated genes (Fig. 3G, Fig. S3F, Table S7-8) were associated with
306 collagen production (*P4HA3*[138] p adj.= 0.013, *COL4A5*[139] p adj.= 0.015) and cell-adhesion
307 (*LTBP2*[140] p adj.= 0.008), which may indicate an alteration in cell spreading and migration with
308 neuronal contact.

309 Taken together, transcriptomic analyses illustrate that initial DRG cell preparations contain
310 multiple cell types, however maturation media enriches for satellite glia. SGs in coculture and SGs
311 cultured alone with NMM treatment are transcriptionally very similar, however minor changes in
312 morphological and functional aspects of SGs do occur with neuronal contact.

313 **Rodent SG (rSG) secreted factors alone do not induce a pseudounipolar morphology in**
314 **iSNs:**

315 The transcriptomic analysis confirmed that rodent satellite glia (rSGs) contribute to the
316 maturation of iSNs, however the molecular mechanisms underlying this process are unknown.
317 We first asked whether this process is mediated by glial secreted factors, using a transwell co-
318 culture system (Fig. 4A). rSGs were cultured for one week on polycarbonate membranes inserted
319 into a well plate, and iSNs were then terminally differentiated in the same wells beneath the
320 membranes, sharing media but never physically touching rSGs, or in wells alone. iSNs were then
321 fixed and stained to visualize neuronal morphology (TUJ1, cytoskeletal marker, green; BRN3a,
322 iSN maturation marker, red) (Fig. 4B), while the rSGs on membranes were dyed and visualized

323 live after two weeks of culture to confirm that a healthy population was present. iSNs differentiated
324 in transwell coculture and alone both presented with predominantly multipolar or immature
325 morphologies, with no significant transition to pseudounipolar morphology (Fig. 4C, Table 3).

326 It is possible that glia only secrete factors critical for the maturation process after they have
327 made physical contact with iSNs. To test this possibility, iSNs plated alone were treated for six
328 days with spent media collected from cocultures (Fig. 4D-F, Table 4). While there are no
329 differences in pseudounipolar morphology, there is a higher frequency of immature neurons in
330 untreated iSNs (immature *adj. residual* = 3.544) compared to spent media treated iSNs (immature
331 *adj. residual* = -3.544), as well as an increased proportion of multipolar cells in spent media treated
332 iSNs (multipolar *adj. residual* = 2.954) compared to untreated iSNs (multipolar *adj. residual* = -
333 2.954). These results are consistent with the idea that rSG-iSN contact, rather than secreted
334 factors, are needed to induce pseudounipolar morphology.

	Morphology Frequencies								
	Immature		**Multipolar**	**Pseudounipolar Transition (PUT) + Pseudounipolar (PU)**					
Condition	**Unipolar**	**Bipolar**	**Multipolar**	**PUT-Bulge**	**PUT-Bell**	**PUT-AB**	**PU-Short**	**PU-Long**	**Totals**
Coculture	0	34	167	18	3	0	1	0	223
iSN Alone	1	42	176	8	6	1	1	1	236
Totals	77		343	39					459

335 **Table 3. Raw frequency of morphology subtypes observed in transwell co-cultured iSNs vs. iSNs terminally**
336 **differentiated alone. X^2 frequency statistic calculated for major morphology groups: Immature, Multipolar, and**
337 **PU(T). X^2= 1.562, df=2, p= 0.4579.**

	Morphology Frequencies								
	Immature		**Multipolar**	**Pseudounipolar Transition (PUT) + Pseudounipolar (PU)**					
Condition	**Unipolar**	**Bipolar**	**Multipolar**	**PUT-Bulge**	**PUT-Bell**	**PUT-AB**	**PU-Short**	**PU-Long**	**Totals**

Media Treated	0	10	225	10	2	0	0	0	247
Untreated	0	26	159	1	3	2	4	0	195
Totals	36		384	22					442

Table 4. Raw frequency of morphology subtypes observed with and without coculture spent media treatment. X^2 frequency statistic calculated for major morphology groups: Immature, Multipolar, and PU(T). X2= 12.69, df=2, p= 0.0018.

Physical contact between rSGs and hiSNs promotes pseudounipolarization:

To determine whether physical contact with satellite glia promotes pseudounipolarization, we designed an assay in which rDRG cells were cultured for two weeks in NMM, then fixed with methanol prior to coculture, preserving surface protein configurations. iSNs were subsequently cultured with the methanol fixed glial cells, in a normal coculture, or alone for one week (Fig. 5A). Cultures were then fixed and stained to visualize neuronal morphology (TUJ1, cytoskeletal marker, green) and contact with rSGs (p75, NGF receptor, magenta) (Fig. 5B). iSNs differentiated in methanol fixed coculture exhibit a phenotype intermediate between iSNs differentiated in normal coculture and those differentiated alone (Fig. 5C, Table 5). The Chi-square frequency test identified significant differences between observed and expected morphology frequencies across all three groups (X^2=131.3, df=6, p<0.001). Interestingly, these results are driven by significant differences between iSNs differentiated in normal coculture conditions (Immature *adj. residual* = -3.543, Multipolar *adj. residual*=-6.471, PUT *adj. residual*= 6.468, PU *adj. residual*=7.893) and iSNs differentiated alone (Immature *adj. residual* = 2.041, Multipolar *adj. residual* = 4.963, PUT *adj. residual*= -5.753, PU *adj. residual*= -3.893), while iSNs differentiated in a methanol fixed coculture exhibited “expected” morphology frequencies, with only significantly fewer pseudounipolar cells than expected (PU *adj. residual*= -4.007). Since PU(T) cells make-up 14.02% of iSNs differentiated in methanol fixed coculture, compared to the 2.26% of iSNs differentiated alone, these results suggest that physical contact between rSGs and iSNs contributes to the changes required for a transition to pseudounipolar morphology.

The degree to which such direct contact truly contributes to this process is unclear, as methanol fixation prevents movement of rSGs in culture, and therefore physical contacts between

364 rSGs and iSNs may be reduced compared to normal cocultures. Overall, the average number of
365 rSG contacts per iSN was significantly reduced in the methanol fixed condition compared to
366 normal cocultures (*t*=23.04, df=470, p<0.0001), with an average of 2 contacts/iSN in methanol
367 fixed coculture vs. 10 contacts/iSN in normal cocultures (Fig. S4A). Significantly more contacts
368 were made to true pseudounipolar cells in methanol fixed coculture compared to less advanced
369 morphologies (Bonferroni post-hoc: PU vs. Multipolar p=0.0038; Bipolar p=0.0053, PUT Bulge
370 p=0.0097) (Fig. S4B). In fact, pseudounipolar iSNs in methanol fixed co-culture were contacted
371 to a similar degree to those in normal coculture, with an average of 9 rSG contacts/ iSN in
372 methanol fixed coculture and 10 rSG contacts/iSN in normal coculture. These results indicate that
373 contact is essential to pseudounipolarization, but downstream signaling and movements of live
374 rSGs may also contribute to this process.

375

	Morphology Frequencies								
	Immature		**Multipolar**	**Pseudounipolar Transition (PUT)**			**Pseudounipolar (PU)**		
Condition	**Unipolar**	**Bipolar**	**Multipolar**	**PUT-Bulge**	**PUT-Bell**	**PUT-AB**	**PU-Short**	**PU-Long**	**Totals**
Methanol Fixed Coculture	2	37	189	35	2	1	4	0	270
Coculture	5	7	105	36	16	10	30	5	214
iSN Alone	1	28	144	4	0	0	0	0	177
Totals	80		438	104			39		661

376 **Table 5: Raw frequencies of morphologies and morphology subtypes observed in methanol fixed coculture,**
377 **normal coculture, and alone. X^2 frequency statistic calculated for major morphology groups: Immature,**
378 **Multipolar, PUT and PU. X2=131.3, df=6, p<0.001.**

379 **Semaphorin-plexin and gap junction signaling play a role in pseudounipolarization of**
380 **iSNs:**

381 We identified two potential pathways whose constituents are appropriately expressed to enable
382 contact mediated SG signaling to iSNs, namely, Sema6a-Plexin A4 and gap junctions. Sema6a,
383 a transmembrane semaphorin protein that is expressed in satellite glia, repels or inhibits axonal
384 growth in developing sensory neurons through engagement with the PlexinA4 receptor[141–144],

385 which is highly expressed in hiSNs (Fig. S4C). Additionally, our sc-RNA seq data set from
386 embryonic DRG satellite glia at the time of pseudounipolarization reveals high expression of
387 *GJA1*, encoding the gap junction protein Connexin-43[88]. *GJA1* was also found to be highly
388 expressed in all NMM treated rDRG glial cultures (Fig. S4D).

389 To test if these pathways promote a pseudounipolar morphology (Fig. 5D), we first knocked
390 down expression of *SEMA6A* in the rSGs using LV-shRNA transduction and puromycin selection.
391 Selected glia were allowed to repopulate and then hiSNs were plated for terminal differentiation
392 in coculture with shRNA-Sema6a expressing glia (shSema6a-rSGs) or shRNA-GFP expressing
393 glia (shGFP-rSGs, control). Cells were cocultured for one week and then fixed and stained to
394 visualize neuronal morphology (TUJ1, cytoskeletal marker, red) and glial expression of Sema6a
395 (Sema6a, magenta; GFP, green) (Fig. 5E). We found that the iSNs differentiated in coculture with
396 shSema6a-rSGs transition to pseudounipolar morphology at a reduced rate compared to controls
397 (Fig. 5F, Table 6), with significantly fewer PU(T) cells (PUT *adj. residual*=-4.772, PU *adj. residual*=-
398 6.861) compared to controls (PUT *adj. residual*=4.772, PU *adj. residual*=6.861), and significantly
399 more multipolar cells (*adj. residual*=9.39) compared to controls (Multipolar *adj. residual*=-9.39.
400 These results indicate that Sema6a-PlexinA4 signaling contributes to pseudounipolarization in
401 this coculture model and may also decrease the incidence of multipolar morphology by inhibiting
402 axonal outgrowth. However, the results also suggest that plexin signaling is not the sole
403 mechanism underlying iSN maturation, since PU(T) cells make up only 10.28% of iSNs
404 differentiated in shSema6a-rSG coculture.

	Morphology Frequencies								
	Immature		**Multipolar**	**Pseudounipolar Transition (PUT)**			**Pseudounipolar (PU)**		
Condition	**Unipolar**	**Bipolar**	**Multipolar**	**PUT-Bulge**	**PUT-Bell**	**PUT-AB**	**PU-Short**	**PU-Long**	**Totals**

shRNA-Sema6a	2	9	242	15	7	2	4	1	282
ShRNA-GFP	20	8	181	38	29	14	53	16	359
Totals	39		423	105			74		641

Table 6. Raw frequency of morphologies observed in shRNA-Sema6a-SG coculture and shRNA-GFP-SG Coculture. X^2 frequency statistic calculated for major morphology groups: Immature, Multipolar, PUT and PU. X^2=94.62, df=3, p<0.001.

To assess the role of satellite glial gap junctions in iSN maturation, we knocked down *GJA1* in the rSGs and plated iSNs for terminal differentiation in coculture with shRNA-GJA1 expressing glia (shGJA1-rSGs) or shRNA-GFP expressing glia (shGFP-rSGs, control) for one week (Fig 5D). Cocultures of hiSNs with shRNA-GJA1 expressing glia (shGJA1-rSGs) or shRNA-GFP expressing glia (shGFP-rSGs, control) were stained to visualize neuronal morphology (TUJ1, cytoskeletal marker, red) and glial expression of GJA1 (GJA1, magenta; GFP, green) (Fig 5G). This experiment was carried out in parallel with the semaphorin knockdown, and therefore we utilized a single group of sh-GFP RNA control samples. Strikingly, iSNs differentiated in coculture with shGJA1-rSGs also transition to pseudounipolar morphology at a reduced rate compared to controls (Fig. 5F, Table 7) with fewer PU(T) cells than expected (PUT *adj. residual*=-5.537, PU *adj. residual*=-7.014), and significantly more multipolar cells than expected (*adj. residual*=10.109). These results suggest that both gap junction and Sema6a/PlexinA mediated signaling contribute to pseudounipolarization.

	Morphology Frequencies								
	Immature		**Multipolar**	**Pseudounipolar Transition (PUT)**			**Pseudounipolar (PU)**		
Condition	**Unipolar**	**Bipolar**	**Multipolar**	**PUT-Bulge**	**PUT-Bell**	**PUT-AB**	**PU-Short**	**PU-Long**	**Totals**
shRNA-GJA1	3	9	277	12	7	4	6	1	319
ShRNA-GFP	20	8	181	38	29	14	53	16	359
Totals	40		458	104			76		678

Table 7. Raw frequency of morphologies observed in shGJA1-rSG coculture and shGFP-rSG Coculture. X^2 frequency statistic calculated for major morphology groups: Immature, Multipolar, PUT and PU. X^2=107.5, df=3, p<0.001.

Cocultured iSNs provide a more physiologically relevant model of neuropathy:

425 iPSC derived neurons often exhibit embryonic phenotypes, which reduces the ability to model
426 complex molecular mechanisms and disease processes [9–15]. To determine whether cocultured
427 iSNs provide a physiologically relevant model of peripheral neuropathy compared to iSNs
428 differentiated alone, we examined the response of these cells to a common form of Chemotherapy
429 Induced Peripheral Neuropathy (CIPN), paclitaxel induced peripheral neuropathy[145,146]. Patients
430 with CIPN experience symptoms of allodynia, paresthesia, numbness, and pain in a stocking
431 glove distribution, due to the degeneration of sensory nerve axon terminals[147]. We assessed the
432 degeneration response of iSNs differentiated in coculture and alone when treated with low dose
433 paclitaxel. At one week of terminal differentiation cultures were treated with paclitaxel
434 chemotherapy or DMSO for 48 hours, then fixed and stained to visualize the neuronal
435 cytoskeleton (TUJ1, Green) and gap junctions in both neurons and glia (GJA1, Magenta) (Fig.
436 6A,C). Neurodegeneration was estimated by quantifying TUJ1 signal.

437 We first tested the impact of low-dose paclitaxel on the degeneration of iSNs differentiated
438 with the Deng et al. 2023[15] protocol, generated by NCATS. Analysis of TUJ1 expression showed
439 that cocultured iSNs were significantly more susceptible to paclitaxel induced degeneration than
440 iSNs differentiated alone (Bonferroni post-hoc: Coculture + Paclitaxel treatment vs. Coculture +
441 DMSO: $p < 0.0001$; vs. iSN Alone + Paclitaxel: <0.0001; vs. iSN Alone + DMSO: $p<0.0001$), which
442 were not significantly impacted by treatment (Bonferroni post-hoc: iSN Alone + Paclitaxel vs. iSN
443 Alone + DMSO $p > 0.9999$) (Fig. 6B). We next tested the impact of the chemotherapy treatment
444 on degeneration of RealDRG™ iSNs from Anatomic, which require a larger dose of paclitaxel to
445 elicit axonal degeneration[148]. Again, iSNs differentiated in coculture were more susceptible to
446 paclitaxel induced degeneration compared to iSNs differentiated alone (Bonferroni post hoc:
447 Coculture + Paclitaxel treatment vs. Coculture + DMSO: $p < 0.0001$; vs. iSN Alone + Paclitaxel:
448 <0.0001; vs. iSN Alone + DMSO: $p<0.0001$), which were not significantly impacted by treatment
449 (iSN Alone + Paclitaxel vs. iSN Alone + DMSO $p > 0.9999$) (Fig. 6D). Together these data indicate

450 that iSNs cocultured with satellite glia provide a more physiologic model for toxin induced
451 neuropathies.

452 **Discussion:**

453 The use of differentiated iPSCs to model human diseases has revolutionized our ability to
454 understand pathology and develop efficacious treatments. While researchers have begun to
455 utilize induced sensory neurons to understand peripheral neuropathies, current differentiation
456 methods produce iSNs with an embryonic phenotype that do not fully recapitulate postnatal
457 functions. In this study, we developed a protocol that enables maturation of iSNs in coculture with
458 rodent satellite glia. We found that contact between iSNs and rSGs, mediated by semaphorin-
459 plexin and glial gap junction signaling, promotes an adult morphology and physiology in the
460 sensory neurons. Ultimately, this system also enables an enhanced model of neuropathy *in vitro*,
461 by increasing iSN susceptibility to chemotherapy induced axonal degeneration at physiologic
462 doses.

463 These studies establish a role for satellite glia in morphologic development of DRG neurons
464 and demonstrate that we can leverage this relationship to reliably produce pseudounipolar iSNs.
465 Previous studies have implicated DRG supporting cells in the morphologic maturation of sensory
466 neurons, with mixed primary cultures of DRG neurons and glia facilitating the transition of sensory
467 neurons to a pseudounipolar morphology[34–36,40]. This result has been recapitulated in induced
468 neuro-mesodermal assembloids[149], however iSNs cocultured with iPSC-derived[16] or primary [21]
469 Schwann cells alone do not exhibit advanced morphology. Based on these studies, we tested the
470 possibility that satellite glia primarily contribute to sensory neuron maturation. *In vivo,* DRG
471 sensory neurons increase physical contact with satellite glia during pseudounipolarization through
472 the development of perikaryal outgrowths that increase contact surface area[40] (Fig. S1B), In the
473 current study, we show that physical contact between glial cells and iSNs is essential to the

474 development of a pseudounipolar morphology, and RNA sequencing and immunohistochemistry
475 indicate that specifically satellite glia are responsible for this effect.

476 Though glial contribution to sensory neuron maturation have been recognized previously,
477 the molecular mechanisms enabling development of pseudounipolar morphology have been
478 unclear. Since our results ruled out glial secreted factors as a direct mechanism of
479 pseudounipolarization, we explored potential contact mediated mechanisms driven by our RNA
480 sequencing data. In iSNs, we observed high expression levels of *Plexina4*, a receptor that
481 interacts with glial semaphorins Sema3a and Sema6a[141–144,150], which have both been implicated
482 in sensory neuron axon development[141–144,151–153]. Since class 3 semaphorins are secreted, we
483 assessed the role of Sema6a, a transmembrane semaphorin[154], in the development of iSN axons.
484 We found knockdown of glial *Sema6a* significantly reduced pseudounipolar formation in
485 cocultured iSNs and instead resulted in a high proportion of multipolar cells. While there was a
486 significant reduction in the proportion of pseudounipolar cells following *Sema6a* knockdown in the
487 satellite glia, this effect was not complete. Factors contributing to observed low levels of
488 pseudounipolarization may include incomplete knockdown of *Sema6a*, compensation via
489 secreted Sema3a, and the possibility that semaphorin-plexin signaling is not the only mechanism
490 underlying this process.

491 In the DRG, satellite glia communicate with adjacent satellite glia and sensory neurons
492 through gap junctions[155,156], contributing to the maintenance of neuronal homeostasis through
493 direct exchange of diverse signaling molecules[157,158]. While little is known regarding gap junction
494 signaling in sensory neuron axon development, communication through gap junctions correlates
495 with neural crest cell differentiation into neuronal cells[159]. Knockdown of glial *GJA1,* like
496 knockdown of Sema6a, significantly reduced the ability of glial cells to induce a transition of iSNs
497 to a pseudounipolar morphology. As was seen following knockdown of Sema6a, knockdown of
498 *GJA1* did not completely abolish pseudounipolarization. Again, this may be explained by

499 incomplete knockdown efficiency, compensation by an alternate connexin, or another parallel
500 signaling mechanism. Future studies need to be carried out to determine whether glial-glial or
501 glial neuronal gap junction signaling contributes to development of pseudounipolar morphology.

502 RNA sequencing also revealed potential intracellular mediators of pseudounipolarization.
503 Multiple molecules implicated in axonal guidance were significantly upregulated in cocultured
504 iSNs, as illustrated in Table 2. These include *CDKL5,* a kinase linked to axonal polarization[98] and
505 *BCL11a,* a transcription factor that suppresses growth of supernumerary neurites and regulates
506 microtubule protein expression[112]. We also observed significant downregulation of *RGMB* which
507 promotes formation of multiple neurites[160]. The identification of cues and molecular pathways that
508 stimulate pseudounipolar morphology may enable further refinements of iSN protocols.

509 Pseudounipolar morphology has multiple implications for sensory neuron physiology, as the
510 axon stem may act as an axon initial segment that potentiates spontaneous activity[36] or as a filter,
511 gating nociceptive action potentials[161,162]. Importantly, we demonstrate that terminal differentiation
512 in coculture yields more physiologically mature iSNs. Using MEA, we found that iSNs in coculture
513 become electrically active earlier than iSNs cultured alone, and fire at a rate more consistent with
514 rodent DRG neurons[54,55]. In addition to the development of an axon stem, the observed differential
515 expression of several ion channels and receptors may contribute to mature firing rates.
516 Upregulation of *SCN10a*, encoding Nav1.8, is of particular importance, as this sodium channel
517 maintains repetitive action potential firing in DRG nociceptors[163] and is integral to pain
518 signaling[72,73,164]. Increased expression of muscarinic receptors *CHRM2* and *CHRM3* may also
519 contribute to spontaneous activity, as acetylcholine has been implicated in the development of
520 bursting and spiking behavior in sympathetic neurons cocultured with satellite glia[165]. Lastly,
521 increased neuronal excitability may reflect a reduction in expression of several potassium
522 channels, namely *KNCT2*[166] and *KCNS1*[167], which have previously been linked to
523 hyperexcitability and neuropathic pain.

524 In this study our goal was to generate iSNs with a more mature adult-like phenotype that
525 would allow us to better model peripheral neuropathies, and we tested the efficacy of modeling
526 toxic neuropathy using chemotherapy treated cocultured iSNs. We found that cocultured iSNs
527 were significantly more susceptible to paclitaxel chemotherapy mediated axonal degeneration
528 compared to iSNs alone. Hyperexcitability of sensory neurons has been shown to contribute to
529 axonal degeneration across multiple neuropathies[6], including chemotherapy induced peripheral
530 neuropathy (CIPN)[145,146], and so the increased baseline excitability of cocultured iSNs may
531 enhance susceptibility to degeneration. Satellite glia may also directly contribute to neuronal
532 degeneration, as studies in rodent models of CIPN indicate that glial release of inflammatory
533 cytokines contribute to degeneration[168–170]. Overall, our results provide new avenues for studying
534 the potential involvement of satellite glial-sensory neuron interactions in the pathogenesis of
535 neuropathies, as this protocol can easily be used to model diabetic peripheral neuropathy,
536 inherited neuropathies, or axonal injury as well.

537 In summary, our work identifies molecular direct contact cues whereby satellite glia support
538 sensory neuron development and establishes an accessible protocol for the reliable differentiation
539 of mature iSNs which can be used to study physiological and pathological changes in sensory
540 neurons and develop novel treatments for peripheral neuropathies.

541 *Limitations of this Study:*

542 This study is limited by the use of rodent glial cells and human derived sensory neurons. Currently,
543 there are no publicly available protocols to differentiate human satellite glia, however several
544 protocols have been developed to induce Schwann Cells[38,171] which share a glial progenitor cell
545 lineage. Adjustments of these protocols such that satellite glia differentiation can be optimized will
546 allow for an advanced iSN differentiation protocol with exclusive use of human cells, and aid in
547 identification of molecular mechanisms underlying normal human sensory neuron development
548 and neuropathy.

549 **Methods:**

550 **Animal Care:** Sprague-Dawley rats were purchased from Charles River Laboratory. Animals were
551 cared for in accordance with NIH standards and guidelines. Experimentation was approved by
552 the Dana Farber Cancer Institute IACUC.

553 **iPSC Culture:** Induced pluripotent stem cells (iPSCs) from LiPSC-GR1.1 (RRID:CVCL_RL65,
554 Male, Hispanic, normal, <1D, umbilical cord blood, Lonza Inc. via NIH RMP, MCB p28) and
555 NCRM5 cell lines (RRID: CVCL_1E75, Male, normal, <1D, umbilical cord blood, Lonza Inc. via
556 NIH RMP, MCB p28) were cultured in feeder-free conditions in Essential-8 Medium (Thermo
557 Fisher; A1517001) using cell culture plates or flasks coated with vitronectin (Thermo Fisher;
558 A14700). iPSCs were passaged with EDTA (Thermo Fisher; 15575020) every 3 days at a 1:6
559 ratio. Cells were treated with the CEPT cocktail for 24 hours after passaging (Chroman 1,
560 MedChem; HY-15392; Emricasan, SelleckChem S7775, Polyamine supplement (1000X), Sigma-
561 Aldrich P8483, Trans-ISRIB, R&D Systems 5284)[172]. Basic characterization including,
562 authentication using G-banded karyotyping, and Mycoplasma detection using Mycoalert kit
563 (Lonza; LT07-318) were carried out at p28. Pluripotency was assessed at p30 using the TaqMan
564 hPSC Scorecard assay (Thermo Fisher; A15876) and analysis software, and significance was
565 determined using the *Student's t-test*. iPSCs (p30) were differentiated into neural crest precursors
566 (NCPs) and immature sensory neurons (SNs) using our published protocol[15].

567 **rDRG-iSN Coculture:**

568 *Rodent DRG glial cell culture:* Sprauge-Dawley day E14.5 rat DRGs were dissected. DRGs were
569 trypsinized (1mg trypsin /mL HBSS) for 50 minutes at 37°C. 40k cells/well were plated on
570 uncoated Lab-Tek™ II Chambered Coverglass (Thermofisher cat#: 155409) with filtered Glia
571 Base Media (DMEM/F12, 10% FBS, 1% Pen. Strep., 0.08% glucose). After a 30-minute
572 incubation at 37°C 7.5% CO_2., chambers were vigorously shaken, and media was fully changed

573 to remove cells in suspension. Remaining glial cells were cultured in Glia Base Media at 37°C
574 7.5% CO_2 for one week with media changes 3x/ week.

575 *Terminal differentiation and iSN- rDRG glia co-culture:* Frozen Neural Precursor Cells (NPCs)
576 were differentiated by NIH-NCATS Stem Cell Laboratory using the protocol outlined in Deng et
577 al., 2023[15]. Lab-Tek™ II Chambered Coverglass (Thermofisher cat#: 155409) were coated with
578 0.005% poly-ornithine solution (Sigma-Alrich cat#: P4957) in dH2O 1 hr at 37°C, washed, and
579 then coated with 5 ug/mL mouse laminin (Thermofisher cat#: 23017015) in dH2O 1 hr at 37°C.
580 NPCs were thawed in NCATS Maturation Media (DMEM/F12+Glutamax, 2% B27,1% N2, 25ng
581 rh- BDNF/b-NGF/GDNF/NT3) + CEPT rock inhibitor cocktail (50nM Chroman-1 (Medchem
582 Express Cat#: HY-15392), 5uM Emricasan (Selleck cat#: S7775), 0.001% Polyamine supplement
583 (Sigma-Alrich cat#: P8483), 0.7uM Trans-ISRIB (Tocris cat#: 5284)). 15k cells/well were plated in
584 NCATS Maturation Media + CEPT on coated cultureware for terminal differentiation alone (iSN-
585 Only), or in coculture with rDRG glial cultures treated with NCATS Maturation Media + CEPT. 24
586 hrs after plating, media was changed to NCATS Maturation Media + 1uM PD0332991 (Tocris cat#:
587 4786). Cells were cultured for one week at 37°C 5% CO_2., with ½ media changes 3x/week.

588 For each experiment throughout this study, we indicate the number of biological replicates used,
589 with each biological sample representing an experiment done with one set of iSNs that were
590 plated and tested individually. The experiment was subsequently replicated on additional sets of
591 cells plated and tested on a different day (the biological replicates). n=4 biological replicates for
592 experiments performed in Figure 1C, n= 2 NCRM5 and n=2 GR1.1.

593 **Quantification of iSN morphology frequency:**

594 *Immunofluorescence:* Cells were fixed for downstream Immunofluorescence (IF) on Day 14. First,
595 cells were fixed with 2% paraformaldehyde (PFA) (EMS cat#: 15710; 1:1 4% PFA to spent media)
596 10 minutes at room temperature (RT), and then in 4% PFA 20 minutes at RT. Cells were washed

597 3x in PBS and stored at 4°C. Fixed cultures were permeabilized with 0.1% Triton-x in PBS 10
598 minutes and blocked in blocking buffer (5% Normal Goat Serum (Cell Signaling Tech. cat#:
599 5425S) in 1x PBS) for 1 hr at RT. Cultures were then incubated overnight at 4°C in primary
600 antibodies (Table 11) diluted in blocking buffer. The following day, cultures were washed and
601 incubated in Alexa-Fluor secondary antibodies (Table 12) and DAPI diluted 1:1000 in blocking
602 buffer for 1 hr at RT. Co-Cultures were stained with mouse anti-human nuclei-CY3 conjugate
603 (Sigma cat#: MAB1281C) for 2 hrs at RT to distinguish human neuronal nuclei from rodent. Cells
604 cultured in Lab-Tek™ II Chambered Coverglass were stored at 4°C in PBS prior to imaging, and
605 cells cultured on coverslips were mounted on slides with fluoromount (Thermofisher cat#:
606 OB10001).

607 *Imaging:* All photomicrographs of cells cultured in Lab-Tek™ II Chambered Coverglass were
608 collected on the Zeiss-980 airy-scan/confocal microscope. Images of all conditions were obtained
609 at 20x with 1.3x zoom and bidirectional scanning in SRY-4 Airy-Scan. Multiplex imaging was
610 utilized with 405, 488, 561, and 639 lasers at 800V gain, 1% laser power, and 0 offset. All images
611 were obtained in a z-stack with 0.35um step size. Systematic random sampling was utilized to
612 image n=50-100 cells/biological replicate across 8-wells. Areas with fused cell bodies and axonal
613 fasciculations were omitted from sampling. All images were 3D airy-scan post processed in Zen
614 Blue software.

615 *Analysis:* All human cells in each photomicrograph were categorized into the following
616 morphologic groups : unipolar (one axonal projection off of the cell body, that does not bifurcate),
617 bipolar (two axonal projections off of opposite cell body poles, ~180° angle), multipolar (more than
618 two axonal projections), Pseudounipolar Transition (PUT)- Bulge (two axonal projections off of the
619 bottom of the cell body, axons form >90° angle), PUT-Bell (two axonal projections off of the bottom
620 of the cell body, axons form a 90° angle or less), PU-Associated Branch (PU-AB,T-shaped
621 pseudounipolar axon with a branch <10uM long), PU-Short (T-shaped pseudounipolar axon, with

622 an axon stem <60um long), PU-Long (T-shaped pseudounipolar axon, with an axon stem >60um
623 long). Human cells were distinguished from rodent cells based on expression of human nuclei-
624 Cy3 marker. Images were blinded and intra-rater or inter-rater reliability was calculated to be
625 >90%. Morphology frequency was compared across morphologic groups: Immature (unipolar
626 and bipolar), Multipolar, Pseudounipolar Transition (PUT-Bulge, PUT-Bell, PUT-AB), and
627 Pseudounipolar (PU-Short and PU-Long) using the Chi-square test in Graphpad Prism 10. Sub-
628 morphologies were pooled into major morphologic categories to reach chi-square test validity
629 requirements. Adjusted residuals with Bonferroni correction were calculated in excel using
630 standard formulas.

631 **Multi-Electrode Array Recording:**

632 *Cell Culture:* rDRG glia were dissected and plated in 48-well, 16 electrode Cytoview-MEA plates
633 (Axion) at 20k cells/well in Glia Media. After a 30-minute incubation at 37°C 7.5% CO_2, plates
634 were vigorously shaken, and media was fully changed to remove cells in suspension. Remaining
635 glial cells were cultured in Glia Media at 37°C 7.5% CO_2 for one week with media changes 3x/
636 week. On the 7th day, iNCPs were thawed and plated in NCATS Maturation Media + CEPT at
637 150k-200k cells/ well, in coculture or alone on coated wells (100ug/mL PDL 1 hr 37°C, 10ug/mL
638 mouse laminin 1 hr 37°C). A fraction of the wells remained glial cells alone as a control, treated
639 with NCATS Maturation Media +CEPT. 24 hrs after plating, media was changed to NCATS
640 Maturation Media + 1uM PD0332991. Cells were cultured for 5-8 weeks at 37°C 5% CO_2., with ½
641 media changes 3x/week. n=4 biological replicates; replicates 1-3 = iPSC Gr1.1, replicate 4 = iPSC
642 NCRM5.

643 *MEA Recording:* MEA recordings were performed on the Maestro Pro recording system from
644 Axion at 37°C 5% CO_2, 1x/week for 5 minutes, after at least 5 minutes of acclimation. AxIS
645 navigator software was used to record standard Spontaneous Neural and Viability properties.
646 Burst Detection was enabled with the following specifications: Single Electrode Minimum #

647 Spikes=5, Network Minimum #Spikes=50, Maximum Interspike Interval= 100s, Mean Firing Rate
648 detection window= 100s. Recordings were carried out weekly, and data was analyzed when an
649 average of 7+ active electrodes was reached for both cocultured iSNs and iSNs alone. Electrodes
650 were considered active with a minimum of 5 spikes/minute.

651 *Analysis:* Data was analyzed at the time point when an average of 7+ electrodes were active in
652 both conditions. Wells with 2 or less active electrodes were excluded from analysis. Glial cells
653 were not active, and therefore were excluded from all analyses aside from # of active electrodes.
654 Data did not follow a normal gaussian distribution, and therefore averages were compared using
655 the Mann-Whitney U test in Graphpad Prism 10. n=# wells, pooled from 4 biological replicates.

656 **RNA sequencing of iSN and rDRG Glia cocultures:**

657 *Cell Culture and RNA Collection:* rDRG glia were dissected and plated in uncoated glass bottom
658 35mm Fluorodishes (WPI cat #: FD35-100) at 250k cells/dish in Glia Media. After 30 minutes at
659 37°C 7.5% CO_2, dishes were vigorously shaken, and media was fully changed to remove cells in
660 suspension. Remaining glial cells were cultured in Glia Media at 37°C 7.5% CO_2 for one week
661 with media changes 3x/ week. On Day 7, cells were either treated with NCATS Maturation Media
662 + 1uM PD0332991, maintained in Glia Media, or co-cultured with iSNs as described above. iSNs
663 were plated at 90k/dish in co-culture or alone, as described above. Cultures were maintained at
664 37°C 5% CO_2., with ½ media changes 3x/week for an additional week. On Day 14, RNA was
665 collected from Glia Media Treated rDRG Glia, NCATS Maturation Media Treated rDRG Glia, iSN-
666 rDRG Glia Co-Culture, and iSN-Only mass cultures using the RNeasy Plus Mini Kit (Qiagen cat#:
667 74134). n=3-4 biological replicates; Coculture: n= 2 iPSC NCRM5, n=1 GR1.1. iSN only: n=4
668 iPSC NCRM5. Glial cells derived from n=4 rats.

669 *RNA sequencing:* mRNA bulk sequencing was carried out at the Dana Farber Cancer Institute
670 Molecular Biology Core Facility. The genomics core team performed RNA QC, rRNA depletion,

671 library preparation (Roche Kapa mRNA Kit), and sequencing on the Illumina NovaSeq 6000.
672 Reads were aligned to both the rat (*Rattus norvegicus*) and human genome using STAR aligner
673 to separate rDRG glia and iSN reads in co-culture. GEO Accession #: GSE272868.

674 *Analysis:* Normalized counts (with raw counts <3 set to NA) were analyzed for differential gene
675 expression using the DESeq2 R package version 1.42.0[173] with an adjusted p-value cutoff of 0.05.
676 Gene Ontology Enrichment Analysis was performed using the clusterProfiler R package version
677 4.10.0[174] with an adjusted p-value cutoff of 0.05.

678 **iSN-rSG co-culture in transwell compartmentalized system:**

679 *Cell Culture:* rDRG glia were dissected as described above and plated at 40k cells/well on
680 uncoated Millicell® Standing Cell Culture Inserts (MilliporeSigma cat#: PIHP01250). rDRG glia
681 were prepared as described above. On the 7th day, iNPCs were plated at 15k cells/ well on sterile
682 12mm #1.5 coverslips, coated as described above, in the same plate for terminal differentiation
683 either in compartmentalized co-culture or alone. Cells were allowed to attach to coverglass for 30
684 min at 37°C 5% CO_2, after which Glia Media was removed from rDRG glial inserts and inserts
685 were transferred to wells with NPCs dedicated for terminal differentiation in compartmentalized
686 co-culture. 24 hrs after iNPC plating, media was changed to NCATS Maturation Media + 1uM
687 PD0332991. Cells were cultured for one week at 37°C 5% $CO_{2.}$, with ½ media changes 3x/week.
688 On the 14th day, rDRG glial culture inserts were moved to new wells and glia attached to insert
689 were visualized with CellTracker Red CMTPX (Thermofisher cat#: C34552). Cells were incubated
690 with 12.5uM dye in DMEM/F12 for 30 min at 37deg 5% CO2, after which media was changed to
691 DMEM/F12 and live cells were imaged at 10x TRITC on the Nikon-Ti E microscope. iSNs adherent
692 to coverglass were fixed for downstream Immunofluorescence (IF) as described above. n=3
693 biological replicates, iPSC Gr1.1.

694 *Imaging and Analysis:* Photomicrographs of cells cultured on coverslips were collected on the
695 Nikon Ni-E confocal microscope at 60x with oil immersion. Images were obtained with 405 and
696 488 lasers, at 30V gain 5% power and 561 30V gain 7% power. All images were obtained in a z-
697 stack with 0.35um step size. Systematic random sampling was utilized to image n=50-100
698 cells/biological replicate across 3 coverslips. Areas with fused cell bodies and axonal
699 fasciculations were omitted from sampling. Inter-rater reliability was calculated >90%. Morphology
700 frequencies and statistics were carried out as described above.

701 **iSN cultures treated with co-culture spent media:**

702 Spent media was collected from iSN-rDRG Glia Co-Cultures over the course of one week and
703 stored at 4°C. On Day 21, iNPCs were plated alone on chambered coverglass in NCATS
704 Maturation Media + CEPT as described above. After 24 hrs, media was either changed to ½ fresh
705 NCATS Maturation Media + 1uM PD0332991 + ½ spent media or maintained in NCATS
706 maturation Media + 1uM PD0332991 as described above. Cells were cultured for one week with
707 3x full media changes maintaining specified ratios. On Day 28, cultures were fixed for IF and
708 images were acquired and analyzed as described. n=3 biological replicates; n= 2 iPSC NCRM5
709 n= 1 iPSC Gr1.1.

710 **iSN-rSG co-culture with glial methanol fixation:**

711 rDRG glia were dissected, plated, prepared, and cultured in chambered coverglass for one week
712 as described above. On Day 7, glia were treated with NCATS maturation media + CEPT, and 24
713 hrs later media was changed to NCATS Maturation Media + 1uM PD0332991. Glia were
714 maintained in NCATS Maturation Media + 1uM PD0332991 an additional week with ½ media
715 changes 3x/week. On day 14, cells were fixed in 95% methanol 7 min at 4°C, washed, and treated
716 with NCATS maturation media + CEPT for downstream iSN co-culture. iNPCs were thawed and
717 plated at 15k cells/well for terminal differentiation in iSN-rDRG Glial Co-Culture with methanol

718 fixation, iSN-rDRG Glial Co-Culture without methanol fixation (prepared as described above), or
719 iSN-only culture (prepared as described above). 24 hrs after iNPC plating, media was changed
720 to NCATS Maturation Media + 1uM PD0332991. Cells were cultured for one week at 37°C 5%
721 $CO_{2.}$, with ½ media changes 3x/week. After one week of coculture, cells were fixed with PFA for
722 downstream IF and images and analyses were carried out as described above. n=4 biological
723 replicates, n=2 NCRM5, n=2 GR1.1.

724 **iSN-rSG co-culture with glial *Sema6a* or *GJA1* sh-RNA knockdown:**

725 rDRG glia were dissected, plated, prepared, and cultured for five days as described above. On
726 Day 5, Glia were transduced with ShRNA-Sema6a-puro-GFPtag lentivirus (Millipore Sigma Cat#:
727 SHCLNV), ShRNA-GJA1-puro-GFPtag lentivirus (Millipore Sigma Cat#: SHCLNV), or ShRNA-
728 GFP-puro control lentivirus (Millipore Sigma cat#: SHC005V) in Glia Media for 24 hrs, after which
729 media was changed. Cells were maintained in Glia Media 72 hrs post-transduction and evaluated
730 for sh-RNA expression using live-imaging in brightfield and FITC on the Nikon-Ti E microscope.
731 Glia were then treated on Day 8 with 1ug/mL puromycin in Glia Media for 48hrs. Media was
732 changed, and selected cells were allowed to proliferate for four days. On Day 14, iNPCs were
733 plated at 15k cells/well in NCATS Maturation Media + CEPT for terminal differentiation in iSN-
734 rDRG Glia Knockdown Co-Culture, iSN rDRG Glia Knockdown Control Co-culturel and iSN-rDRG
735 Glia Co-Culture Control (prepared as described above). 24 hrs after iNPC plating, media was
736 changed to NCATS Maturation Media + 1uM PD0332991, and cells were co-cultured for one week
737 at 37°C 5% $CO_{2.}$, with ½ media changes 3x/week. On Day 21, co-cultures were fixed for IF as
738 described. n=4 biological replicates, 2/ iPSC line.

739 **Modeling chemotherapy induced axonal degeneration:**

740 *Chemotherapy treatment of iSN co-culture with rDRG glia:* rDRG glia were prepared as described
741 above. iSNs generated with the Deng et al. 2023[15] protocol, were plated at 15k cells/well in rDRG

742 glial co-culture or alone and maintained in culture for 7 days as described above. On day 14, cells
743 were treated with 60nM Paclitaxel (Sigma Aldrich cat #: T7402) or 0.2% DMSO (Sigma Aldrich
744 cat#: D2650) in NCATS Maturation Media + 1uM PD0332991 for 48 hrs. n=4, iPSC NCRM5.
745 Anatomic RealDRG iSNs were plated at 5k cells/well in rDRG glial co-culture or alone and
746 maintained in culture for 7 days as described above. On day 14, cells were treated with 600nM
747 Paclitaxel (Sigma Aldrich cat #: T7402) or 0.2% DMSO (Sigma Aldrich cat#: D2650) in NCATS
748 Maturation Media + 1uM PD0332991 for 48 hrs. n=4, Anatomic RealDRGs are derived from one
749 genetic iPSC line. Cells were then fixed as described above for IF.

750 *Immunofluorescence (IF):* Fixed cultures were permeabilized with 0.1% Triton-x in PBS 10
751 minutes, and blocked in blocking buffer (5% Normal Donkey Serum (Sigma Aldrich cat#: D9663)
752 in PBS) for 1 hr at RT. Next, they were incubated overnight at 4°C in primary antibodies (Table
753 11) diluted in blocking buffer. The following day, cultures were washed and incubated in Alexa-
754 Fluor secondary antibodies (Table 12) and DAPI diluted 1:1000 in blocking buffer for 1 hr at RT.
755 Cells were washed and stored in PBS at 4°C prior to imaging.

756 *Imaging:* All photomicrographs of cells cultured in Lab-Tek™ II Chambered Coverglass were
757 collected on the Zeiss-980 airy-scan/confocal microscope. Images of all conditions were obtained
758 at 20x with 1.3x zoom and bidirectional scanning in SRY-4 Airy-Scan configuration. Multiplex
759 imaging was utilized with 405, 488, 561, lasers at 800V gain, 1% laser power, and 0 offset. All
760 images were obtained in a z-stack with 0.35um step size. Systematic random sampling was
761 utilized to image n=16 fields/biological replicate across 6-wells. All images were 3D airy-scan post
762 processed in Zen Blue software.

763 *Analysis:* Particle analysis was carried out on gray-scale TUJ1 channel image stacks. Threshold
764 was manually set at the brightest z-stack slice for each image, and percent area occupied by
765 TUJ1 pixels was quantified for each image stack. Average values were calculated for each field.
766 Field averages were compared between treatment groups and culture conditions using two-way

767 ANOVA analysis with the Bonferroni post-hoc test in Graphpad Prism. n=64 fields from 4 biological

768 replicates.

Primary Antibody	Supplier:Cat #	Concentration	Experiment(s)
rbt anti-BRN3a	Abcam: ab245230	1:250	Co-culture in compartmentalized system, Spent media treatment
rbt anti-dsRed	Takara:632496	1:1000	*in vivo* DRG morphology
gt anti-GJA1	Abcam: ab87645	1:200	Connexin-43/GJA1 knockdown co-culture, Chemotherapy treatment co-culture
rbt anti-Fabp7	ThermoFisher: PA531864	1:200	Identification of glial subtypes
Mse anti-human nuclei-CY3	Millipore Sigma: MAB1281C	1:200	Co-culture, RealDRG co-culture, Methanol fixation co-culture
rbt anti-MBP	Abcam: ab218011	1:250	Identification of glial subtypes
rbt anti-P75/ngfr	Abcam: ab52987	1:100/ 1:200	Co-culture, RealDRG co-culture, Methanol fixation co-culture, Identification of glial subtypes
rbt anti-OCT6	Abcam: ab259952	1:200	Identification of glial subtypes
Mouse anti-S100b	Sigma: S2532	1:1000	Identification of glial subtypes
rbt anti-Sema6a	Thermofisher: PA581009	1:100	Sema6a knockdown co-culture
ms anti-TUJ1	Biolegend: 801202	1:1000	Co-culture, RealDRG co-culture, Co-culture in compartmentalized system, Methanol fixation co-culture, Spent media treatment, Sema6a knockdown co-culture Connexin-43/GJA1 knockdown co-culture, Chemotherapy treatment co-culture

769 **Table 11. Primary antibodies.**

Secondary	Supplier:Cat #	Concentration	Experiment(s)

Antibody			
gt anti-Ms Alexa 488	Thermofisher: A11001	1:1000	Co-Culture, RealDRG co-culture, Methanol Fixation co-culture, Co-culture in compartmentalized system, Spent media treatment, Identification of Glial Subtypes
gt anti Rbt Alexa 647	Thermofisher: A21245	1:1000	Co-Culture, RealDRG co-culture, Methanol Fixation co-culture
gt anti-Rbt Alexa 546	Thermofisher: A11035	1:1000	Co-culture in compartmentalized system, Spent media treatment, Identification of Glial Subtypes
dnky anti-Ms Alexa 568	Thermofisher: A10037	1:1000	Sema6a Knockdown coculture, Connexin-43/GJA1 knockdown coculture, CIPN chemotherapy treatment coculture
dnky anti-Gt Alexa 647	Thermofisher: A21447	1:1000	Connexin-43/GJA1 knockdown coculture, Chemotherapy treatment coculture
dnky anti-Rbt Alexa 647	Thermofisher: A31573	1:1000	Sema6a knockdown coculture
dnky anti-Rbt Alexa 546	Thermofisher: A10040	1:1000	*in vivo* DRG morphology

770 **Table 12. Secondary antibodies.**

771

772 **Figure Legends:**

773 **Figure 1: Human iSNs differentiated in coculture with embryonic rodent DRG glia exhibit**
774 **more mature morphology and physiology.** A) Schematic illustrating protocol to terminally
775 differentiate iSNs in coculture with embryonic rat DRG glia (rDRG). Briefly, DRGs are dissected
776 from E14.5 rat embryos. After 30 minutes, cultureware is shaken and cells in suspension are
777 removed. Glia are cultured for 1 week, after which iNCPs are thawed and plated in coculture or
778 alone for 1 week of maturation. B) Photomicrographs representing distinct iSN morphologies
779 observed. TUJ1= Green, p75= Magenta, Human Nuclei= Red, DAPI= Cyan. Scale=50um. PU=
780 pseudounipolar. PU-AB: white arrowhead indicates accessory branch. PU-Long: white arrowhead
781 indicates the PU-Long neuron in this field. C) Frequency of each morphology observed in
782 coculture and alone, displayed as percentages. 4 biological replicates, 2 iPSC cell lines. D.
783 Representative raster plots over 2.5 minutes of MEA recording. Black lines indicate individual

spikes and blue lines indicate bursts. E) Average number of active electrodes when average was > 7 (5-7 weeks). Coculture n= 28 wells, iSN alone n=17 wells, Glia alone n=16 wells from 4 biological replicates. F-H) Number of spikes (F), mean firing rate (G), and number of bursts (H) when average # active electrodes were >7. Wells with <2 active electrodes were excluded. Coculture n= 26 wells, iSN alone n=15 wells from 4 biological replicates. I) Average burst duration in seconds when average # active electrodes were >7. Wells with <2 active electrodes and 0 bursts were excluded. Coculture n=24 wells, iSN alone n=14 wells from 4 biological replicates. J) Interburst Interval in seconds when average # active electrodes were >7. Wells with <2 active electrodes and <2 bursts were excluded. Coculture n= 22 wells, iSN alone n=13 wells from 4 biological replicates. F-J) Mann-Whitney U tests performed in Graphpad Prism 10, $p<0.05$=significant, $p<0.0001$=****.

Figure 2. iNCPs terminally differentiated in co-culture more advanced in neuronal differentiation compared to iNCPs alone. A) Volcano plot illustrating differential gene expression in coculture vs. alone. B) GO analysis terms upregulated in coculture vs. iSNs alone, related to neuronal development. C) GO analysis terms downregulated in coculture vs. iSNs alone, related to neuronal development. Coculture n=3, iSN alone n=4. P adj.<0.05.

Figure 3. Rodent DRG satellite glia (rSGs) are responsible for advanced maturation of iSNs. A) Volcano plot illustrating differential gene expression in NCATS Maturation Media treated rDRG glia vs. rDRG glia maintained in base glia media B-C) GO analysis terms upregulated (B) and downregulated (C) in NCATS Maturation Media treated rDRG glia vs. rDRG glia maintained in base glia media. D) Volcano plot illustrating differential gene expression in cocultured rDRG glia vs. rDRG glia maintained in base glia media E-F) GO analysis terms upregulated (E) and downregulated (F) in cocultured rDRG glia vs. rDRG glia maintained in base glia media. G) Volcano plot illustrating differential gene expression in cocultured rDRG glia vs. NCATS Maturation Media treated rDRG glia. n=3-4/group. P adj.<0.05.

Figure 4. rSG secreted factors do not induce pseudounipolar morphology in iSNs. A) Schematic illustrating transwell coculture protocol. B) Representative photomicrographs of iSNs cultured in transwell coculture or alone. TUJ1= Green, BRN3a=Red, DAPI= Blue. Scale= 50um. C) Frequency of each morphology observed in coculture and alone, displayed as percentages .n= 3 biological replicates D) Schematic illustrating protocol for iSN treatment with coculture spent media. E) Representative photomicrographs of iSNs treated with coculture spent media or untreated. TUJ1= Green, BRN3a=Red, DAPI= Blue. Scale=50um. F) Frequency of each morphology observed in Coculture Media treated and untreated iSNs, displayed as percentages. 3 biological replicates.

822 **Figure 5. Physical contact between rSGs and iSNs is essential to pseudounipolarization.**
823 A) Schematic illustrating protocol for iSN coculture with methanol fixed glia. B) Representative
824 photomicrographs of iSNs in coculture with methanol fixed glia, normal glia, or alone. TUJ1=
825 Green, p75=Magenta, Human Nuclei= Red, DAPI= Cyan. iSNs alone were not stained for human
826 nuclei. Scale= 50um. C) Frequency of each morphology observed in cocultured iSNs with
827 methanol fixed glia and normal glia, displayed as percentages. n=4 biological replicates. D)
828 Schematic illustrating protocol for iSN coculture with Sema6a, GJA1, and GFP knockdown in glia.
829 All three conditions were run in parallel. E) Representative photomicrographs of iSNs in coculture
830 with SEMA6a knockdown glia or GFP knockdown glia. Sema6a=Magenta, TUJ1= Red,
831 GFP=Green, DAPI=Cyan. Scale=50um. F) Frequency of each morphology observed in iSNs
832 cocultured with SEMA6a knockdown, GFP knockdown, and GJA1 Knockdown glia, displayed as
833 percentages. n=4 biological replicates. G) Representative photomicrographs of iSNs in coculture
834 with GJA1 knockdown glia or GFP knockdown glia. GJA1=Magenta, TUJ1= Red, GFP=Green,
835 DAPI=Cyan. Scale=50um.

836 **Figure 6. Cocultured iSNs are more susceptible to paclitaxel mediated neurodegeneration.**
837 A) Representative photomicrographs of Deng et al. 2023 generated iSNs in coculture or alone,
838 treated with either 0.2% DMSO or 60nM paclitaxel. TUJ1= Green, GJA1=Magenta, Human
839 Nuclei= Red, DAPI= Cyan. iSNs alone were not stained for human nuclei. Scale= 50um. B)
840 Percent area occupied by TUJ1 particles in cocultured iSNs and iSNs differentiated alone + 0.2%
841 DMSO or 60nM Paclitaxel. Two-Way ANOVA with Bonferroni post-hoc calculated in Graphpad
842 Prism 10, $p<0.05$= significant, $p<0.0001$=****. n=64 fields from 4 biological replicates. C)
843 Representative photomicrographs of Anatomic RealDRG iSNs in coculture or alone, treated with
844 either 0.2% DMSO or 600nM paclitaxel. TUJ1= Green, GJA1=Magenta, Human Nuclei= Red,
845 DAPI= Cyan. iSNs alone were not stained for human nuclei. Scale= 50um. D) Percent area
846 occupied by TUJ1 particles in cocultured iSNs and iSNs differentiated alone + 0.2% DMSO or
847 600nM Paclitaxel. Two-Way ANOVA with Bonferroni post-hoc calculated in Graphpad Prism 10,
848 $p<0.05$= significant, $p<0.0001$=****. n=64 fields from 4 biological replicates.

849 **Acknowledgements:** NCI R01 CA205255. Schematics created with Biorender.

850 **Declaration of Interests:** C.J.W. is a founder of Nocion, Quralis, and Blackbox Bio, and is a
851 member of the SAB of Lundbeck Pharma and Tafalgie Therapeutics. I.S. is currently CSO at
852 FUJIFILM Cellular Dynamics. All other authors have no interests to disclose.

853 **Author Contributions**: Conceptualization: CJL, OYT, RAS. Generation of NCPs: KG, VJ, DC,
854 PO, CT, IS. Performance of experiments: CJL, MFPM, ES, SD, VP, SZ, OYT. Analysis: CJL,
855 MFPM, MT, TM. Funding Acquisition: RAS. Project Administration: CJL, RAS. Supervision: RAS,
856 CW. Writing: CJL, RAS, with input from all authors.

857

858 **<u>Supplemental Methods:</u>**

859 **Animal Care:**

860 Sprague-Dawley rats were purchased from Charles River Laboratory. Ntrk2-CreER/C57BL/6 mice
861 and lox-tdtomato/C57BL/6 mice were shared by Dr. David Ginty, Harvard Medical School. PLP1-
862 GFP/C57BL/6 mice were shared by Dr. Lisa Goodrich, Harvard Medical School. Animals were

863 cared for in accordance with NIH standards and guidelines. Experimentation was approved by
864 the Dana Farber Cancer Institute IACUC.

865 **Tamoxifen induced sparse labeling of Ntrk2+ sensory neurons with tdtomato *in vivo*:**

866 Ntrk-CrER mice were crossed with lox-tdtomato mice and subsequently crossed with PLP1-
867 GFP/C57BL/6 mice. Timed pregnant Ntrk-CreER/lox-tdtomato/PLP-1GFP mice were weighed
868 and tamoxifen (TMXF) dose was calculated at 40ug/g body weight. 2mg/mL Tamoxifen (TMXF)
869 was stored in methanol at -80C and the final TMXF dose was diluted in 100uL corn oil. Diluted
870 TMXF was vortexed 45 minutes and dried in a Speedvac to remove methanol from the mixture,
871 leaving TMXF in corn-oil alone. Injections were carried out intraperitoneally at E12.5-E14.5 to
872 sustain expression and sacrifice at E14.5, E16.5, E18.5, P5. At time of sacrifice, embryonic
873 lumbar DRGs were dissected, and expression of tdtomato and PLP1-GFP was evaluated via
874 epifluorescence. DRGs were then drop fixed in 4% paraformaldehyde at 4°C overnight. The next
875 day, DRGs were washed 3x with 1XPBS and stored at 4°C in 1X PBS until staining. n=3+ embyros
876 total per age group.

877 **Quantification of DRG sensory neuron morphology frequency *in vivo*:**

878 *Immunofluorescence*: Fixed DRGs were permeabilized 2 hrs in 0.5% tritonX in PBS, and then
879 blocked in 5% Normal Donkey Serum (NDS)/0.5% tritonX in PBS 4-5hrs at RT. They were then
880 incubated in rbt anti-dsRed (Takara Cat#: 632496) primary antibody diluted 1:1000 in blocking
881 buffer at 4°C overnight, and washed the next day with 1X PBS. Next, DRGs were incubated with
882 dnky anti-rbt 546 (Thermofisher Cat#: A10040) secondary antibody diluted 1:500 in blocking
883 buffer for 3 hrs at RT. After staining, DRGs were stored at 4°C in 1XPBS, or gradually transferred
884 to methanol for tissue clearing.

885 *DRG Tissue Clearing:* Stained DRGs stored in PBS were gradually transferred to methanol with
886 10 minute incubations in the following concentrations: 25%, 50%, 75%, and 100%. After methanol
887 dehydration, each DRG was transferred to a slide and placed within a slide spacer (VWR
888 Cat#102096-614). BABB solution (1 Benzyl Alcohol:2 Benzyl Benzoate) was added to the DRG
889 and incubated 2-3min, after which it was replaced with fresh BABB, and steps were repeated until
890 the tissue was cleared. Then, a circular coverslip was mounted on top with tissue embedded in
891 BABB solution.

892 *Imaging:* Confocal images were acquired on the Nikon Ni-E confocal microscope, first at 20X to
893 visualize the entire DRG, and then at 40x to visualize individually labeled neurons. Images were
894 acquired at x resolution, 2.4 speed, 0.2-0.3um step, with 488 and 561 laser at 1.04 laser power,
895 36 gain, 0 offset. All cells labeled with tdtomato in the DRG were imaged from the top to bottom
896 of neuronal cell bodies.

897 *Analysis:* Images were blinded after acquisition, and NIS elements software was used to visualize
898 all cell morphology in 2D and/or 3D. All labeled cells were categorized into the following
899 morphologic groups: bipolar (elongated cell body, with an axon emanating from the two opposite
900 poles of the cell body with ~180° angle between), intermediate (round cell body with two axons
901 forming <180° angle between), and pseudounipolar (one axon stem emanating from cell body,
902 forming a T-Shape axon). Cells were considered apoptotic with condensed cell bodies small, and
903 no axons attached.

904 **Anatomic RealDRG iSN co-culture with rDRG glia:** Frozen RealDRG iSNs were purchased
905 from Anatomic (cat#: 1020). rDRG glia were dissected, plated, prepared, and cultured for one
906 week as described above. On Day 7, RealDRG iSNs were thawed in Chrono-Senso-MM
907 (Anatomic) and plated at 15k, 9k, or 5k cells/well either in rDRG glia co-culture in NCATS
908 Maturation Media. Lab-Tek™ II Chambered Coverglass were coated with 0.01% Poly-ornithine

solution for 1 hr at 37°C, washed with dPBS, and coated with iMatrix-511 (Reprocell cat#:NP892-021) 1:50 in dPBS 3 hrs at 37°C for iSN-only culture control. After 24 hrs, media was either changed to NCATS maturation Media + 1uM PD0332991. Cells were cultured for one week with 3x ½ media changes. On Day 14, cells were fixed for downstream IF and analysis as described in text. n=3 biological replicates at densities indicated.

Treatment of rDRG glia with neuronal maturation media: rDRG glia were dissected, plated, prepared, and cultured for one week as described above. On Day 7, glia were either treated with NCATS Maturation Media + CEPT and cultured at 37°C 5% CO_2 or maintained in Glia Media at 37°C 7.5% CO_2. After 24 hrs, NCATS Maturation Media + CEPT was changed to NCATS Maturation Media + 1uM PD0332991. Glia were matured for an additional week with ½ media changes 3x/week and fixed for downstream Immunofluorescence (IF) on Day 14. First, cells were fixed with 2% paraformaldehyde (PFA) (EMS cat#: 15710; 1:1 4% PFA to spent media) 10 minutes at room temperature (RT), and then in 4% PFA 20 minutes at RT. Cells were washed 3x in PBS and stored at 4°C for downstream experimentation. n=4 biological replicates.

Identification of Glial Subtypes in rDRG Glial cultures with IF:
Immunofluorescence: Fixed rDRG glial cultures treated with and without NCATS maturation medium were stained using the protocol described in text.

Imaging: All photomicrographs of cells cultured in Lab-Tek™ II Chambered Coverglass were collected on the Zeiss-980 airy-scan/confocal microscope. Images of all conditions were obtained at 20x with 1.3x zoom and bidirectional scanning in SRY-4 Airy-Scan configuration. Multiplex imaging was utilized with 405, 488, 561, lasers. All images were obtained in a z-stack with 0.35um step size. Systematic random sampling was utilized to image n=12-15 fields/biological replicate across 8-wells. All images were 2D airy-scan post processed in Zen Blue software. n=4 biological replicates.

Analysis: Particle analysis was carried out on glial marker channels. Threshold was manually set at brightest z-stack slice for each image, and percent area occupied by particles, average particle size, and average mean gray value were quantified for each image stack. Average values were calculated for each field, and averages were compared between treatment groups using the t-test function in excel where n=# of fields.

Quantification of rSG-iSN contacts in coculture with methanol fixation:

Immunofluorescence and Imaging: IF and imaging were performed as described in text. n=4 biological replicates

Analysis: Number of rSGs contacting individual iSNs was quantified using the CellCounter plugin in FIJI. Contact was defined as apposition between P75+, human Nuc. Cy3- processes with TUJ1+, Human Nuc. Cy3+ cell body and neurites. Number of rSGs were marked by individual DAPI+, Human Nuc. Cy3- nuclei and rSGs contacting iSNs without a nucleus present in the field were not counted. Contacts were counted per individual iSN, and each iSN was categorized into defined morphologic categories. Average number of total glial contacts/cell was compared using the t-test function and average number of total glial contacts/cell for each morphologic category was compared using Two-way ANOVA with Bonferroni post-hoc test in GraphPad Prism 10.

Supplemental Figure Legends:

Figure S1. Human iSNs differentiated in coculture with embryonic rodent DRG glia exhibit advanced morphology and physiology. A) Timeline for pseudounipolar transition was established *in vivo* in embryonic mice expressing tamoxifen induced NTRK2-tdtomato. Morphology frequencies from whole DRGs were quantified and categorized as apoptotic (light gray), bipolar (dark gray), intermediate (pink), or pseudounipolar (red). DRG NTRK2+ neurons became pseudounipolar between days E14.5 and E16.5, indicated by black arrow. E14.5 3-5 DRGs were quantified. B) Photomicrographs illustrating physical contact between satellite glia and DRG neurons during pseudounipolarization. Green= PLP1, Red= Ntrk-tdtomato. Scale= 20um. C-D) C. Representative photomicrographs of Anatomic RealDRGs terminally differentiated in coculture or alone with NCATS maturation media and Anatomic's proprietary media Senso-MM. D. Photomicrographs depicting transitional and pseudounipolar morphologies observed in cocultured Anatomic RealDRGs. TUJ1=Green, p75=Magenta, human nuclei = Red, DAPI=Cyan. RealDRGs alone were not stained for human nuclei. Scale=50um.E-H) Average number of active electrodes during weekly MEA recordings for fourbiological replicates. Cocultured iSNs=purple, iSNs alone= orange, Glia alone= green. Average >7 active electrodes were observed in both cocultured iSNs and iSNs alone at 7 weeks in replicate 1, 5 weeks in replicate 2, 6 weeks in replicate 3, and 5 weeks in replicate 4.

Figure S2. iNCPs terminally differentiated in co-culture more advanced in neuronal differentiation compared to iNCPs alone. A) Principal component analysis and B) Hierarchal Cluster analysis of RNA sequencing reads from cocultured iSN and iSNs alone.

Figure S3. Figure 3. Rodent DRG satellite glia (rSGs) are responsible for advanced maturation of iSNs. A) Representative photomicrographs of glial cultures maintained in glial base media for 1 week and treated with NCATS Maturation Media for 1 week (Maturation Media) or maintained in glial base media for 2 weeks (Glia Media). S100b= Green, FABP7/OCT6/P75= Red, DAPI= Cyan. Scale = 50 um. B) Representative photomicrographs of glial cultures maintained in glial base media for 1 week and treated with NCATS Maturation Media for 1 week (Maturation Media) or maintained in glial base media for 2 weeks (Glia Only), iSNs in coculture and iSNs alone. Glial Cultures: S100b=Magenta, MBP=Green, DAPI=Cyan, iSN cultures: TUJ1=Magenta, MBP=Green, DAPI= Cyan. No MBP signal was detected in any culture condition. Scale=50um. C) Schematic of glial culture protocol for RNA sequencing. D-E) Principal component analysis (D) and Hierarchal Cluster analysis (E) of RNA sequencing reads from rDRG glia in coculture, treated with maturation media, and maintained in base glia media. F) GO terms significantly downregulated in cocultured glia compared to glia treated with maturation media. P adj.<0.05.

Figure S4. Physical contact between rSGs and hiSNs is essential to pseudounipolarization. A) Total rSG-iSN contacts per individual iSN in coculture with methanol fixed glia or in normal coculture. T-test performed in GraphPad Prism 10, ****=p<0.0001. B) Average number of rSG-iSN contacts per individual iSN in coculture with methanol fixed glia or in normal coculture, partitioned by morphology of iSN. Two-way ANOVA with Bonferroni post-hoc test calculated in GraphPad Prism 10. P<0.05=*, P<0.01=**, P< 0.0001=****. C) PlexinA4 mRNA reads normalized to TUBB3 (TUJ1) mRNA reads in cocultured iSNs and iSNs

differentiated alone. D) GJA1 mRNA reads normalized to S100b mRNA reads in cocultured and maturation media treated glia.

Supplemental Index:

1. Document S1: Supplemental Methods and Figure Legends
2. Document S2: Supplemental Figures 1-4
3. Supplemental Tables Containing Large Datasets:
    a. S1: Cocultured iSN vs iSN Alone DGE
    b. S2: Cocultured iSN vs iSN Alone GO
    c. S3: NMM treated rDRG Glia vs rDRG Glia alone in base DGE
    d. S4: NMM treated rDRG Glia vs rDRG Glia alone in base GO
    e. S5: Cocultured rDRG Glia vs rDRG Glia Alone in base DGE
    f. S6: Cocultured rDRG Glia vs rDRG Glia alone in base GO
    g. S7: Cocultured rDRG Glia vs NMM treated rDRG Glia DGE
    h. S8: Cocultured rDRG Glia vs NMM Treated rDRG Glia GO

References:

1. Meltzer, S., Santiago, C., Sharma, N., and Ginty, D.D. (2021). The cellular and molecular basis of somatosensory neuron development. Neuron *109*, 3736–3757. https://doi.org/10.1016/j.neuron.2021.09.004.

2. Zenker, W., and Högl, E. (1976). The prebifurcation section of the axon of the rat spinal ganglion cell. Cell Tissue Res. *165*, 345–363. https://doi.org/10.1007/BF00222438.

3. Nascimento, A.I., Mar, F.M., and Sousa, M.M. (2018). The intriguing nature of dorsal root ganglion neurons: Linking structure with polarity and function. Prog. Neurobiol. *168*, 86–103. https://doi.org/10.1016/j.pneurobio.2018.05.002.

4. Sharma, N., Flaherty, K., Lezgiyeva, K., Wagner, D.E., Klein, A.M., and Ginty, D.D. (2020). The emergence of transcriptional identity in somatosensory neurons. Nature *577*, 392–398. https://doi.org/10.1038/s41586-019-1900-1.

5. Körner, J., and Lampert, A. (2022). Functional subgroups of rat and human sensory neurons: a systematic review of electrophysiological properties. Pflugers Arch. Eur. J. Physiol. *474*, 367–385. https://doi.org/10.1007/s00424-021-02656-6.

6. Saporta, M.A., Bacha, A., and Shy, M.E. (2022). Peripheral neuropathies. In Neurobiology of Brain Disorders: Biological Basis of Neurological and Psychiatric Disorders, Second Edition (Elsevier), pp. 165–184. https://doi.org/10.1016/B978-0-323-85654-6.00006-X.

7. Rowe, R.G., and Daley, G.Q. (2019). Induced pluripotent stem cells in disease modelling and drug discovery. Nat. Rev. Genet. *20*, 377–388. https://doi.org/10.1038/s41576-019-0100-z.

8. Nicholson, M.W., Ting, C.Y., Chan, D.Z.H., Cheng, Y.C., Lee, Y.C., Hsu, C.C., Huang, C.Y., and Hsieh, P.C.H. (2022). Utility of iPSC-Derived Cells for Disease Modeling, Drug Development, and Cell Therapy. Cells *11*. https://doi.org/10.3390/cells11111853.

9. Chambers, S.M., Qi, Y., Mica, Y., Lee, G., Zhang, X.J., Niu, L., Bilsland, J., Cao, L., Stevens, E., Whiting, P., et al. (2012). Combined small-molecule inhibition accelerates developmental timing and converts human pluripotent stem cells into nociceptors. Nat.

1041 Biotechnol. *30*, 715–720. https://doi.org/10.1038/nbt.2249.

1042 10. Guimarães, M.Z.P., De Vecchi, R., Vitória, G., Sochacki, J.K., Paulsen, B.S., Lima, I.,
1043 Rodrigues da Silva, F., da Costa, R.F.M., Castro, N.G., Breton, L., et al. (2018).
1044 Generation of iPSC-Derived Human Peripheral Sensory Neurons Releasing Substance P
1045 Elicited by TRPV1 Agonists. Front. Mol. Neurosci. *11*, 1–17.
1046 https://doi.org/10.3389/fnmol.2018.00277.

1047 11. Hulme, A.J., McArthur, J.R., Maksour, S., Miellet, S., Ooi, L., Adams, D.J., Finol-
1048 Urdaneta, R.K., and Dottori, M. (2020). Molecular and Functional Characterization of
1049 Neurogenin-2 Induced Human Sensory Neurons. Front. Cell. Neurosci. *14*, 1–18.
1050 https://doi.org/10.3389/fncel.2020.600895.

1051 12. Umehara, Y., Toyama, S., Tominaga, M., Matsuda, H., Takahashi, N., Kamata, Y.,
1052 Niyonsaba, F., Ogawa, H., and Takamori, K. (2020). Robust induction of neural crest
1053 cells to derive peripheral sensory neurons from human induced pluripotent stem cells.
1054 Sci. Rep. *10*, 1–10. https://doi.org/10.1038/s41598-020-60036-z.

1055 13. Nickolls, A.R., Lee, M.M., Espinoza, D.F., Szczot, M., Lam, R.M., Wang, Q., Beers, J.,
1056 Zou, J., Nguyen, M.Q., Solinski, H.J., et al. (2020). Transcriptional Programming of
1057 Human Mechanosensory Neuron Subtypes from Pluripotent Stem Cells. Cell Rep. *30*,
1058 932-946.e7. https://doi.org/10.1016/j.celrep.2019.12.062.

1059 14. Kalia, A.K., Rösseler, C., Granja-Vazquez, R., Ahmad, A., Pancrazio, J.J., Neureiter, A.,
1060 Zhang, M., Sauter, D., Vetter, I., Andersson, A., et al. (2023). How to differentiate induced
1061 pluripotent stem cells into sensory neurons for disease modelling: a comparison of two
1062 protocols. Res. Sq., 1–47. https://doi.org/10.21203/rs.3.rs-3127017/v1.

1063 15. Deng, T., Jovanovic, V.M., Tristan, C.A., Weber, C., Chu, P.H., Inman, J., Ryu, S.,
1064 Jethmalani, Y., Ferreira de Sousa, J., Ormanoglu, P., et al. (2023). Scalable generation of
1065 sensory neurons from human pluripotent stem cells. Stem Cell Reports *18*, 1030–1047.
1066 https://doi.org/10.1016/j.stemcr.2023.03.006.

1067 16. Clark, A.J., Kaller, M.S., Galino, J., Willison, H.J., Rinaldi, S., and Bennett, D.L.H. (2017).
1068 Co-cultures with stem cell-derived human sensory neurons reveal regulators of peripheral
1069 myelination. Brain *140*, 898–913. https://doi.org/10.1093/brain/awx012.

1070 17. McDermott, L.A., Weir, G.A., Themistocleous, A.C., Segerdahl, A.R., Blesneac, I.,
1071 Baskozos, G., Clark, A.J., Millar, V., Peck, L.J., Ebner, D., et al. (2019). Defining the
1072 Functional Role of Na V 1.7 in Human Nociception. Neuron *101*, 905-919.e8.
1073 https://doi.org/10.1016/j.neuron.2019.01.047.

1074 18. Odawara, A., Shibata, M., Ishibashi, Y., Nagafuku, N., Matsuda, N., and Suzuki, I. (2022).
1075 In Vitro Pain Assay Using Human iPSC-Derived Sensory Neurons and Microelectrode
1076 Array. Toxicol. Sci. *188*, 131–141. https://doi.org/10.1093/toxsci/kfac045.

1077 19. Wheeler, H.E., Wing, C., Delaney, S.M., Komatsu, M., and Dolan, M.E. (2015). Modeling
1078 chemotherapeutic neurotoxicity with human induced pluripotent stem cell-derived
1079 neuronal cells. PLoS One *10*, 1–16. https://doi.org/10.1371/journal.pone.0118020.

1080 20. Vojnits, K., Mahammad, S., Collins, T.J., and Bhatia, M. (2019). Chemotherapy-Induced
1081 Neuropathy and Drug Discovery Platform Using Human Sensory Neurons Converted
1082 Directly from Adult Peripheral Blood. Stem Cells Transl. Med. *8*, 1180–1191.
1083 https://doi.org/10.1002/sctm.19-0054.

1084 21. Xiong, C., Chua, K.C., Stage, T.B., Priotti, J., Kim, J., Altman-Merino, A., Chan, D., Saraf,
1085 K., Canato Ferracini, A., Fattahi, F., et al. (2020). Human Induced Pluripotent Stem Cell
1086 Derived Sensory Neurons are Sensitive to the Neurotoxic Effects of Paclitaxel. Clin.
1087 Transl. Sci., 1–14. https://doi.org/10.1111/cts.12912.

1088 22. Chen, Y., Saski, Y., DiAntonio, A., and Milbrandt, J. (2021). SARM1 is required in human
1089 derived sensory neurons for injury- induced and neurotoxic axon degeneration. Exp.
1090 Neurol. *339*. https://doi.org/10.4049/jimmunol.1801473.The.

1091 23. Schinke, C., Fernandez Vallone, V., Ivanov, A., Peng, Y., Körtvelyessy, P., Nolte, L.,
1092 Huehnchen, P., Beule, D., Stachelscheid, H., Boehmerle, W., et al. (2021). Modeling
1093 chemotherapy induced neurotoxicity with human induced pluripotent stem cell (iPSC) -
1094 derived sensory neurons. Neurobiol. Dis. *155*, 105391.
1095 https://doi.org/10.1016/j.nbd.2021.105391.

1096 24. Snavely, A.R., Heo, K., Petrova, V., Ho, T.S.Y., Huang, X., Hermawan, C., Kagan, R.,
1097 Deng, T., Singeç, I., Chen, L., et al. (2022). Bortezomib-induced neurotoxicity in human
1098 neurons is the consequence of nicotinamide adenine dinucleotide depletion. DMM Dis.
1099 Model. Mech. *15*. https://doi.org/10.1242/dmm.049358.

1100 25. Rana, P., Luerman, G., Hess, D., Rubitski, E., Adkins, K., and Somps, C. (2017).
1101 Utilization of iPSC-derived human neurons for high-throughput drug-induced peripheral
1102 neuropathy screening. Toxicol. Vitr. *45*, 111–118.
1103 https://doi.org/10.1016/j.tiv.2017.08.014.

1104 26. Jayakar, S., Shim, J., Jo, S., Bean, B.P., Singeç, I., and Woolf, C.J. (2021). Developing
1105 nociceptor-selective treatments for acute and chronic pain. Sci. Transl. Med. *13*.
1106 https://doi.org/10.1126/scitranslmed.abj9837.

1107 27. Matsuda, S., and Uehara, Y. (1984). Prenatal development of the rat dorsal root ganglia -
1108 A scanning electron-microscopic study. Cell Tissue Res. *235*, 13–18.
1109 https://doi.org/10.1007/BF00213717.

1110 28. Barber, R.P., and Vaughn, J.E. (1986). Differentiation of dorsal root ganglion cells with
1111 processes in their synaptic target zone of embryonic mouse spinal cord: a retrograde
1112 tracer study. J. Neurocytol. *15*, 207–218. https://doi.org/10.1007/BF01611657.

1113 29. Matsuda, S., Baluk, P., Shimizu, D., and Fujiwara, T. (1996). Dorsal root ganglion neuron
1114 development in chick and rat. Anat. Embryol. (Berl). *193*, 475–480.
1115 https://doi.org/10.1007/BF00185878.

1116 30. Kiss, F. (1932). SYMPATHETIC ELEMENTS IN THE CRANIAL AND SPINAL GANGLIA.
1117 J. Anat. *66*, 488–498.

1118 31. Fisher, B.Y.C., and Ranson, S.W. (1933). ON THE SO-CALLED SYMPATHETIC CELLS
1119 IN TI. J. Anat. *68*, 1–10.

1120 32. Truex, R.C. (1943). DEGENERATE VERSUS MULTIPOLAR NEURONS INT SENSORY
1121 GANGLIA. J. Nerv. Ment. Dis. *97*, 606.

1122 33. Bhatt, S., Diaz, R., and Trainor, P.A. (2013). Signals and switches in mammalian neural
1123 crest cell differentiation. Cold Spring Harb. Perspect. Biol. *5*.
1124 https://doi.org/10.1101/cshperspect.a008326.

1125 34. Mudge, A.W. (1984). Schwann cells induce morphological transformation of sensory
1126 neurones in vitro. Nature *309*, 367–369. https://doi.org/10.1038/309367a0.

1127 35. Takahashi, K., and Ninomiya, T. (1987). Morphological changes of dorsal root ganglion
1128 cells in the process-forming period. Prog. Neurobiol. *29*, 393–410.
1129 https://doi.org/10.1016/0301-0082(87)90020-7.

1130 36. Nascimento, A.I., Da Silva, T.F., Fernandes, E.C., Luz, L.L., Mar, F.M., Safronov, B. V.,
1131 and Sousa, M.M. (2022). Sensory neurons have an axon initial segment that initiates
1132 spontaneous activity in neuropathic pain. Brain *145*, 1632–1640.
1133 https://doi.org/10.1093/brain/awac078.

1134 37. Jones, I., Yelhekar, T.D., Wiberg, R., Kingham, P.J., Johansson, S., Wiberg, M., and
1135 Carlsson, L. (2018). Development and validation of an in vitro model system to study
1136 peripheral sensory neuron development and injury. Sci. Rep. *8*, 1–15.
1137 https://doi.org/10.1038/s41598-018-34280-3.

1138 38. Kim, H.S., Kim, J.Y., Song, C.L., Jeong, J.E., and Cho, Y.S. (2020). Directly induced
1139 human Schwann cell precursors as a valuable source of Schwann cells. Stem Cell Res.
1140 Ther. *11*, 257. https://doi.org/10.1186/s13287-020-01772-x.

1141 39. Pannese, E. (1969). Electron microscopical study on the development of the satellite cell
1142 sheath in spinal ganglia. J. Comp. Neurol. *135*, 381–421.
1143 https://doi.org/10.1002/cne.901350403.

1144 40. Matsuda, S., Kobayashi, N., Mominoki, K., Wakisaka, H., Mori, M., and Murakami, S.
1145 (2000). Morphological transformation of sensory ganglion neurons and satellite cells. Acta
1146 Anat. Nippon. *73*, 612–613.

1147 41. Wall, P.D., and Devor, M. (1983). Sensory afferent impulses originate from dorsal root
1148 ganglia as well as from the periphery in normal and nerve injured rats. Pain *17*, 321–339.
1149 https://doi.org/10.1016/0304-3959(83)90164-1.

1150 42. Amir, R., and Devor, M. (1997). Spike-evoked suppression and burst patterning in dorsal
1151 root ganglion neurons of the rat. J. Physiol. *501*, 183–196. https://doi.org/10.1111/j.1469-
1152 7793.1997.183bo.x.

1153 43. Amir, R., Michaelis, M., and Devor, M. (2002). Burst discharge in primary sensory
1154 neurons: Triggered by subthreshold oscillations, maintained by depolarizing
1155 afterpotentials. J. Neurosci. *22*, 1187–1198. https://doi.org/10.1523/jneurosci.22-03-
1156 01187.2002.

1157 44. Djouhri, L., Koutsikou, S., Fang, X., McMullan, S., and Lawson, S.N. (2006).
1158 Spontaneous pain, both neuropathic and inflammatory, is related to frequency of
1159 spontaneous firing in intact C-fiber nociceptors. J. Neurosci. *26*, 1281–1292.
1160 https://doi.org/10.1523/JNEUROSCI.3388-05.2006.

1161 45. Ma, C., and LaMotte, R.H. (2007). Multiple sites for generation of ectopic spontaneous
1162 activity in neurons of the chronically compressed dorsal root ganglion. J. Neurosci. *27*,
1163 14059–14068. https://doi.org/10.1523/JNEUROSCI.3699-07.2007.

1164 46. Liu, C.N., Wall, P.D., Ben-Dor, E., Michaelis, M., Amir, R., and Devor, M. (2000). Tactile
1165 allodynia in the absence of C-fiber activation: Altered firing properties of DRG neurons
1166 following spinal nerve injury. Pain *85*, 503–521. https://doi.org/10.1016/S0304-
1167 3959(00)00251-7.

1168 47. Xie, W., Strong, J.A., Kim, D., Shahrestani, S., and Zhang, J.M. (2012). Bursting activity
1169 in myelinated sensory neurons plays a key role in pain behavior induced by localized

1170 inflammation of the rat sensory anglion. Neuroscience *206*, 212–223.
1171 https://doi.org/10.1016/j.neuroscience.2012.01.007.Bursting.

1172 48. Zheng, Q., Xie, W., Lückemeyer, D.D., Lay, M., Wang, X.W., Dong, X., Limjunyawong,
1173 N., Ye, Y., Zhou, F.Q., Strong, J.A., et al. (2022). Synchronized cluster firing, a distinct
1174 form of sensory neuron activation, drives spontaneous pain. Neuron *110*, 209-220.e6.
1175 https://doi.org/10.1016/j.neuron.2021.10.019.

1176 49. North, R.Y., Li, Y., Ray, P., Rhines, L.D., Tatsui, C.E., Rao, G., Johansson, C.A., Zhang,
1177 H., Kim, Y.H., Zhang, B., et al. (2019). Electrophysiological and transcriptomic correlates
1178 of neuropathic pain in human dorsal root ganglion neurons. Brain *142*, 1215–1226.
1179 https://doi.org/10.1093/brain/awz063.

1180 50. Zhang, X., Chen, Y., Wang, C., and Huang, L.Y.M. (2007). Neuronal somatic ATP
1181 release triggers neuron-satellite glial cell communication in dorsal root ganglia. Proc. Natl.
1182 Acad. Sci. U. S. A. *104*, 9864–9869. https://doi.org/10.1073/pnas.0611048104.

1183 51. Rozanski, G.M., Li, Q., and Stanley, E.F. (2013). Transglial transmission at the dorsal
1184 root ganglion sandwich synapse: Glial cell to postsynaptic neuron communication. Eur. J.
1185 Neurosci. *37*, 1221–1228. https://doi.org/10.1111/ejn.12132.

1186 52. Huang, L.Y.M., Gu, Y., and Chen, Y. (2013). Communication between neuronal somata
1187 and satellite glial cells in sensory ganglia. Glia *61*, 1571–1581.
1188 https://doi.org/10.1002/glia.22541.

1189 53. Kim, Y.S., Anderson, M., Park, K., Zheng, Q., Agarwal, A., Gong, C., Saijilafu, Young,
1190 L.A., He, S., LaVinka, P.C., et al. (2016). Coupled Activation of Primary Sensory Neurons
1191 Contributes to Chronic Pain. Neuron *91*, 1085–1096.
1192 https://doi.org/10.1016/j.neuron.2016.07.044.

1193 54. Newberry, K., Wang, S., Hoque, N., Kiss, L., Ahlijanian, M.K., Herrington, J., and Graef,
1194 J.D. (2016). Development of a spontaneously active dorsal root ganglia assay using
1195 multiwell multielectrode arrays. J. Neurophysiol. *115*, 3217–3228.
1196 https://doi.org/10.1152/jn.01122.2015.

1197 55. Black, B.J., Atmaramani, R., Kumaraju, R., Plagens, S., Romero-Ortega, M., Dussor, G.,
1198 Price, T.J., Campbell, Z.T., and Pancrazio, J.J. (2018). Adult mouse sensory neurons on
1199 microelectrode arrays exhibit increased spontaneous and stimulus-evoked activity in the
1200 presence of interleukin-6. J. Neurophysiol. *120*, 1374–1385.
1201 https://doi.org/10.1152/jn.00158.2018.

1202 56. Hiranuma, M., Okuda, Y., Fujii, Y., Richard, J.P., and Watanabe, T. (2024).
1203 Characterization of human iPSC-derived sensory neurons and their functional
1204 assessment using multi electrode array. Sci. Rep. *14*, 1–8.
1205 https://doi.org/10.1038/s41598-024-55602-8.

1206 57. Frith, T.J.R., Granata, I., Wind, M., Stout, E., Thompson, O., Neumann, K., Stavish, D.,
1207 Heath, P.R., Ortmann, D., Hackland, J.O.S., et al. (2018). Human axial progenitors
1208 generate trunk neural crest cells in vitro. Elife *7*, 1–27.
1209 https://doi.org/10.7554/eLife.35786.

1210 58. Libby, A.R.G., Joy, D.A., Elder, N.H., Bulger, E.A., Krakora, M.Z., Gaylord, E.A.,
1211 Mendoza-Camacho, F., Butts, J.C., and McDevitt, T.C. (2021). Axial elongation of
1212 caudalized human organoids mimics aspects of neural tube development. Dev. *148*.
1213 https://doi.org/10.1242/dev.198275.

1214 59. Kee, Y., and Bronner-Fraser, M. (2005). To proliferate or to die: Role of Id3 in cell cycle
1215 progression and survival of neural crest progenitors. Genes Dev. *19*, 744–755.
1216 https://doi.org/10.1101/gad.1257405.

1217 60. Heng, Y.H.E., McLeay, R.C., Harvey, T.J., Smith, A.G., Barry, G., Cato, K., Plachez, C.,
1218 Little, E., Mason, S., Dixon, C., et al. (2014). NFIX regulates neural progenitor cell
1219 differentiation during hippocampal morphogenesis. Cereb. Cortex *24*, 261–279.
1220 https://doi.org/10.1093/cercor/bhs307.

1221 61. Martynoga, B., Mateo, J.L., Zhou, B., Andersen, J., Achimastou, A., Urbán, N., van den
1222 Berg, D., Georgopoulou, D., Hadjur, S., Wittbrodt, J., et al. (2013). Epigenomic enhancer
1223 annotation reveals a key role for NFIX in neural stem cell quiescence. Genes Dev. *27*,
1224 1769–1786. https://doi.org/10.1101/gad.216804.113.

1225 62. Harris, L., Genovesi, L.A., Gronostajski, R.M., Wainwright, B.J., and Piper, M. (2015).
1226 Nuclear factor one transcription factors: Divergent functions in developmental versus
1227 adult stem cell populations. Dev. Dyn. *244*, 227–238. https://doi.org/10.1002/dvdy.24182.

1228 63. Zalucki, O., Harris, L., Harvey, T.J., Harkins, D., Widagdo, J., Oishi, S., Matuzelski, E.,
1229 Ling Hilary Yong, X., Schmidt, H., Anggono, V., et al. (2019). NFIX-mediated inhibition of
1230 neuroblast branching regulates migration within the adult mouse ventricular-
1231 subventricular zone. Cereb. Cortex *29*, 3590–3604.
1232 https://doi.org/10.1093/cercor/bhy233.

1233 64. He, J.C., Neves, S.R., Jordan, J.D., and Iyengar, R. (2006). Role of the Go/i signaling
1234 network in the regulation of neurite outgrowth. Can. J. Physiol. Pharmacol. *84*, 687–694.
1235 https://doi.org/10.1139/Y06-025.

1236 65. Bromberg, K., Iyengar, R., and He, J. (2011). Regulation of neurite outgrowth by Gi/o
1237 signaling pathways. Front Biosci *13*, 4544–4557.

1238 66. Wolf, D., Hofbrucker-MacKenzie, S.A., Izadi, M., Seemann, E., Steiniger, F., Schwintzer,
1239 L., Koch, D., Kessels, M.M., and Qualmann, B. (2019). Ankyrin repeat-containing N-Ank
1240 proteins shape cellular membranes. Nat. Cell Biol. *21*, 1191–1205.
1241 https://doi.org/10.1038/s41556-019-0381-7.

1242 67. Kim, S.J., Woo, Y., Kim, H.J., Goo, B.S., Nhung, T.T.M., Lee, S.A., Suh, B.K., Mun, D.J.,
1243 Kim, J.H., and Park, S.K. (2022). Retinoic acid-induced protein 14 controls dendritic spine
1244 dynamics associated with depressive-like behaviors. Elife *11*, 1–30.
1245 https://doi.org/10.7554/eLife.77755.

1246 68. Christiansen, J.H., Coles, E.G., and Wilkinson, D.G. (2000). Molecular control of neural
1247 crest formation, migration and differentiation. Curr. Opin. Cell Biol. *12*, 719–724.
1248 https://doi.org/10.1016/S0955-0674(00)00158-7.

1249 69. Lian, Y., Wu, C., Liu, L., and Li, X. (2024). Prediction of cell-cell communication patterns
1250 of dorsal root ganglion cells: single-cell RNA sequencing data analysis. Neural Regen.
1251 Res. *19*, 1367–1374. https://doi.org/10.4103/1673-5374.384067.

1252 70. Bennett, D.L., Clark, X.A.J., Huang, J., Waxman, S.G., and Dib-Hajj, S.D. (2019). The
1253 role of voltage-gated sodium channels in pain signaling. Physiol. Rev. *99*, 1079–1151.
1254 https://doi.org/10.1152/physrev.00052.2017.

1255 71. Jarvis, M.F., Honore, P., Shieh, C.C., Chapman, M., Joshi, S., Zhang, X.F., Kort, M.,
1256 Carroll, W., Marron, B., Atkinson, R., et al. (2007). A-803467, a potent and selective

1257 Nav1.8 sodium channel blocker, attenuates neuropathic and inflammatory pain in the rat.
1258 Proc. Natl. Acad. Sci. U. S. A. *104*, 8520–8525.
1259 https://doi.org/10.1073/pnas.0611364104.

1260 72. Jones, J., Correll, D.J., Lechner, S.M., Jazic, I., Miao, X., Shaw, D., Simard, C., Osteen,
1261 J.D., Hare, B., Beaton, A., et al. (2023). Selective Inhibition of Na V 1.8 with VX-548 for
1262 Acute Pain . N. Engl. J. Med. *389*, 393–405. https://doi.org/10.1056/nejmoa2209870.

1263 73. Jo, S., Zhang, H.X.B., and Bean, B.P. (2023). Use-Dependent Relief of Inhibition of
1264 Nav1.8 Channels by A-887826. Mol. Pharmacol. *103*, 221–229.
1265 https://doi.org/10.1124/molpharm.122.000593.

1266 74. Haberberger, R., Scholz, A., Kummer, W., and Kress, M. (2000). M2-receptor subtype
1267 does not mediate muscarine-induced increases in [Ca2+](i) in nociceptive neurons of rat
1268 dorsal root ganglia. J. Neurophysiol. *84*, 1934–1941.
1269 https://doi.org/10.1152/jn.2000.84.4.1934.

1270 75. Tata, A.M., Vilaró, M.T., and Mengod, G. (2000). Muscarinic receptor subtypes
1271 expression in rat and chick dorsal root ganglia. Mol. Brain Res. *82*, 1–10.
1272 https://doi.org/10.1016/S0169-328X(00)00165-0.

1273 76. De Angelis, F., Marinelli, S., Fioretti, B., Catacuzzeno, L., Franciolini, F., Pavone, F., and
1274 Tata, A.M. (2014). M2 receptors exert analgesic action on DRG sensory neurons by
1275 negatively modulating VR1 activity. J. Cell. Physiol. *229*, 783–790.
1276 https://doi.org/10.1002/jcp.24499.

1277 77. Xian, X.C., and Nicol, G.D. (2007). Manipulation of the potassium channel Kv1.1 and its
1278 effect on neuronal excitability in rat sensory neurons. J. Neurophysiol. *98*, 2683–2692.
1279 https://doi.org/10.1152/jn.00437.2007.

1280 78. Wang, J.J., and Li, Y. (2016). KCNQ potassium channels in sensory system and neural
1281 circuits. Acta Pharmacol. Sin. *37*, 25–33. https://doi.org/10.1038/aps.2015.131.

1282 79. Smith, P.A. (2020). K+ Channels in Primary Afferents and Their Role in Nerve Injury-
1283 Induced Pain. Front. Cell. Neurosci. *14*. https://doi.org/10.3389/fncel.2020.566418.

1284 80. Bhattacharya, D., Rothstein, M., Azambuja, A.P., and Simoes-Costa, M. (2018). Control
1285 of neural crest multipotency by wnt signaling and the Lin28/let-7 axis. Elife *7*, 1–24.
1286 https://doi.org/10.7554/eLife.40556.

1287 81. Shoval, I., and Kalcheim, C. (2012). Antagonistic activities of Rho and Rac GTPases
1288 underlie the transition from neural crest delamination to migration. Dev. Dyn. *241*, 1155–
1289 1168. https://doi.org/10.1002/dvdy.23799.

1290 82. Kurisaki, T., Masuda, A., Osumi, N., Nabeshima, Y.I., and Fujisawa-Sehara, A. (1998).
1291 Spatially- and temporally-restricted expression of meltrin α (ADAM12) and β (ADAM19) in
1292 mouse embryo. Mech. Dev. *73*, 211–215. https://doi.org/10.1016/S0925-4773(98)00043-
1293 4.

1294 83. Samad, T.A., Rebbapragada, A., Bell, E., Zhang, Y., Sidis, Y., Jeong, S.J., Campagna,
1295 J.A., Perusini, S., Fabrizio, D.A., Schneyer, A.L., et al. (2005). DRAGON, a bone
1296 morphogenetic protein co-receptor. J. Biol. Chem. *280*, 14122–14129.
1297 https://doi.org/10.1074/jbc.M410034200.

1298 84. Zorick, T.S., Syroid, D.E., Arroyo, E., Scherer, S.S., and Lemke, G. (1996). The
1299 transcription factors SCIP and Krox-20 mark distinct stages and cell fates in Schwann cell

1300 differentiation. Mol. Cell. Neurosci. *8*, 129–145. https://doi.org/10.1006/mcne.1996.0052.

1301 85. Wu, J., Peng, D., Voehler, M., Sanders, C., and Li, J. (2013). Structure and Expression of
1302 a Novel Compact Myelin Protein - Small VCP-Interacting Protein (SVIP). Biochem.
1303 Biophys. Res. Commun. *440*. https://doi.org/10.1016/j.bbrc.2013.09.056.Structure.

1304 86. Kastriti, M.E., Faure, L., Von Ahsen, D., Bouderlique, T.G., Boström, J., Solovieva, T.,
1305 Jackson, C., Bronner, M., Meijer, D., Hadjab, S., et al. (2022). Schwann cell precursors
1306 represent a neural crest-like state with biased multipotency. EMBO J. *41*, 1–28.
1307 https://doi.org/10.15252/embj.2021108780.

1308 87. Frank, M. (2000). MAL, a proteolipid in glycosphingolipid enriched domains: Functional
1309 implications in myelin and beyond. Prog. Neurobiol. *60*, 531–544.
1310 https://doi.org/10.1016/S0301-0082(99)00039-8.

1311 88. Tasdemir-Yilmaz, O.E., Druckenbrod, N.R., Olukoya, O.O., Dong, W., Yung, A.R.,
1312 Bastille, I., Pazyra-Murphy, M.F., Sitko, A.A., Hale, E.B., Vigneau, S., et al. (2021).
1313 Diversity of developing peripheral glia revealed by single-cell RNA sequencing. Dev. Cell
1314 *56*, 2516-2535.e8. https://doi.org/10.1016/j.devcel.2021.08.005.

1315 89. Avraham, O., Chamessian, A., Feng, R., Yang, L., Halevi, A.E., Moore, A.M., Gereau,
1316 R.W., and Cavalli, V. (2022). Profiling the molecular signature of satellite glial cells at the
1317 single cell level reveals high similarities between rodents and humans. Pain *163*, 2348–
1318 2364. https://doi.org/10.1097/j.pain.0000000000002628.

1319 90. Mapps, A.A., Thomsen, M.B., Boehm, E., Zhao, H., Hattar, S., and Kuruvilla, R. (2022).
1320 Diversity of satellite glia in sympathetic and sensory ganglia. Cell Rep. *38*.
1321 https://doi.org/10.1016/j.celrep.2022.110328.

1322 91. Cinquina, V., Calvigioni, D., Piscitelli, F., Keimpema, E., Di Marzo, V., Verkhratsky, A.,
1323 and Harkany, T. (2023). Astrocytes modulate neuronal development by S100A6
1324 signaling. bioRxiv.

1325 92. O'Malley, A.M., Shanley, D.K., Kelly, A.T., and Barry, D.S. (2014). Towards an
1326 understanding of semaphorin signalling in the spinal cord. Gene *553*, 69–74.
1327 https://doi.org/10.1016/j.gene.2014.10.005.

1328 93. Fujii, S., Yoshida, S., Inagaki, E., Hatou, S., Tsubota, K., Takahashi, M., Shimmura, S.,
1329 and Sugita, S. (2019). Immunological Properties of Neural Crest Cells Derived from
1330 Human Induced Pluripotent Stem Cells. Stem Cells Dev. *28*, 28–43.
1331 https://doi.org/10.1089/scd.2018.0058.

1332 94. Mehler, V.J., Burns, C.J., Stauss, H., Francis, R.J., and Moore, M.L. (2020). Human
1333 iPSC-Derived Neural Crest Stem Cells Exhibit Low Immunogenicity. Mol. Ther. Methods
1334 Clin. Dev. *16*, 161–171. https://doi.org/10.1016/j.omtm.2019.12.015.

1335 95. Li, C., Wang, S., Chen, Y., and Zhang, X. (2018). Somatosensory Neuron Typing with
1336 High-Coverage Single-Cell RNA Sequencing and Functional Analysis. Neurosci. Bull. *34*,
1337 200–207. https://doi.org/10.1007/s12264-017-0147-9.

1338 96. Ray, P., Torck, A., Quigley, L., Wangzhou, A., Neiman, M., Rao, C., Lam, T., Kim, J.Y.,
1339 Kim, T.H., Zhang, M.Q., et al. (2018). Comparative transcriptome profiling of the human
1340 and mouse dorsal root ganglia: An RNA-seq-based resource for pain and sensory
1341 neuroscience research https://doi.org/10.1097/j.pain.0000000000001217.

1342 97. Fernández-Montoya, J., Avendaño, C., and Negredo, P. (2018). The glutamatergic
1343 system in primary somatosensory neurons and its involvement in sensory input-
1344 dependent plasticity. Int. J. Mol. Sci. *19*. https://doi.org/10.3390/ijms19010069.

1345 98. Nawaz, M.S., Giarda, E., Bedogni, F., Montanara, P. La, Ricciardi, S., Ciceri, D., Alberio,
1346 T., Landsberger, N., Rusconi, L., and Kilstrup-Nielsen, C. (2016). CDKL5 and shootin1
1347 interact and concur in regulating neuronal polarization. PLoS One *11*.
1348 https://doi.org/10.1371/journal.pone.0148634.

1349 99. Bushlin, I., Petralia, R.S., Wu, F., Harel, A., Mughal, M.R., Mattson, M.P., and Yao, P.J.
1350 (2008). Clathrin assembly protein AP180 and CALM differentially control axogenesis and
1351 dendrite outgrowth in embryonic hippocampal neurons. J. Neurosci. *28*, 10257–10271.
1352 https://doi.org/10.1523/JNEUROSCI.2471-08.2008.

1353 100. Montanara, P. La, Hervera, A., Baltussen, L.L., Hutson, T.H., Palmisano, I., De Virgiliis,
1354 F., Kong, G., Chadwick, J., Gao, Y., Bartus, K., et al. (2020). Cyclin-dependent-like
1355 kinase 5 is required for pain signaling in human sensory neurons and mouse models. Sci.
1356 Transl. Med. *12*, 1–36. https://doi.org/10.1126/SCITRANSLMED.AAX4846.

1357 101. Hori, K., and Hoshino, M. (2017). Neuronal migration and AUTS2 syndrome. Brain Sci. *7*.
1358 https://doi.org/10.3390/brainsci7050054.

1359 102. Lentz, S.I., Miner, J.H., Sanes, J.R., and Snider, W.D. (1997). Distribution of the ten
1360 known laminin chains in the pathways and targets of developing sensory axons. J. Comp.
1361 Neurol. *378*, 547–561. https://doi.org/10.1002/(SICI)1096-
1362 9861(19970224)378:4<547::AID-CNE9>3.0.CO;2-2.

1363 103. Liu, C., Lin, C., Whitaker, D.T., Bakeri, H., Bulgakov, O. V., Liu, P., Lei, J., Dong, L., Li,
1364 T., and Swaroop, A. (2013). Prickle1 is expressed in distinct cell populations of the
1365 central nervous system and contributes to neuronal morphogenesis. Hum. Mol. Genet.
1366 *22*, 2234–2246. https://doi.org/10.1093/hmg/ddt075.

1367 104. Agrawal, M., and Welshhans, K. (2021). Local Translation Across Neural Development: A
1368 Focus on Radial Glial Cells, Axons, and Synaptogenesis. Front. Mol. Neurosci. *14*, 1–18.
1369 https://doi.org/10.3389/fnmol.2021.717170.

1370 105. Kumar, S., Chakraborty, S., Barbosa, C., Brustovetsky, T., Brustovetsky, N., and
1371 Obukhov, A.G. (2012). Mechanisms controlling neurite outgrowth in a
1372 pheochromocytoma cell line: The role of TRPC channels. J. Cell. Physiol. *227*, 1408–
1373 1419. https://doi.org/10.1002/jcp.22855.

1374 106. Joseph, D.J., Williams, D.J., and MacDermott, A.B. (2011). Modulation of neurite
1375 outgrowth by activation of calcium-permeable kainate receptors expressed by rat
1376 nociceptive-like dorsal root ganglion neurons. Dev. Neurobiol. *71*, 818–835.
1377 https://doi.org/10.1002/dneu.20906.

1378 107. Bakos, J., Bacova, Z., Grant, S.G., Castejon, A.M., and Ostatnikova, D. (2015). Are
1379 Molecules Involved in Neuritogenesis and Axon Guidance Related to Autism
1380 Pathogenesis? NeuroMolecular Med. *17*, 297–304. https://doi.org/10.1007/s12017-015-
1381 8357-7.

1382 108. Wang, T., Liu, Y., Xu, X.H., Deng, C.Y., Wu, K.Y., Zhu, J., Fu, X.Q., He, M., and Luo,
1383 Z.G. (2011). Lgl1 activation of Rab10 Promotes axonal membrane trafficking underlying
1384 neuronal polarization. Dev. Cell *21*, 431–444.
1385 https://doi.org/10.1016/j.devcel.2011.07.007.

1386 109. Stegeman, S., Jolly, L.A., Premarathne, S., Gecz, J., Richards, L.J., Mackay-Sim, A., and
1387 Wood, S.A. (2013). Loss of Usp9x Disrupts Cortical Architecture, Hippocampal
1388 Development and TGFβ-Mediated Axonogenesis. PLoS One *8*, 1–12.
1389 https://doi.org/10.1371/journal.pone.0068287.

1390 110. Luo, X., Salgueiro, Y., Beckerman, S., Lemmon, V., Tsoulfas, P., and Park, K. (2013).
1391 Three-dimensional evaluation of retinal ganglion cell axon regeneration and pathfinding in
1392 whole mouse tissue after injury. Exp. Neurol. *247*, 653–662.
1393 https://doi.org/10.1016/j.expneurol.2013.03.001.Three-dimensional.

1394 111. Mutalik, S.P., and Gupton, S.L. (2021). Glycosylation in axonal guidance. Int. J. Mol. Sci.
1395 *22*. https://doi.org/10.3390/ijms22105143.

1396 112. Kuo, T.Y., Hong, C.J., and Hsueh, Y.P. (2009). Bcl11A/CTIP1 regulates expression of
1397 DCC and MAP1b in control of axon branching and dendrite outgrowth. Mol. Cell.
1398 Neurosci. *42*, 195–207. https://doi.org/10.1016/j.mcn.2009.07.006.

1399 113. Hall, A., and Lalli, G. (2010). Rho and Ras GTPases in Axon Growth, Guidance, and
1400 Branching. Cold Spring Harb. Perspect. Biol., 1–18.

1401 114. Luxey, M., Jungas, T., Laussu, J., Audouard, C., Garces, A., and Davy, A. (2013). Eph:
1402 Ephrin-B1 Forward Signaling Controls Fasciculation Of Sensory And Motor Axons. Dev.
1403 Biol. *383*, 264–274. https://doi.org/10.1016/j.ydbio.2013.09.010.

1404 115. Laumonnerie, C., Da Silva, R. V., Kania, A., and Wilson, S.I. (2014). Netrin 1 and Dcc
1405 signalling are required for confinement of central axons within the central nervous
1406 system. Dev. *141*, 594–603. https://doi.org/10.1242/dev.099606.

1407 116. Balmer, C.W., and Lamantia, A.S. (2004). Loss of Gli3 and Shh Function Disrupts
1408 Olfactory Axon Trajectories. J. Comp. Neurol. *472*, 292–307.
1409 https://doi.org/10.1002/cne.20053.

1410 117. Butler, S.J., and Tear, G. (2007). Getting axons onto the right path: The role of
1411 transcription factors in axon guidance. Development *134*, 439–448.
1412 https://doi.org/10.1242/dev.02762.

1413 118. Zhao, L.L., Zhang, T., Huang, W.X., Guo, T.T., and Gu, X.S. (2023). Transcriptional
1414 regulatory network during axonal regeneration of dorsal root ganglion neurons: laser-
1415 capture microdissection and deep sequencing. Neural Regen. Res. *18*, 2056–2066.
1416 https://doi.org/10.4103/1673-5374.366494.

1417 119. Shamay-Ramot, A., Khermesh, K., Porath, H.T., Barak, M., Pinto, Y., Wachtel, C.,
1418 Zilberberg, A., Lerer-Goldshtein, T., Efroni, S., Levanon, E.Y., et al. (2015). Fmrp
1419 Interacts with Adar and Regulates RNA Editing, Synaptic Density and Locomotor Activity
1420 in Zebrafish. PLoS Genet. *11*, 1–28. https://doi.org/10.1371/journal.pgen.1005702.

1421 120. John, A., Brylka, H., Wiegreffe, C., Simon, R., Liu, P., Jüttner, R., Bryan Crenshaw, I.,
1422 Luyten, F.P., Jenkins, N.A., Copeland, N.G., et al. (2012). Bcl11a is required for neuronal
1423 morphogenesis and sensory circuit formation in dorsal spinal cord development.
1424 Development *139*, 1831–1841. https://doi.org/10.1242/dev.072850.

1425 121. Wang, S.H.J., Celic, I., Choi, S.Y., Riccomagno, M., Wang, Q., Sun, L.O., Mitchell, S.P.,
1426 Vasioukhin, V., Huganir, R.L., and Kolodkin, A.L. (2014). Dlg5 regulates dendritic spine
1427 formation and synaptogenesis by controlling subcellular N-cadherin localization. J.
1428 Neurosci. *34*, 12745–12761. https://doi.org/10.1523/JNEUROSCI.1280-14.2014.

1429 122. Noseda, R., Belin, S., Piguet, F., Vaccari, I., Scarlino, S., Brambilla, P., Boneschi, F.M.,
1430 Feltri, M.L., Wrabetz, L., Quattrini, A., et al. (2013). DDIT4/REDD1/RTP801 is a novel
1431 negative regulator of schwann cell myelination. J. Neurosci. *33*, 15295–15305.
1432 https://doi.org/10.1523/JNEUROSCI.2408-13.2013.

1433 123. Gunsch, G., Paradie, E., and Townsend, K.L. (2023). Peripheral nervous system glia in
1434 support of metabolic tissue functions. Trends Endocrinol. Metab. *34*, 622–639.
1435 https://doi.org/10.1016/j.tem.2023.07.004.

1436 124. Birren, S.J., Goodrich, L. V., and Segal, R.A. (2024). Satellite Glial Cells: No Longer the
1437 Most Overlooked Glia. Cold Spring Harb. Perspect. Biol., a041367.
1438 https://doi.org/10.1101/cshperspect.a041367.

1439 125. Narayanan, S.P., Flores, A.I., Wang, F., and Macklin, W.B. (2009). Akt signals through
1440 the mammalian target of rapamycin pathway to regulate CNS myelination. J. Neurosci.
1441 *29*, 6860–6870. https://doi.org/10.1523/JNEUROSCI.0232-09.2009.

1442 126. Lebeau, P., Al-Hashimi, A., Sood, S., Lhoták, Š., Yu, P., Gyulay, G., Paré, G., Wayne
1443 Chen, S.R., Trigatti, B., Prat, A., et al. (2017). Endoplasmic reticulum stress and Ca2+
1444 depletion differentially modulate the sterol regulatory protein PCSK9 to control lipid
1445 metabolism. J. Biol. Chem. *292*, 1510–1523. https://doi.org/10.1074/jbc.M116.744235.

1446 127. Bartz, F., Kern, L., Erz, D., Zhu, M., Gilbert, D., Meinhof, T., Wirkner, U., Erfle, H.,
1447 Muckenthaler, M., Pepperkok, R., et al. (2009). Identification of Cholesterol-Regulating
1448 Genes by Targeted RNAi Screening. Cell Metab. *10*, 63–75.
1449 https://doi.org/10.1016/j.cmet.2009.05.009.

1450 128. Elbaz, B., Yang, L., Vardy, M., Isaac, S., Rader, B.L., Kawaguchi, R., Traka, M., Woolf,
1451 C.J., Renthal, W., and Popko, B. (2022). Sensory neurons display cell-type-specific
1452 vulnerability to loss of neuron-glia interactions. Cell Rep. *40*, 111130.
1453 https://doi.org/10.1016/j.celrep.2022.111130.

1454 129. Meriau, P., Weill, L., Puccio, H., and Agulhon, C. (2024). Frataxin deficiency in
1455 proprioceptive neurons is causal to inflammatory and glial responses in dorsal root
1456 ganglia.

1457 130. Krishnan, A., Bhavanam, S., and Zochodne, D. (2018). An intimate role for adult dorsal
1458 root ganglia resident cycling cells in the generation of local macrophages and satellite
1459 glial cells. J. Neuropathol. Exp. Neurol. *77*, 929–941. https://doi.org/10.1093/jnen/nly072.

1460 131. Hall, B.E., Macdonald, E., Cassidy, M., Yun, S., Sapio, M.R., Ray, P., Doty, M., Nara, P.,
1461 Burton, M.D., Shiers, S., et al. (2022). Transcriptomic analysis of human sensory neurons
1462 in painful diabetic neuropathy reveals inflammation and neuronal loss. Sci. Rep. *12*, 1–
1463 16. https://doi.org/10.1038/s41598-022-08100-8.

1464 132. Mocciaro, A., Berdougo, E., Zeng, K., Black, E., Vagnarelli, P., Earnshaw, W., Gillespie,
1465 D., Jallepalli, P., and Schiebel, E. (2010). Vertebrate cells genetically deficient for
1466 Cdc14A or Cdc14B retain DNA damage checkpoint proficiency but are impaired in DNA
1467 repair. J. Cell Biol. *189*, 631–639. https://doi.org/10.1083/jcb.200910057.

1468 133. Park, B.S., Jo, H.W., and Jung, J. (2015). Expression profile of aminoacyl-tRNA
1469 synthetases in dorsal root ganglion neurons after peripheral nerve injury. J. Mol. Histol.
1470 *46*, 115–122. https://doi.org/10.1007/s10735-014-9601-4.

1471 134. Ninomiya, K., Ohta, K., Yamashita, K., Mizuno, K., and Ohashi, K. (2021). PLEKHG4B

1472 enables actin cytoskeletal remodeling during epithelial cell-cell junction formation. J. Cell
1473 Sci. *134*. https://doi.org/10.1242/jcs.249078.

1474 135. Repetto, D., Camera, P., Melani, R., Morello, N., Russo, I., Calcagno, E., Tomasoni, R.,
1475 Bianchi, F., Berto, G., Giustetto, M., et al. (2014). p140Cap regulates memory and
1476 synaptic plasticity through src-mediated and citron-N-mediated actin reorganization. J.
1477 Neurosci. *34*, 1542–1553. https://doi.org/10.1523/JNEUROSCI.2341-13.2014.

1478 136. Aruga, J., and Mikoshiba, K. (2003). Identification and characterization of Slitrk, a novel
1479 neuronal transmembrane protein family controlling neurite outgrowth. Mol. Cell. Neurosci.
1480 *24*, 117–129. https://doi.org/10.1016/S1044-7431(03)00129-5.

1481 137. Chu, Y., Jia, S., Xu, K., Liu, Q., Mai, L., Liu, J., Fan, W., and Huang, F. (2023). Single-cell
1482 transcriptomic profile of satellite glial cells in trigeminal ganglion. Front. Mol. Neurosci. *16*,
1483 1–16. https://doi.org/10.3389/fnmol.2023.1117065.

1484 138. Luo, Y., Xu, W., Chen, H., Warburton, D., Dong, R., Qian, B., Selman, M., Gualdie, J.,
1485 Kolb, M., and Shi, W. (2015). A novel profibrotic mechanism mediated by TGF-β-
1486 stimulated collagen prolyl hydroxylase expression in fibrotic lung mesenchymal cells. J.
1487 Pathol. *236*, 13384–13394. https://doi.org/10.1002/path.4530.A.

1488 139. Chen, P., Cescon, M., and Bonaldo, P. (2015). The Role of Collagens in Peripheral Nerve
1489 Myelination and Function. Mol. Neurobiol. *52*, 216–225. https://doi.org/10.1007/s12035-
1490 014-8862-y.

1491 140. Vehviläinen, P., Hyytiäinen, M., and Keski-Oja, J. (2009). Matrix association of latent
1492 TGF-beta binding protein-2 (LTBP-2) is dependent on fibrillin-1. J. Cell. Physiol. *221*,
1493 586–593. https://doi.org/10.1002/jcp.21888.

1494 141. Suto, F., Ito, K., Uemura, M., Shimizu, M., Shinkawa, Y., Sanbo, M., Shinoda, T., Tsuboi,
1495 M., Takashima, S., Yagi, T., et al. (2005). Plexin-A4 mediates axon-repulsive activities of
1496 both secreted and transmembrane semaphorins and plays roles in nerve fiber guidance.
1497 J. Neurosci. *25*, 3628–3637. https://doi.org/10.1523/JNEUROSCI.4480-04.2005.

1498 142. Mauti, O., Domanitskaya, E., Andermatt, I., Sadhu, R., and Stoeckli, E.T. (2007).
1499 Semaphorin6A acts as a gate keeper between the central and the peripheral nervous
1500 system. Neural Dev. *2*, 1–17. https://doi.org/10.1186/1749-8104-2-28.

1501 143. Haklai-Topper, L., Mlechkovich, G., Savariego, D., Gokhman, I., and Yaron, A. (2010).
1502 Cis interaction between Semaphorin6A and Plexin-A4 modulates the repulsive response
1503 to Sema6A. EMBO J. *29*, 2635–2645. https://doi.org/10.1038/emboj.2010.147.

1504 144. Lowry Curley, J., Catig, G.C., Horn-Ranney, E.L., and Moore, M.J. (2014). Sensory axon
1505 guidance with semaphorin 6A and nerve growth factor in a biomimetic choice point
1506 model. Biofabrication *6*. https://doi.org/10.1088/1758-5082/6/3/035026.

1507 145. Pease-Raissi, S.E., Pazyra-Murphy, M.F., Li, Y., Wachter, F., Fukuda, Y.,
1508 Fenstermacher, S.J., Barclay, L.A., Bird, G.H., Walensky, L.D., and Segal, R.A. (2017).
1509 Paclitaxel Reduces Axonal Bclw to Initiate IP3R1-Dependent Axon Degeneration. Neuron
1510 *96*, 373-386.e6. https://doi.org/10.1016/j.neuron.2017.09.034.

1511 146. Li, Y., Pazyra-Murphy, M.F., Avizonis, D., Russo, M.T., Tang, S., Chen, C.Y., Hsueh,
1512 Y.P., Bergholz, J.S., Jiang, T., Zhao, J.J., et al. (2022). Sarm1 activation produces
1513 cADPR to increase intra-axonal Ca++ and promote axon degeneration in PIPN. J. Cell
1514 Biol. *221*. https://doi.org/10.1083/jcb.202106080.

1515 147. Chen, X., Gan, Y., Au, N.P.B., and Ma, C.H.E. (2024). Current understanding of the
1516 molecular mechanisms of chemotherapy-induced peripheral neuropathy. Front. Mol.
1517 Neurosci. *17*. https://doi.org/10.3389/fnmol.2024.1345811.

1518 148. Paulson, S., McCabe, G., Winkler, M., Findley, T., Pascua, A., Gordon, K., Walsh, P., and
1519 Truong, V. (2024). Scalable and Efficient Generation of iPSC-derived Human Sensory
1520 Neurons for CIPN and Pain Research. In SLAS.

1521 149. Rockel, A.F., Wagner, N., Spenger, P., Ergün, S., and Wörsdörfer, P. (2023). Neuro-
1522 mesodermal assembloids recapitulate aspects of peripheral nervous system development
1523 in vitro. Stem Cell Reports *18*, 1155–1165. https://doi.org/10.1016/j.stemcr.2023.03.012.

1524 150. Lu, D., Shang, G., He, X., Bai, X. chen, and Zhang, X. (2021). Architecture of the
1525 Sema3A/PlexinA4/Neuropilin tripartite complex. Nat. Commun. *12*, 1–13.
1526 https://doi.org/10.1038/s41467-021-23541-x.

1527 151. Kitsukawa, T., Shimizu, M., Sanbo, M., Hirata, T., Taniguchi, M., Bekku, Y., Yagi, T., and
1528 Fujisawa, H. (1997). Neuropilin-semaphorin III/D-mediated chemorepulsive signals play a
1529 crucial role in peripheral nerve projection in mice. Neuron *19*, 995–1005.
1530 https://doi.org/10.1016/S0896-6273(00)80392-X.

1531 152. Xu, X.M., Fisher, D.A., Zhou, L., White, F.A., Ng, S., Snidpper, W.D., and Luo, Y. (2000).
1532 The transmembrane protein semaphorin 6A repels embryonic sympathetic axons. J.
1533 Neurosci. *20*, 2638–2648. https://doi.org/10.1523/jneurosci.20-07-02638.2000.

1534 153. Lerman, O., Ben-Zvi, A., Yagil, Z., and Behar, O. (2007). Semaphorin3A accelerates
1535 neuronal polarity in vitro and in its absence the orientation of DRG neuronal polarity in
1536 vivo is distorted. Mol. Cell. Neurosci. *36*, 222–234.
1537 https://doi.org/10.1016/j.mcn.2007.07.003.

1538 154. Nakamura, F., Kalb, R.G., and Strittmatter, S.M. (2000). Molecular basis of semaphorin-
1539 mediated axon guidance. J. Neurobiol. *44*, 219–229. https://doi.org/10.1002/1097-
1540 4695(200008)44:2<219::AID-NEU11>3.0.CO;2-W.

1541 155. Pannese, E. (2010). The structure of the perineuronal sheath of satellite glial cells
1542 (SGCs) in sensory ganglia. Neuron Glia Biol. *6*, 3–10.
1543 https://doi.org/10.1017/S1740925X10000037.

1544 156. Kolos, E.A., and Korzhevsky, D.E. (2024). Gap Junction Protein Connexin-43 in a Rat
1545 Dorsal Root Ganglion. Cell tissue biol. *18*, 189–198.
1546 https://doi.org/10.1134/S1990519X23700049.

1547 157. Retamal, M.A., Riquelme, M.A., Stehberg, J., and Alcayaga, J. (2017). Connexin43
1548 hemichannels in satellite glial cells, can they influence sensory neuron activity? Front.
1549 Mol. Neurosci. *10*, 1–9. https://doi.org/10.3389/fnmol.2017.00374.

1550 158. Hanani, M., and Spray, D.C. (2020). Emerging importance of satellite glia in nervous
1551 system function and dysfunction. Nat. Rev. Neurosci. *21*, 485–498.
1552 https://doi.org/10.1038/s41583-020-0333-z.

1553 159. Keane, R.W., Mehta, P.P., Rose, B., Honig, L.S., Loewenstein, W.R., and Rutishauser,
1554 U. (1988). Neural differentiation, NCAM-mediated adhesion, and gap junctional
1555 communication in neuroectoderm. A study in vitro. J. Cell Biol. *106*, 1307–1319.
1556 https://doi.org/10.1083/jcb.106.4.1307.

1557 160. Ma, C.H.E., Brenner, G.J., Omura, T., Samad, O.A., Costigan, M., Inquimbert, P.,

1558 Niederkofler, V., Salie, R., Sun, C.C., Lin, H.Y., et al. (2011). The BMP coreceptor RGMb
1559 promotes while the endogenous BMP antagonist noggin reduces neurite outgrowth and
1560 peripheral nerve regeneration by modulating BMP signaling. J. Neurosci. *31*, 18391–
1561 18400. https://doi.org/10.1523/JNEUROSCI.4550-11.2011.

1562 161. Sundt, D., Gamper, N., and Jaffe, D.B. (2015). Spike propagation through the dorsal root
1563 ganglia in an unmyelinated sensory neuron: A modeling study. J. Neurophysiol. *114*,
1564 3140–3153. https://doi.org/10.1152/jn.00226.2015.

1565 162. Hao, H., Ramli, R., Wang, C., Liu, C., Shah, S., Mullen, P., Lall, V., Jones, F., Shao, J.,
1566 Zhang, H., et al. (2023). Dorsal root ganglia control nociceptive input to the central
1567 nervous system https://doi.org/10.1371/journal.pbio.3001958.

1568 163. Han, C., Estacion, M., Huang, J., Vasylyev, D., Zhao, P., Dib-Hajj, S.D., and Waxman,
1569 S.G. (2015). Human Nav1.8: Enhanced persistent and ramp currents contribute to distinct
1570 firing properties of human DRG neurons. J. Neurophysiol. *113*, 3172–3185.
1571 https://doi.org/10.1152/jn.00113.2015.

1572 164. Lai, J., Gold, M.S., Kim, C.S., Biana, D., Ossipov, M.H., Hunterc, J.C., and Porreca, F.
1573 (2002). Inhibition of neuropathic pain by decreased expression of the tetrodotoxin-
1574 resistant sodium channel, NaV1.8. Pain *95*, 143–152. https://doi.org/10.1016/S0304-
1575 3959(01)00391-8.

1576 165. Enes, J., Haburcák, M., Sona, S., Gerard, N., Mitchell, A.C., Fu, W., and Birren, S.J.
1577 (2020). Satellite glial cells modulate cholinergic transmission between sympathetic
1578 neurons. PLoS One *15*, 1–21. https://doi.org/10.1371/journal.pone.0218643.

1579 166. Tomasello, D.L., Hurley, E., Wrabetz, L., and Bhattacharjee, A. (2017). Slick (Kcnt2)
1580 sodium-activated potassium channels limit peptidergic nociceptor excitability and
1581 hyperalgesia. J. Exp. Neurosci. *11*. https://doi.org/10.1177/1179069517726996.

1582 167. Tsantoulas, C., Denk, F., Signore, M., Nassar, M.A., Futai, K., and McMahon, S.B.
1583 (2018). Mice lacking Kcns1 in peripheral neurons show increased basal and neuropathic
1584 pain sensitivity. Pain *159*, 1641–1651. https://doi.org/10.1097/j.pain.0000000000001255.

1585 168. Warwick, R.A., and Hanani, M. (2013). The contribution of satellite glial cells to
1586 chemotherapy-induced neuropathic pain. Eur. J. Pain (United Kingdom) *17*, 571–580.
1587 https://doi.org/10.1002/j.1532-2149.2012.00219.x.

1588 169. Leo, M., Schmitt, L.I., Kutritz, A., Kleinschnitz, C., and Hagenacker, T. (2021). Cisplatin-
1589 induced activation and functional modulation of satellite glial cells lead to cytokine-
1590 mediated modulation of sensory neuron excitability. Exp. Neurol. *341*.
1591 https://doi.org/10.1016/j.expneurol.2021.113695.

1592 170. Schmitt, L.I., Leo, M., Kutritz, A., Kleinschnitz, C., and Hagenacker, T. (2020). Activation
1593 and functional modulation of satellite glial cells by oxaliplatin lead to hyperexcitability of
1594 sensory neurons in vitro. Mol. Cell. Neurosci. *105*, 103499.
1595 https://doi.org/10.1016/j.mcn.2020.103499.

1596 171. Majd, H., Amin, S., Ghazizadeh, Z., Cesiulis, A., Arroyo, E., Lankford, K., Majd, A.,
1597 Farahvashi, S., Chemel, A.K., Okoye, M., et al. (2023). Deriving Schwann cells from
1598 hPSCs enables disease modeling and drug discovery for diabetic peripheral neuropathy.
1599 Cell Stem Cell *30*, 632-647.e10. https://doi.org/10.1016/j.stem.2023.04.006.

1600 172. Chen, Y., Tristan, C.A., Chen, L., Jovanovic, V.M., Malley, C., Chu, P.H., Ryu, S., Deng,

1601 T., Ormanoglu, P., Tao, D., et al. (2021). A versatile polypharmacology platform promotes
1602 cytoprotection and viability of human pluripotent and differentiated cells (Springer US)
1603 https://doi.org/10.1038/s41592-021-01126-2.

1604 173. Love, M.I., Huber, W., and Anders, S. (2014). Moderated estimation of fold change and
1605 dispersion for RNA-seq data with DESeq2. Genome Biol. *15*, 1–21.
1606 https://doi.org/10.1186/s13059-014-0550-8.

1607 174. Wu, T., Hu, E., Xu, S., Chen, M., Guo, P., Dai, Z., Feng, T., Zhou, L., Tang, W., Zhan, L.,
1608 et al. (2021). clusterProfiler 4.0: A universal enrichment tool for interpreting omics data.
1609 Innovation *2*, 100141. https://doi.org/10.1016/j.xinn.2021.100141.

1610

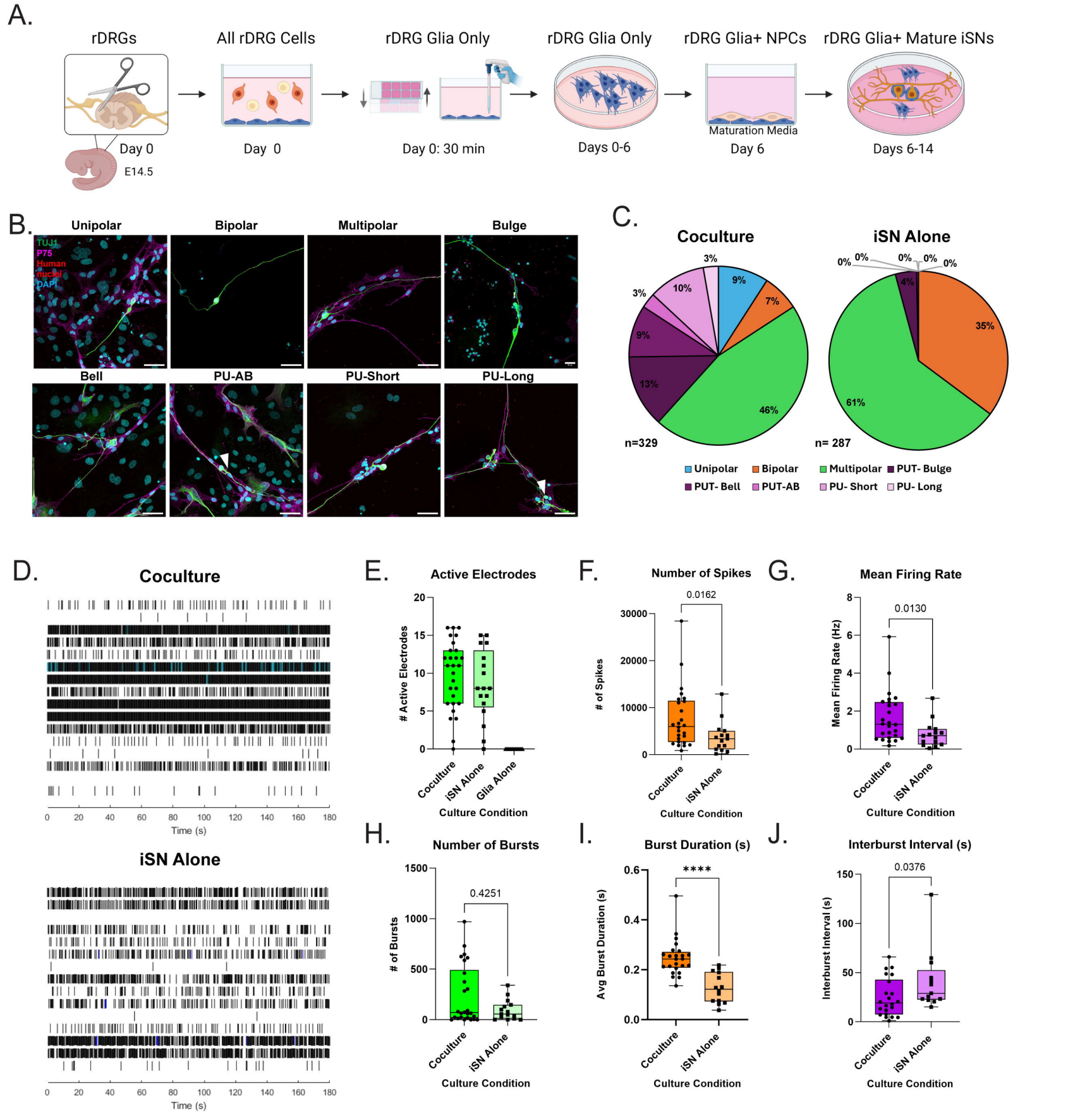
A.
rDRGs
All rDRG Cells
rDRG Glia Only
rDRG Glia Only
rDRG Glia+ NPCs
rDRG Glia+ Mature iSNs
Day 0
E14.5
Day 0
Day 0: 30 min
Days 0-6
Maturation Media
Day 6
Days 6-14
B.
Unipolar
Bipolar
Multipolar
Bulge
TUJ1
P75
Human nuclei
DAPI
Bell
PU-AB
PU-Short
PU-Long
C.
Coculture
iSN Alone
n=329
n= 287
Unipolar
Bipolar
Multipolar
PUT- Bulge
PUT- Bell
PUT-AB
PU- Short
PU- Long
D.
Coculture
iSN Alone
Time (s)
E.
Active Electrodes
Active Electrodes
Coculture
iSN Alone
Glia Alone
Culture Condition
F.
Number of Spikes
0.0162
# of Spikes
Culture Condition
G.
Mean Firing Rate
0.0130
Mean Firing Rate (Hz)
Culture Condition
H.
Number of Bursts
0.4251
# of Bursts
Culture Condition
I.
Burst Duration (s)
****
Avg Burst Duration (s)
Culture Condition
J.
Interburst Interval (s)
0.0376
Interburst Interval (s)
Culture Condition

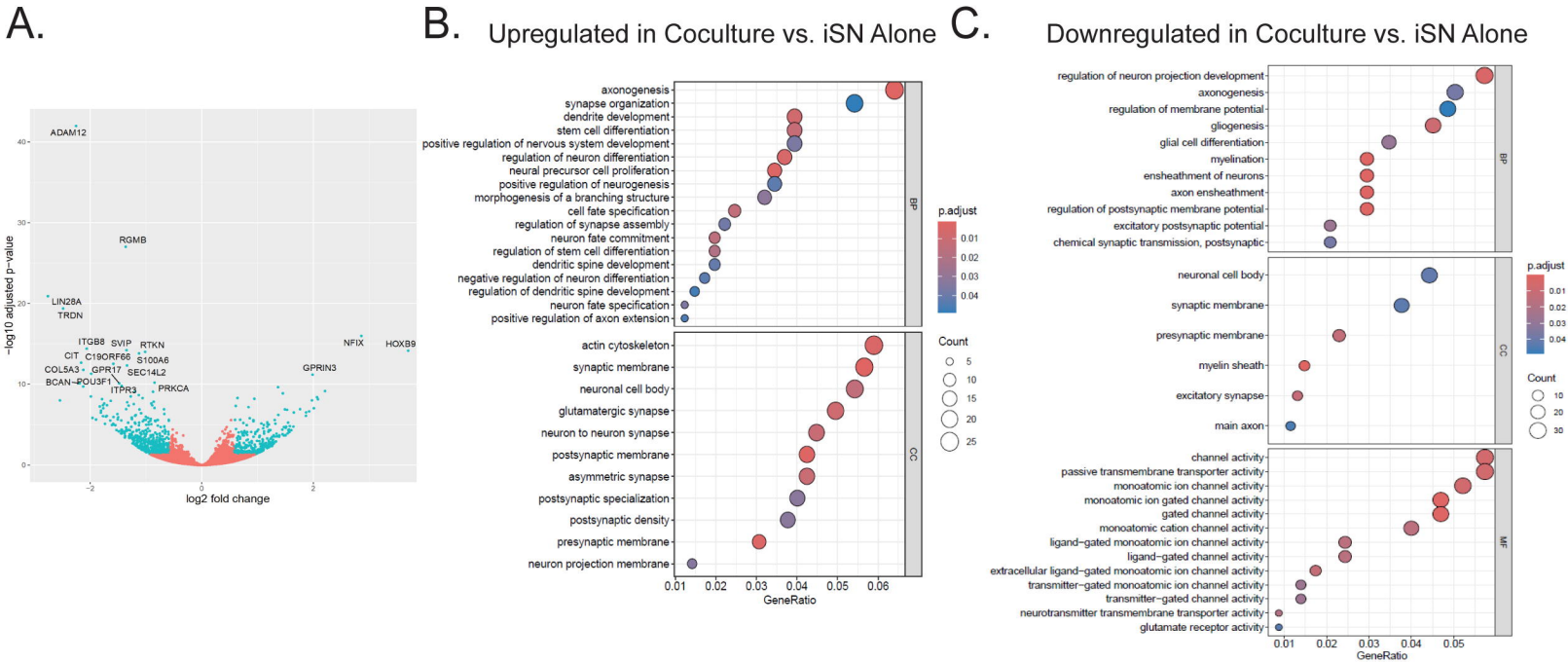
A.
ADAM12
RGMB
LIN28A
TRDN
ITGB8
SVIP
RTKN
CIT
C19ORF66
S100A6
COL5A3
GPR17
SEC14L2
BCAN
POU3F1
ITPR3
PRKCA
NFIX
HOXB9
GPRIN3
−log10 adjusted p−value
log2 fold change
B. Upregulated in Coculture vs. iSN Alone
axonogenesis
synapse organization
dendrite development
stem cell differentiation
positive regulation of nervous system development
regulation of neuron differentiation
neural precursor cell proliferation
positive regulation of neurogenesis
morphogenesis of a branching structure
cell fate specification
regulation of synapse assembly
neuron fate commitment
regulation of stem cell differentiation
dendritic spine development
negative regulation of neuron differentiation
regulation of dendritic spine development
neuron fate specification
positive regulation of axon extension
actin cytoskeleton
synaptic membrane
neuronal cell body
glutamatergic synapse
neuron to neuron synapse
postsynaptic membrane
asymmetric synapse
postsynaptic specialization
postsynaptic density
presynaptic membrane
neuron projection membrane
BP
CC
p.adjust
Count
GeneRatio
C. Downregulated in Coculture vs. iSN Alone
regulation of neuron projection development
axonogenesis
regulation of membrane potential
gliogenesis
glial cell differentiation
myelination
ensheathment of neurons
axon ensheathment
regulation of postsynaptic membrane potential
excitatory postsynaptic potential
chemical synaptic transmission, postsynaptic
neuronal cell body
synaptic membrane
presynaptic membrane
myelin sheath
excitatory synapse
main axon
channel activity
passive transmembrane transporter activity
monoatomic ion channel activity
monoatomic ion gated channel activity
gated channel activity
monoatomic cation channel activity
ligand−gated monoatomic ion channel activity
ligand−gated channel activity
extracellular ligand−gated monoatomic ion channel activity
transmitter−gated monoatomic ion channel activity
transmitter−gated channel activity
neurotransmitter transmembrane transporter activity
glutamate receptor activity
BP
CC
MF
p.adjust
Count
GeneRatio

A.

NMM Treated Alone vs. Glia Media Alone

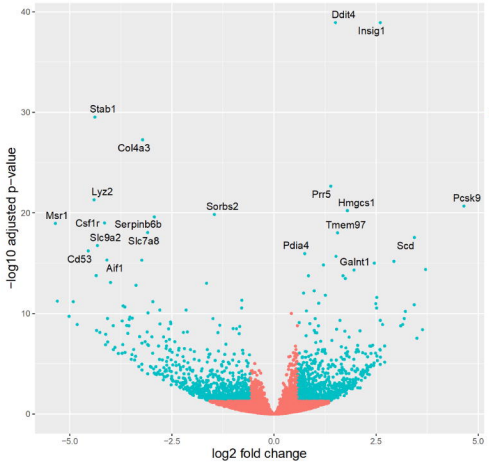

B.

Upregulated in NMM Treated Glia Alone

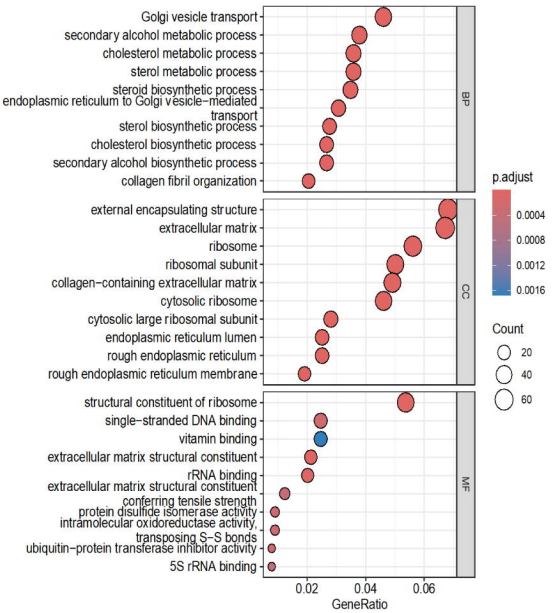

C.

Downregulated in NMM Treated Glia Alone

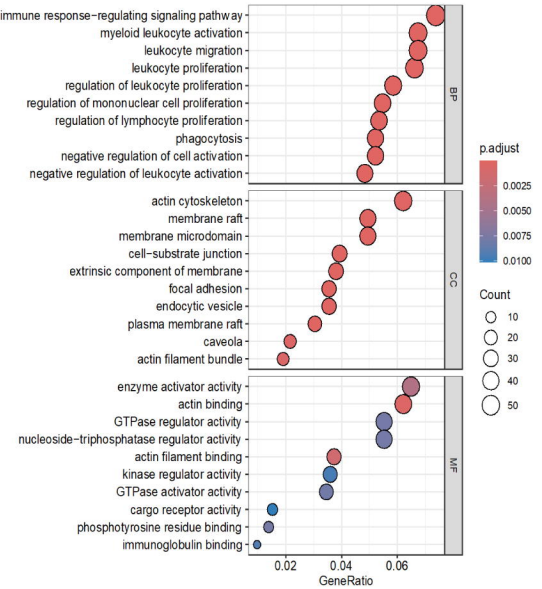

D.

Coculture vs. Glia Media Alone

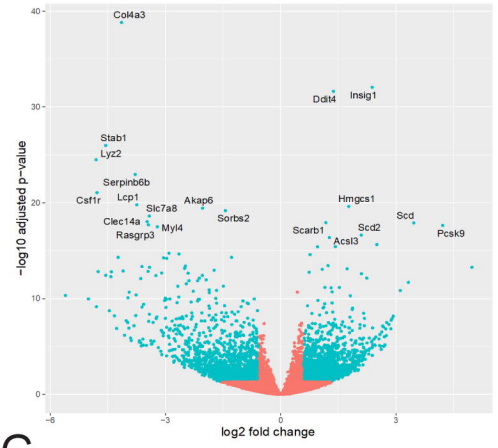

E.

Upregulated in Coculture

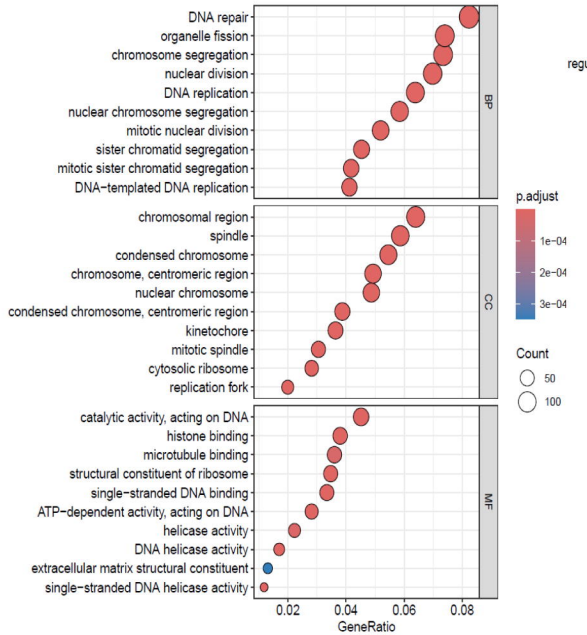

F.

Dowregulated in Coculture

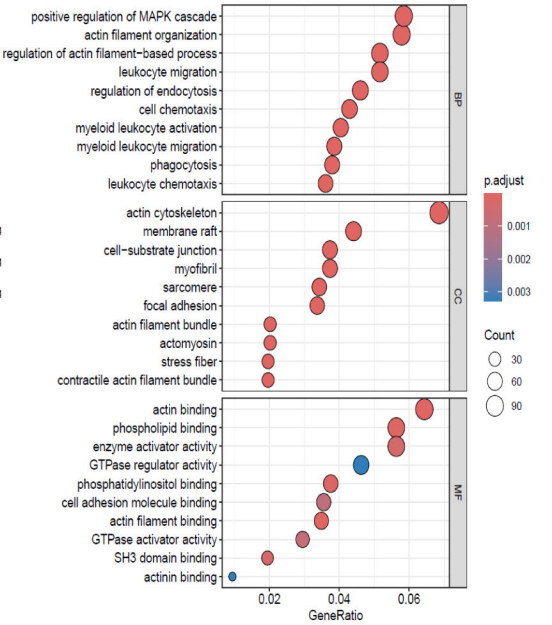

G.

Coculture vs. NMM Treated Alone

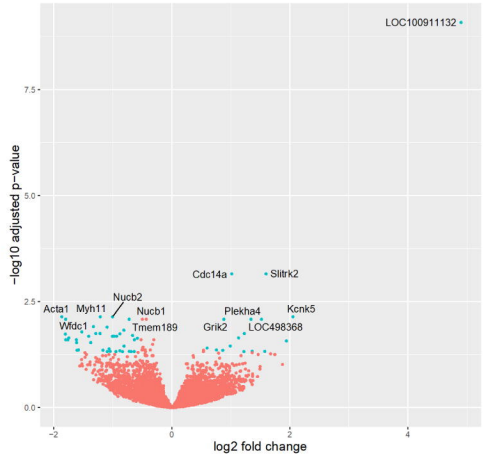

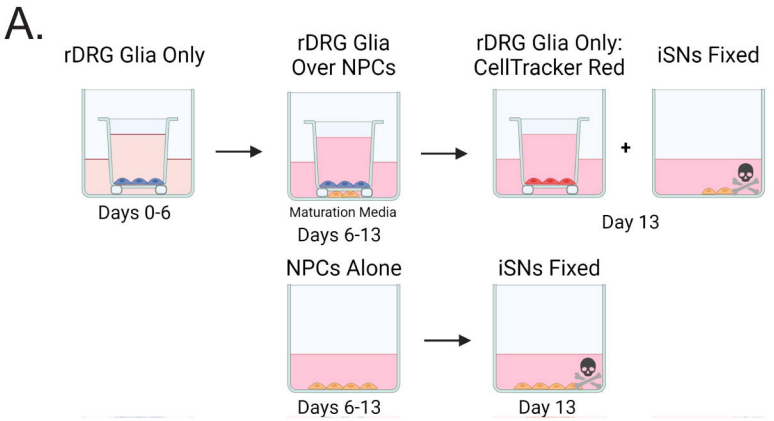
A.
rDRG Glia Only
Days 0-6
rDRG Glia Over NPCs
Maturation Media
Days 6-13
rDRG Glia Only: CellTracker Red
iSNs Fixed
Day 13
NPCs Alone
Days 6-13
iSNs Fixed
Day 13

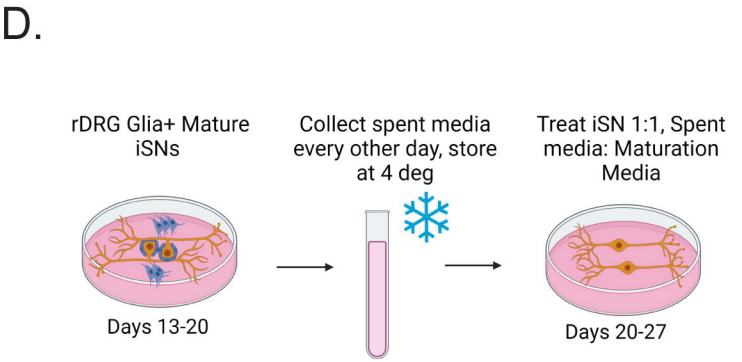
D.
rDRG Glia+ Mature iSNs
Days 13-20
Collect spent media every other day, store at 4 deg
Treat iSN 1:1, Spent media: Maturation Media
Days 20-27

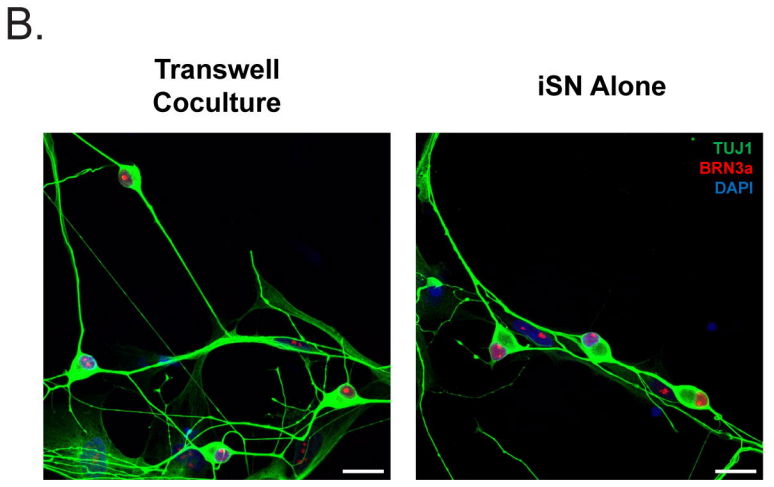
B.
Transwell Coculture
iSN Alone
TUJ1
BRN3a
DAPI

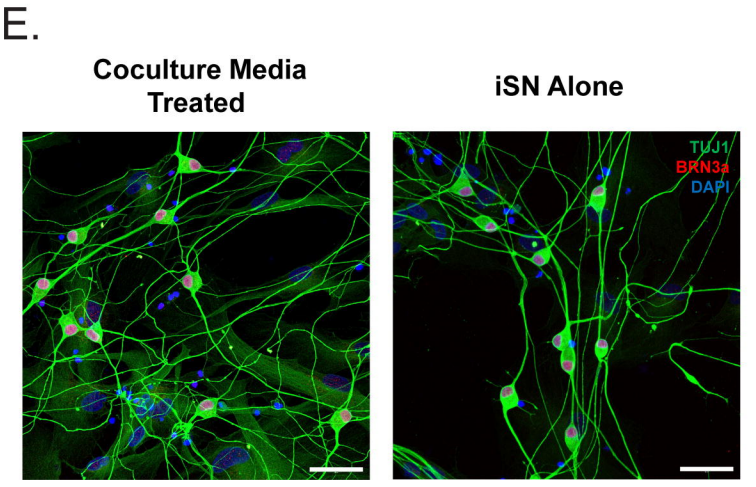
E.
Coculture Media Treated
iSN Alone
TUJ1
BRN3a
DAPI

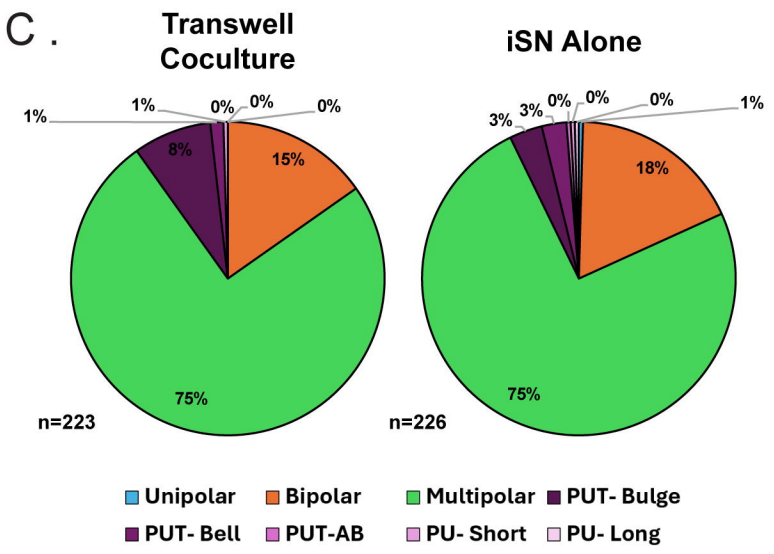
C .
Transwell Coculture
iSN Alone
1%
1%
0%
0%
0%
8%
15%
75%
n=223
3%
3%
0%
0%
0%
1%
18%
75%
n=226
Unipolar
Bipolar
Multipolar
PUT- Bulge
PUT- Bell
PUT-AB
PU- Short
PU- Long

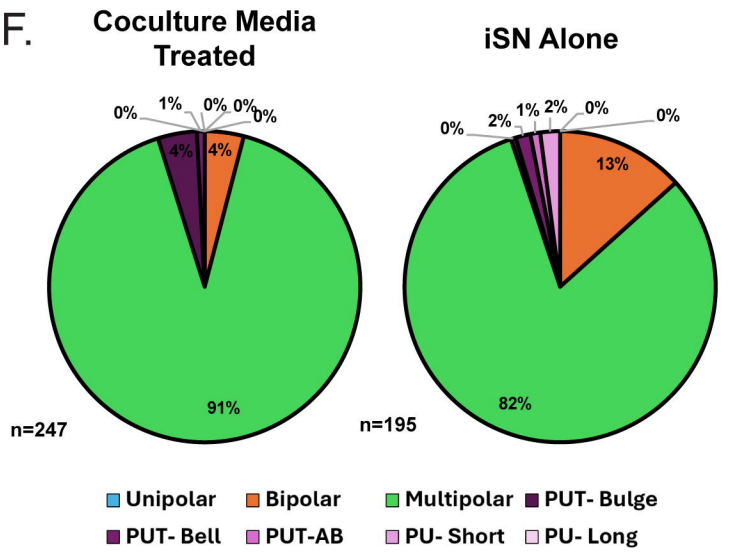
F.
Coculture Media Treated
iSN Alone
0%
1%
0%
0%
0%
4%
4%
91%
n=247
0%
2%
1%
2%
0%
0%
13%
82%
n=195
Unipolar
Bipolar
Multipolar
PUT- Bulge
PUT- Bell
PUT-AB
PU- Short
PU- Long

A.

rDRG Glia Only
rDRG Glia Only: Maturation Media
rDRG Glia Only: Methanol Fixation
rDRG Glia+ NPCs
rDRG Glia+ Mature iSNs
Days 0-6
Days 6-13
Day 13 AM
Day 13 PM
Days 13-20

B.

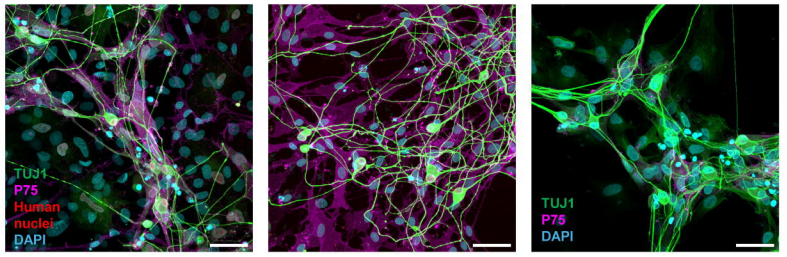
Methanol Fixed Glia, 2wks
Coculture Control
iSN Alone
TUJ1
P75
Human nuclei
DAPI
TUJ1
P75
DAPI

C.

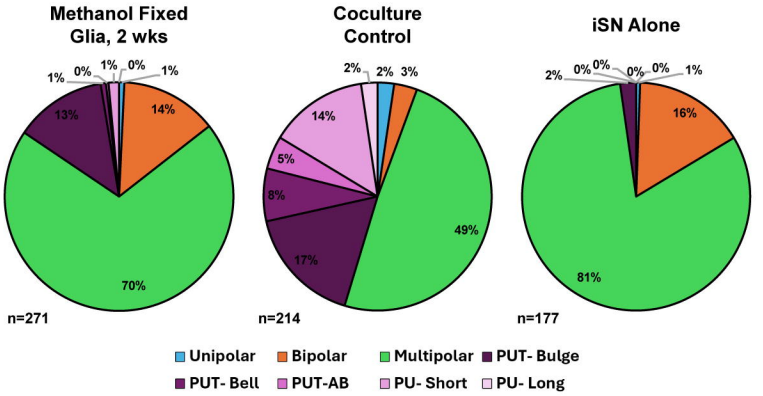
Methanol Fixed Glia, 2 wks
Coculture Control
iSN Alone
1%
0%
1%
0%
1%
13%
14%
70%
n=271
2%
2%
3%
14%
5%
8%
17%
49%
n=214
2%
0%
0%
0%
0%
1%
16%
81%
n=177
Unipolar
Bipolar
Multipolar
PUT- Bulge
PUT- Bell
PUT-AB
PU- Short
PU- Long

D.

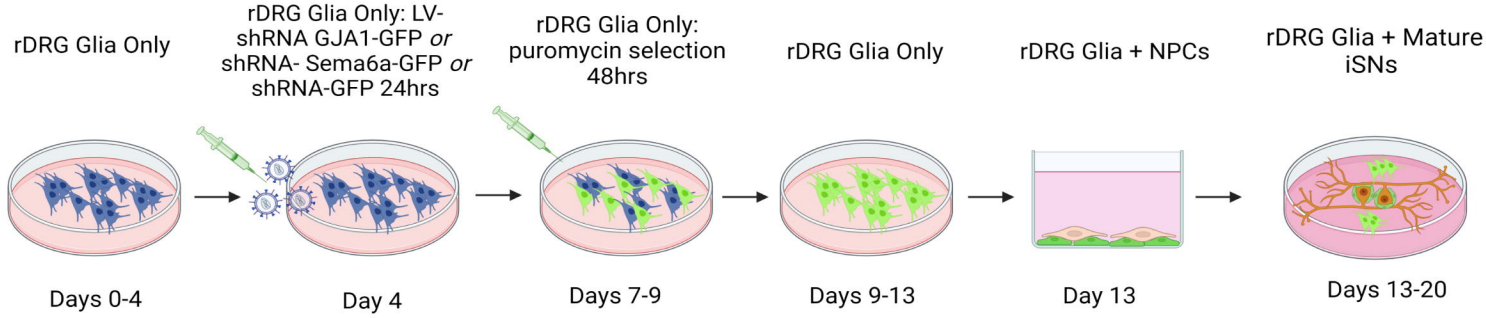
rDRG Glia Only
rDRG Glia Only: LV-shRNA GJA1-GFP *or* shRNA- Sema6a-GFP *or* shRNA-GFP 24hrs
rDRG Glia Only: puromycin selection 48hrs
rDRG Glia Only
rDRG Glia + NPCs
rDRG Glia + Mature iSNs
Days 0-4
Day 4
Days 7-9
Days 9-13
Day 13
Days 13-20

E.

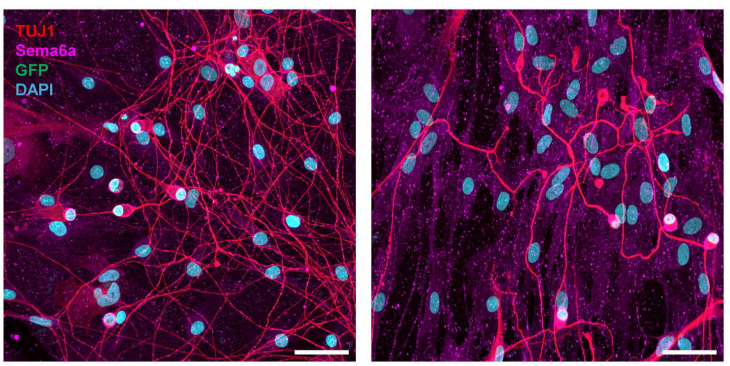
Sh-Sema6a rDRG Glia Coculture
Sh-GFP rDRG Glia Coculture
TUJ1
Sema6a
GFP
DAPI

G.

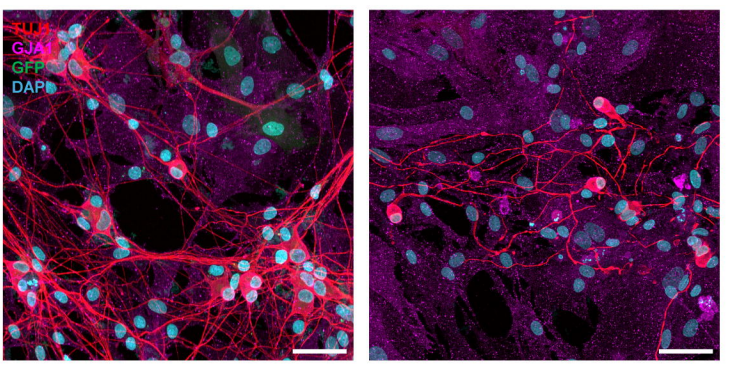
Sh-GJA1 rDRG Glia Coculture
Sh-GFP rDRG Glia Coculture
TUJ1
GJA1
GFP
DAPI

F.

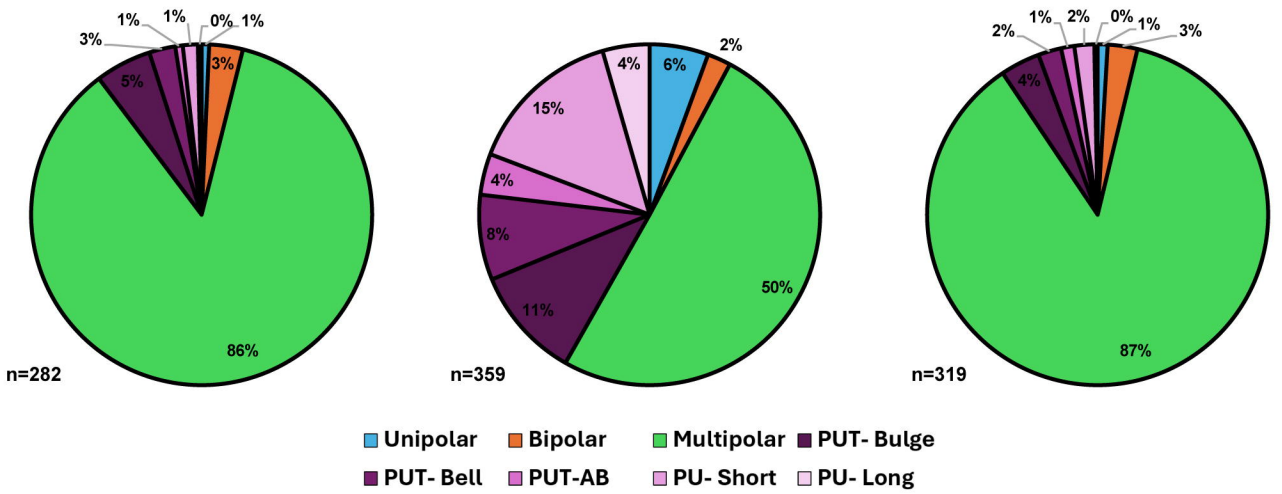
Sh-RNA-Sema6a Coculture
3%
1%
1%
0%
1%
3%
5%
86%
n=282
Sh-RNA-GFP Coculture
4%
6%
2%
15%
4%
8%
11%
50%
n=359
Sh-RNA-GJA1 Coculture
2%
1%
2%
0%
1%
3%
4%
87%
n=319
Unipolar
Bipolar
Multipolar
PUT- Bulge
PUT- Bell
PUT-AB
PU- Short
PU- Long

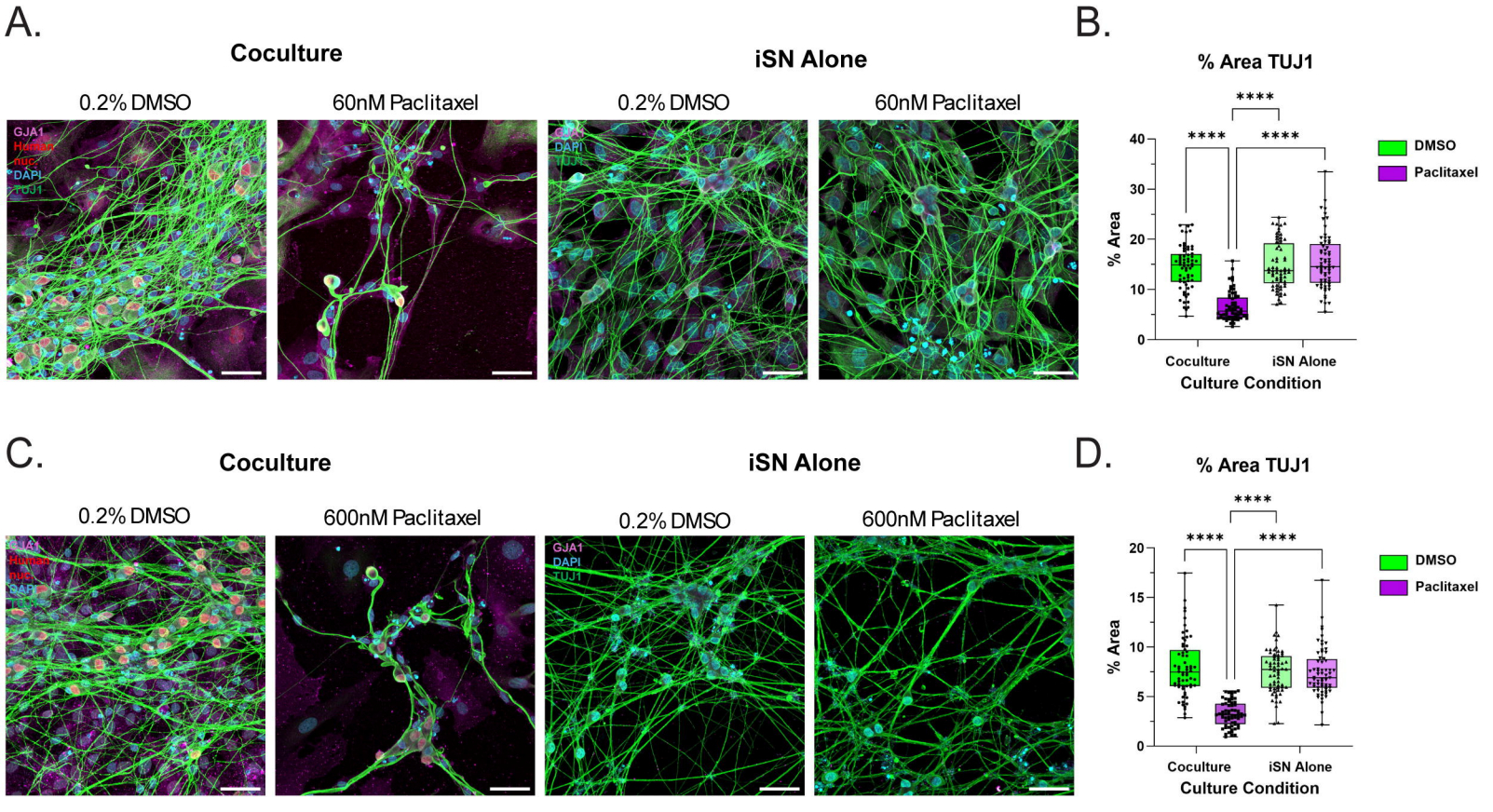
A.
Coculture
iSN Alone
0.2% DMSO
60nM Paclitaxel
0.2% DMSO
60nM Paclitaxel
GJA1
Human nuc
DAPI
TUJ1
B.
% Area TUJ1
****
****
****
40
30
20
10
0
% Area
DMSO
Paclitaxel
Coculture
iSN Alone
Culture Condition
C.
Coculture
iSN Alone
0.2% DMSO
600nM Paclitaxel
0.2% DMSO
600nM Paclitaxel
GJA1
DAPI
TUJ1
D.
% Area TUJ1
****
****
****
20
15
10
5
0
% Area
DMSO
Paclitaxel
Coculture
iSN Alone
Culture Condition

S1.

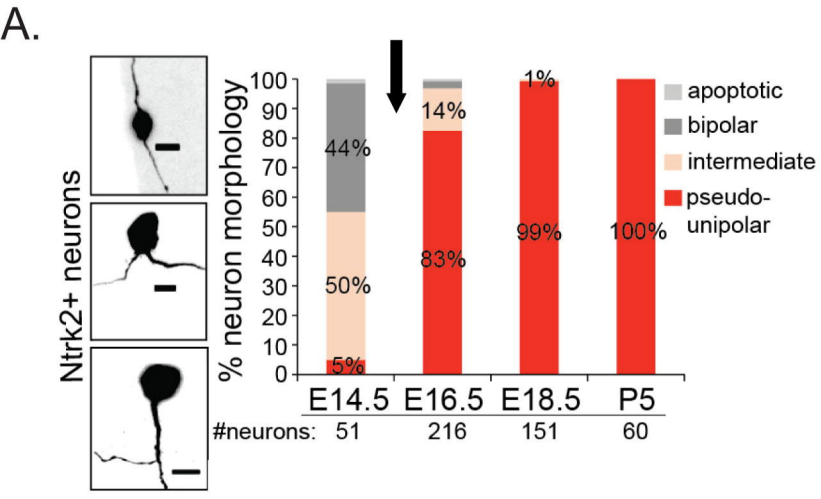
A.
Ntrk2+ neurons
% neuron morphology
100
90
80
70
60
50
40
30
20
10
0
44%
50%
5%
14%
83%
1%
99%
100%
apoptotic
bipolar
intermediate
pseudo-unipolar
E14.5
E16.5
E18.5
P5
#neurons: 51 216 151 60

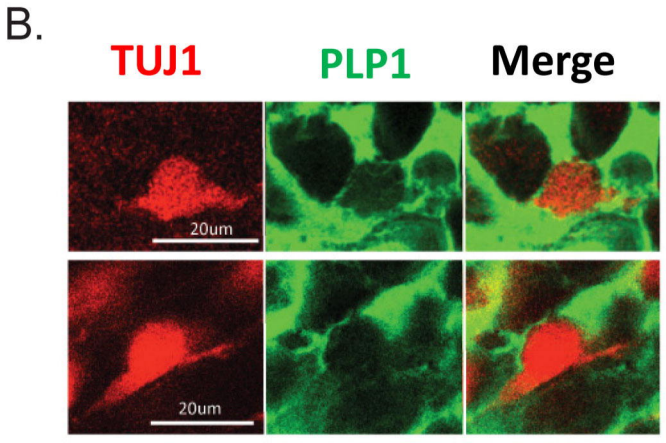
B.
TUJ1
PLP1
Merge
20um
20um

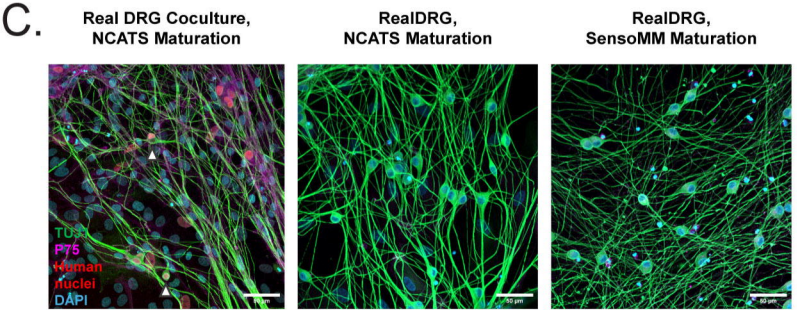
C.
Real DRG Coculture, NCATS Maturation
RealDRG, NCATS Maturation
RealDRG, SensoMM Maturation
TUJ1
P75
Human
nuclei
DAPI

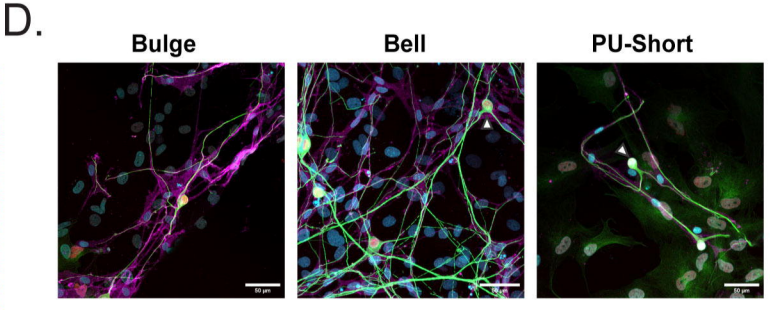
D.
Bulge
Bell
PU-Short

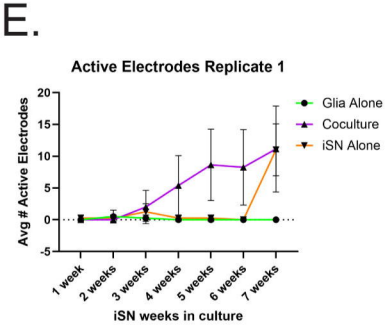
E.
Active Electrodes Replicate 1
Avg # Active Electrodes
Glia Alone
Coculture
iSN Alone
1 week
2 weeks
3 weeks
4 weeks
5 weeks
6 weeks
7 weeks
iSN weeks in culture

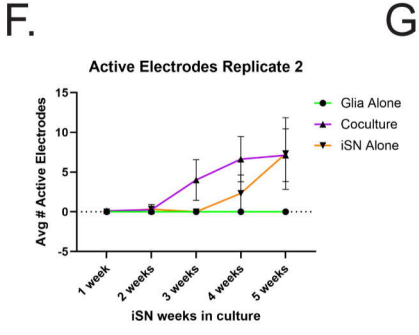
F.
Active Electrodes Replicate 2
Avg # Active Electrodes
Glia Alone
Coculture
iSN Alone
1 week
2 weeks
3 weeks
4 weeks
5 weeks
iSN weeks in culture

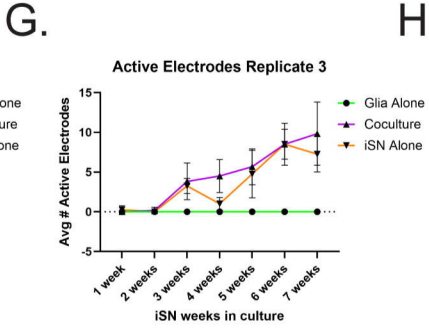
G.
Active Electrodes Replicate 3
Avg # Active Electrodes
Glia Alone
Coculture
iSN Alone
1 week
2 weeks
3 weeks
4 weeks
5 weeks
6 weeks
7 weeks
iSN weeks in culture

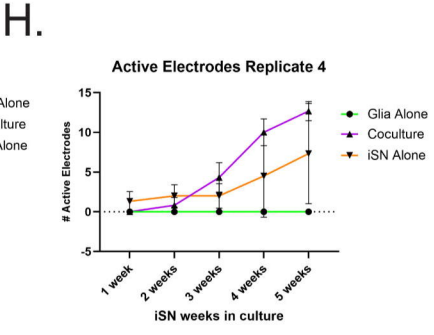
H.
Active Electrodes Replicate 4
Active Electrodes
Glia Alone
Coculture
iSN Alone
1 week
2 weeks
3 weeks
4 weeks
5 weeks
iSN weeks in culture

S2.

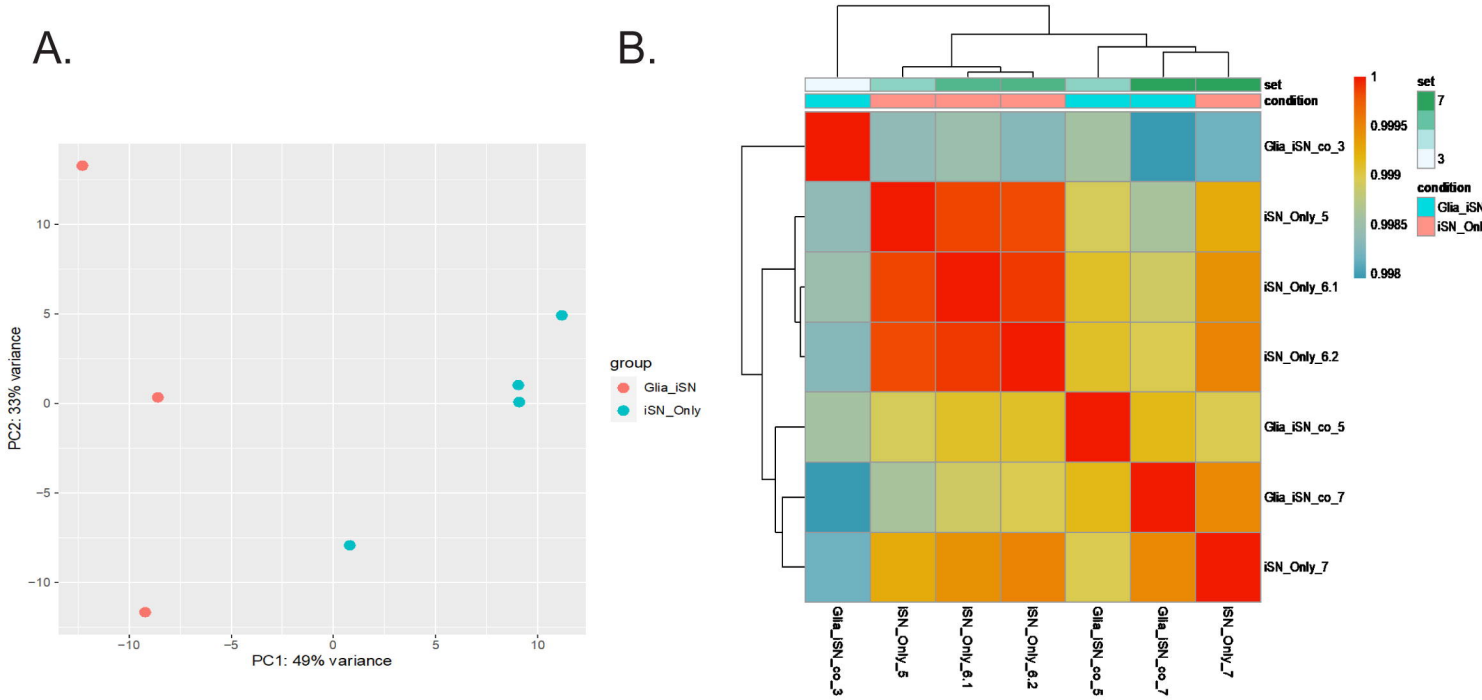
A.
B.
PC2: 33% variance
PC1: 49% variance
10
5
0
−5
−10
group
Glia_iSN
iSN_Only
set
condition
Glia_iSN_co_3
iSN_Only_5
iSN_Only_6.1
iSN_Only_6.2
Glia_iSN_co_5
Glia_iSN_co_7
iSN_Only_7
1
0.9995
0.999
0.9985
0.998
set
7
3
condition
Glia_iSN
iSN_Only

S3.

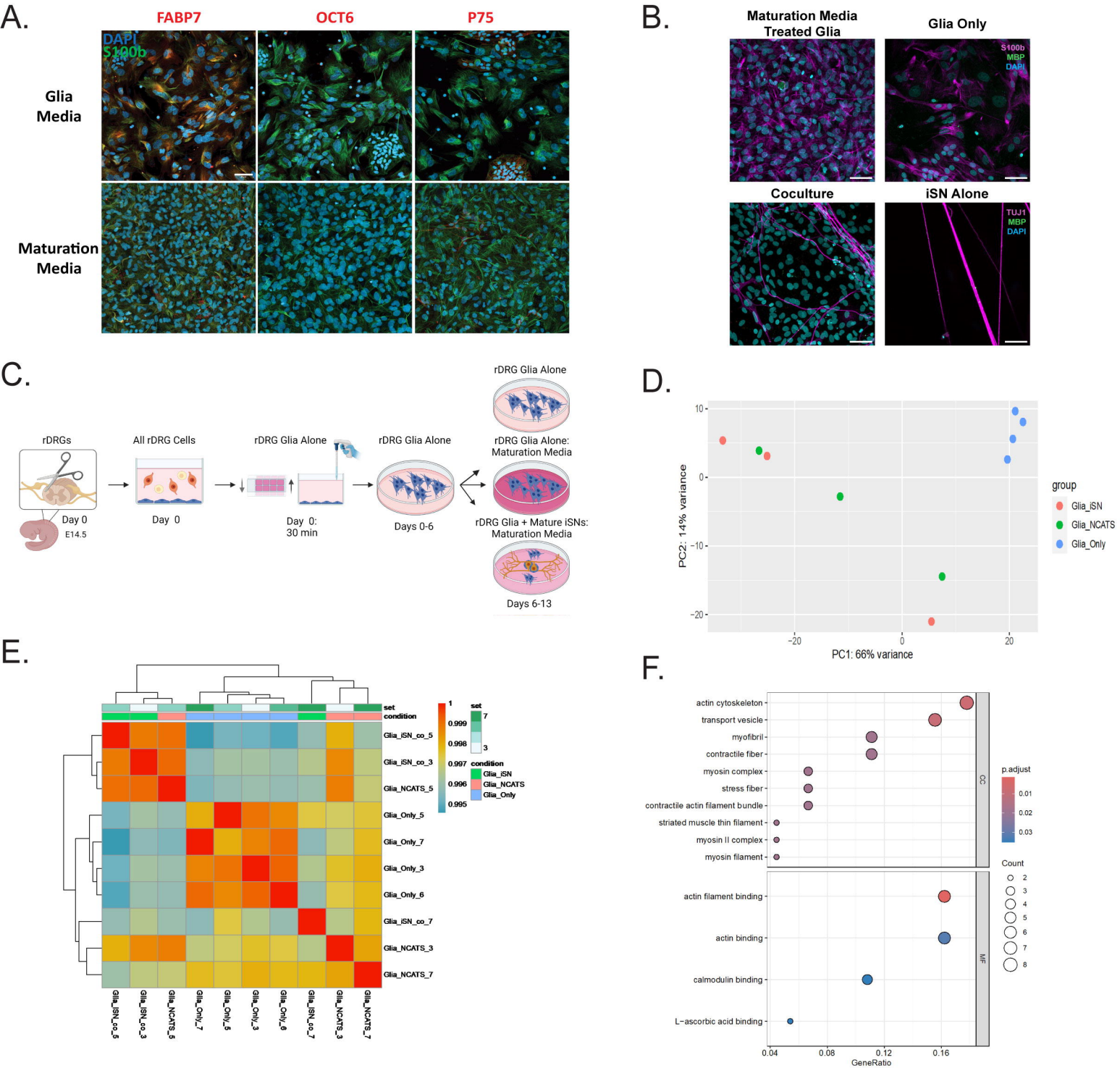
A.
FABP7
OCT6
P75
DAPI
S100b
Glia Media
Maturation Media
B.
Maturation Media Treated Glia
Glia Only
S100b
MBP
DAPI
Coculture
iSN Alone
TUJ1
MBP
DAPI
C.
rDRGs
Day 0
E14.5
All rDRG Cells
Day 0
rDRG Glia Alone
Day 0:
30 min
rDRG Glia Alone
Days 0-6
rDRG Glia Alone
rDRG Glia Alone:
Maturation Media
rDRG Glia + Mature iSNs:
Maturation Media
Days 6-13
D.
PC2: 14% variance
PC1: 66% variance
group
Glia_iSN
Glia_NCATS
Glia_Only
E.
set
condition
Glia_iSN_co_5
Glia_iSN_co_3
Glia_NCATS_5
Glia_Only_5
Glia_Only_7
Glia_Only_3
Glia_Only_6
Glia_iSN_co_7
Glia_NCATS_3
Glia_NCATS_7
condition
Glia_iSN
Glia_NCATS
Glia_Only
F.
actin cytoskeleton
transport vesicle
myofibril
contractile fiber
myosin complex
stress fiber
contractile actin filament bundle
striated muscle thin filament
myosin II complex
myosin filament
CC
actin filament binding
actin binding
calmodulin binding
L-ascorbic acid binding
MF
p.adjust
Count
GeneRatio

S4.

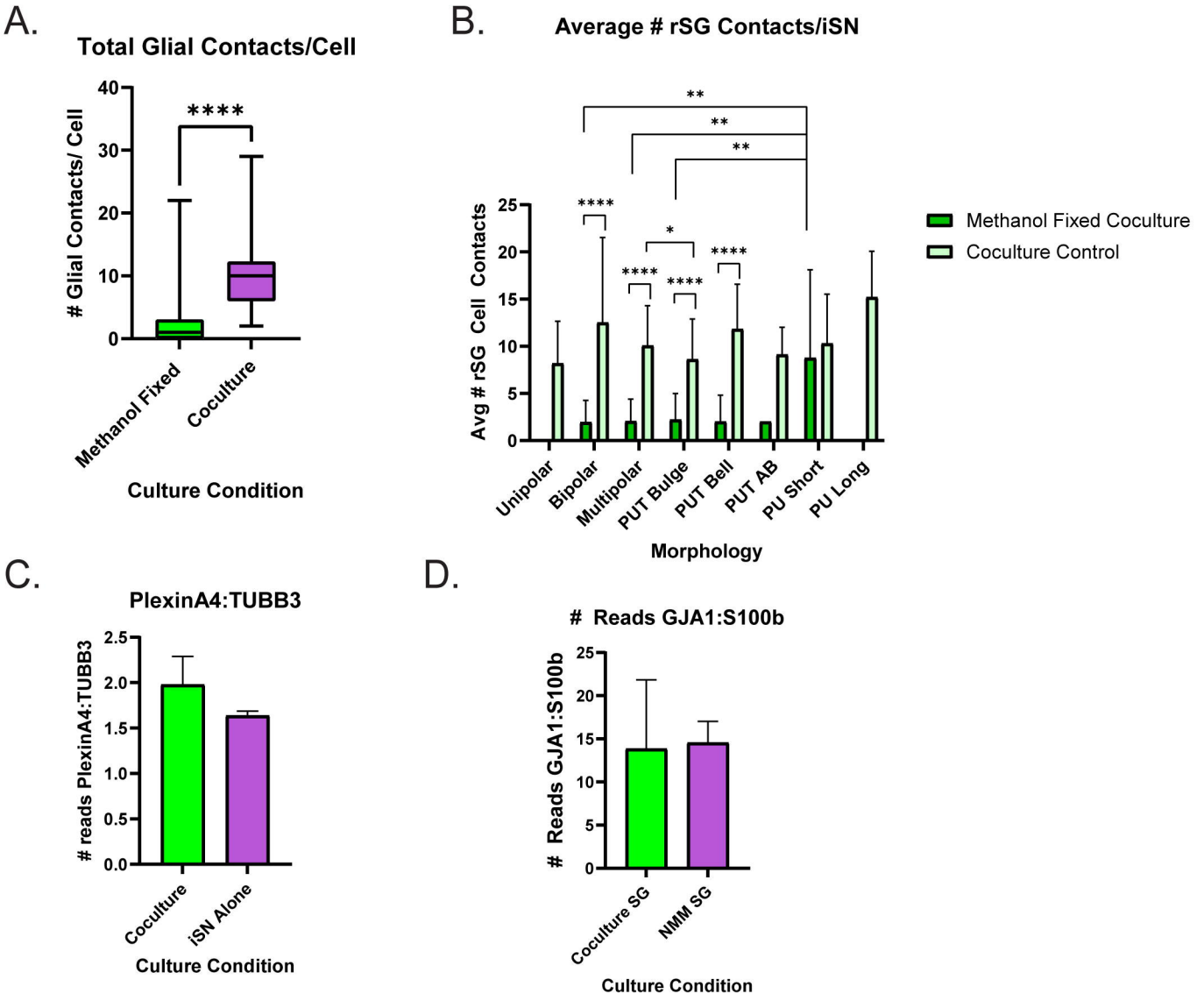
A.
Total Glial Contacts/Cell
Glial Contacts/ Cell
****
Methanol Fixed
Coculture
Culture Condition
B.
Average # rSG Contacts/iSN
Avg # rSG Cell Contacts
Methanol Fixed Coculture
Coculture Control
Unipolar
Bipolar
Multipolar
PUT Bulge
PUT Bell
PUT AB
PU Short
PU Long
Morphology
C.
PlexinA4:TUBB3
reads PlexinA4:TUBB3
Coculture
iSN Alone
Culture Condition
D.
Reads GJA1:S100b
Reads GJA1:S100b
Coculture SG
NMM SG
Culture Condition